

THE DEEP X-RAY RADIO BLAZAR SURVEY (DXRBS)

I. Methods and First Results ¹

Eric S. Perlman^{2,3}

Space Telescope Science Institute, 3700 San Martin Drive, Baltimore, MD 21218, USA.

Email: perlman@stsci.edu

Paolo Padovani^{4,5}

Dipartimento di Fisica, II Università di Roma “Tor Vergata”,

Via della Ricerca Scientifica 1, I-00133 Roma, Italy.

Paolo Giommi⁴

SAX Science Data Center, ASI, Viale Regina Margherita 202, I-00198, Italy.

Rita Sambruna^{2,6}

Laboratory for High Energy Astrophysics, Mail Code 660.2

Goddard Space Flight Center, Greenbelt, MD 20771, USA

Laurence R. Jones

School of Physics & Astronomy, University of Birmingham, Birmingham B15 2TT, UK.

Anastasios Tzioumis and John Reynolds

Australia Telescope National Facility, CSIRO, PO Box 76, Epping NSW 2121, Australia

ABSTRACT

We have undertaken a survey of archived, pointed ROSAT PSPC data for blazars by correlating the ROSAT WGACAT database with several publicly

¹Based on observations collected at the European Southern Observatory, La Silla, Chile; Kitt Peak National Observatory, Cerro Tololo Interamerican Observatory, and the Australia Telescope National Facility

²Visiting astronomer at Kitt Peak National Observatory

³Visiting astronomer at Cerro Tololo Interamerican Observatory

⁴Visiting astronomer at the European Southern Observatory, La Silla, Chile

⁵Currently on leave at the Space Telescope Science Institute, 3700 San Martin Drive, Baltimore, MD 21218, USA

⁶Presently at: Pennsylvania State University, Department of Astronomy, 525 Davey Lab, University Park, PA 16803

available radio catalogs, restricting our candidate list to serendipitous flat radio spectrum sources ($\alpha_r \leq 0.70$, where $S_\nu \propto \nu^{-\alpha}$). Here we discuss our survey methods, identification procedure and first results. Our survey is found to be $\sim 95\%$ efficient at finding flat-spectrum radio-loud quasars (FSRQs, 59 of our first 85 IDs) and BL Lacertae objects (22 of our first 85 IDs), a figure which is comparable to or greater than that achieved by other radio and X-ray survey techniques.

The identifications presented here show that all previous samples of blazars (even when taken together) did not representatively survey the blazar population, missing critical regions of (L_X, L_R) parameter space within which large fractions of the blazar population lie. Particularly important is the identification of a large population of FSRQs ($\gtrsim 25\%$ of DXRBS FSRQs) with ratios of X-ray to radio luminosity $\gtrsim 10^{-6}$ ($\alpha_{rx} \lesssim 0.78$). In addition, due to our greater sensitivity, DXRBS has already more than doubled the number of FSRQs in complete samples with 5 GHz (radio) luminosities between $10^{31.5}$ and $10^{33.5}$ erg s $^{-1}$ Hz $^{-1}$ and fills in the region of parameter space between X-ray selected and radio-selected samples of BL Lacs. DXRBS is the very first sample to contain statistically significant numbers of blazars at low luminosities, approaching what should be the lower end of the FSRQ luminosity function.

Subject headings: BL Lacertae objects: general – Quasars: general – radio continuum – surveys – X-rays

1. Introduction

Blazars are the most extreme variety of AGN known. Their signal properties include irregular, rapid variability; high optical polarization; core-dominant radio morphology; apparent superluminal motion; flat ($\alpha_r < 0.5$) radio spectra; and a broad continuum extending from the radio through the gamma-rays (these properties are reviewed in detail by Urry & Padovani 1995). The broadband emission from blazars is dominated by non-thermal processes (most likely synchrotron and inverse-Compton radiation), likely emitted by a relativistic jet pointed close to our line of sight (as originally proposed by Blandford & Rees in 1978). The beaming hypothesis has been successful in reproducing the luminosity function of samples of blazars (e.g., Padovani & Urry 1990, 1991, 1992; Urry, Padovani & Stickel 1991), allowing the derivation of class properties such as the range of Lorentz factors Γ and opening angles in the radio band (and also in other bands for BL Lacs).

However, the small size of these samples (30-50 objects) has prevented detailed modeling of the luminosity function, especially at low powers, yielding considerable uncertainties on the derived parameters.

Due to the rarity and low space-density of blazars, which make up considerably less than 5% of all AGN (Padovani 1997), “pencil-beam” surveys of the type carried out by, e.g., Castander et al. (1996), are poorly suited for finding blazars. As has already been noted by Perlman et al. (1996a), wide-angle surveys with appropriately restrictive search parameters are much more efficacious. Indeed, it is thanks to the advent of such surveys that complete samples of blazars exist today. With the advent of modern archival techniques and deeper wide-angle surveys, it is now possible to combine survey techniques and develop surveys which can sample the blazar luminosity function deeply and representatively. Several such projects are currently underway (§ 3).

This paper describes the DXRBS blazar survey and its goals, and presents our first 85 firm identifications. The main result presented here is that previous blazar samples are not representative of the blazar class, missing approximately half of the FSRQ population and a somewhat smaller part of the BL Lac population. The newly identified DXRBS blazars expand the range of L_X/L_R values found among blazars with emission lines by an order of magnitude, and for the first time samples the low-luminosity end of the luminosity function of FSRQs with reasonable statistics. In Section 2, we describe the methods used to find blazar candidates and prepare for optical observations. Section 3 contains a detailed discussion on the subject of classification of flat-spectrum radio sources. Section 4 describes the results of our optical spectroscopy and the makeup of the DXRBS blazar sample as of April 1997. Section 5 discusses the redshift distribution of both the BL Lac and FSRQ subsamples. Section 6 contains a discussion of the properties of the sample, and the implications of these first results for unified schemes and upon our picture of the blazar class. In Section 7, we discuss the topic of selection effects. The conclusions of this work are summarized in Section 8.

2. Survey Methods

2.1. The Catalogs

The Deep X-ray Radio Blazar Survey (DXRBS) uses a cross-correlation of all serendipitous sources in the publicly available database of ROSAT sources, WGACAT (White, Giommi & Angelini 1995), having quality flag ≥ 5 (to avoid problematic detections) with a number of publicly available radio catalogs. North of the celestial equator, we used

the 20 cm and 6 cm Green Bank survey catalogs NORTH20CM and GB6 (White & Becker 1992; Gregory et al. 1996), while south of the equator, we used the Parkes-MIT-NRAO catalog PMN (Griffith & Wright 1993). All sources with radio spectral index $\alpha_r \leq 0.7$ at a few GHz were selected as blazar candidates.

For objects north of the celestial equator, 6-20 cm radio spectral indices were obtained directly from the cross-correlation of the GB6 and NORTH20CM catalogs. For sources at southern declinations, the lack of a comparably deep radio survey at a second frequency required a different strategy. In the band $0^\circ > \delta > -15^\circ$, we cross-correlated the sources with the public NVSS database (Condon et al. 1997); our selection of candidates is still not completed in this declination range, since the NVSS is not yet 100% complete. Further south, the positional accuracy of the NVSS, which covers the sky north of -40° , decreases somewhat (Condon et al. 1997). In this region, we conducted a snapshot survey with the Australia Telescope Compact Array (ATCA) at 3.6 and 6 cm (note that the positional accuracy of the ATCA snapshots deteriorate significantly at $\delta > -15^\circ$ due to the East-West nature of the array), to get also radio spectral indices unaffected by variability (see § 7). The first set of ATCA observations (of 163 X-ray/radio sources) took place 11-13 November 1995. A second set of 55 X-ray/radio sources (some of which have preliminarily been classified as blazar candidates based upon the 6-20 cm spectral index computed from their PMN and NVSS fluxes) were observed in October 1997 to complete the coverage of the southern sample. These ATCA observations will be discussed in a future paper. We had originally requested observations at 6 and 20 cm at the ATCA as well, to match our northern sample, but the time allocation committee decided otherwise, based on the instrumental configuration. Note that, as the NVSS has a much smaller beam size than the GB6 survey, it is preferable to use, whenever possible, the NORTH20CM 20 cm fluxes to derive spectral indices. Extra care was taken in the $0^\circ > \delta > -15^\circ$ region, where we had to resort to the NVSS for this purpose, to include the flux from all sources in a 2 arcmin radius. We stress, however, that this problem is severe only for extended, steep-spectrum radio sources, and not for the core-dominated, flat-spectrum sources we are interested in.

2.2. The Criteria

We have identified as our highest priority sources those which meet the following four criteria:

1. $\alpha_{6-20} \leq 0.7$ for $\delta > -15^\circ$; $\alpha_{3.6-6} \leq 0.7$ for $\delta < -15^\circ$
2. $|b| > 10^\circ$;

3. $F(20 \text{ cm}) > 100 \text{ mJy}$ for $0 < \delta < 75^\circ$;
4. $F(6 \text{ cm}) \gtrsim 50 \text{ mJy}$ for $\delta < 0^\circ$.

These criteria were chosen in order to ensure that a well defined, flux-limited sample can be achieved. Over 200 candidate blazars met the above defining criteria (details are given below). In addition, 98 previously identified but serendipitously observed objects meet our criteria (see § 4.3). Lower-galactic-latitude and lower-flux sources were assigned to a lower-priority list, but are useful in order to fill in higher L_X/L_R areas of parameter space. No pre-selection was imposed on WGACAT in the region $75^\circ \geq \delta \geq -90^\circ$, although for ease of identification we avoided the regions within 5° of the Large and Small Magellanic Clouds, as well as M31.

Note that although we have not imposed any cut in X-ray flux, our sample will have both radio and X-ray flux limits, the latter depending on the region of the sky surveyed due to the serendipitous nature of WGACAT (similarly to the EMSS). Depending on the length of each individual exposure and the distance from the center of the PSPC field, the X-ray flux limits appropriate for each source will vary between $\sim 10^{-14}$ and $\sim 10^{-12} \text{ erg cm}^{-2} \text{ s}^{-1}$. The slightly different radio flux limits north and south of the equator are simply explained: For $\delta > 0^\circ$ (and $\leq 75^\circ$, the limit of the GB6 catalog), it is easy to see that all sources with $F(20 \text{ cm}) > 100 \text{ mJy}$ (the limit of the NORTH20CM catalog) and $\alpha_r \leq 0.7$ will be above the much lower flux limit of the GB6 catalog ($\sim 25 \text{ mJy}$; note that the converse does not hold). For $\delta < 0^\circ$, on the other hand, our radio flux limit is the completeness limit of the PMN survey, which (while declination dependent; see Griffith & Wright 1993) averages about 50 mJy.

2.3. The Cross-correlations

The actual cross-correlations were done as follows: north of $\delta > 0^\circ$ WGACAT was correlated with the GB6 catalog with a correlation radius of one arc minute. The resulting sample, which included 1,119 sources, was then correlated with the NORTH20CM, this time with a correlation radius of 3 arc minutes, as the positional uncertainties of the NORTH20CM catalog are considerably worse than those of the GB6 catalog (160 arcsec at the 90% level compared to 10-15 arcsec at the 1σ level). This produced a list of 570 sources, 262 of which are unclassified (see below for details on the classification of WGACAT sources). The 6-20 cm spectral index was then calculated and 89 sources turned out to have $\alpha_r \leq 0.7$ and $|b| > 10^\circ$. The total number of candidates in the south is still growing. The correlation of WGACAT with the PMN catalog, with a correlation radius of one

arcmin, produced a list of 541 objects, 310 of which are unclassified. Of these, 223 are at $|b| > 10^\circ$ and $\delta < 0^\circ$ (the PMN sample reaches $\delta \sim 10^\circ$). So far, 103 have turned out to have $\alpha_r \leq 0.7$, but this number is bound to increase with the analysis of our October 1997 ATCA observations and the completion of the NVSS (almost complete as of October 1997).

To evaluate our completeness it is important to derive WGACAT positional error circles. This was done as follows. WGACAT was cross-correlated with the Hipparcos Input Catalog (see e.g., Torra & Turon 1985) and the offsets between the two databases were obtained for 6 bins of the distance from the WGACAT field center (0 - 10 arcmin, 10 - 20 arcmin etc.). One σ positional errors were then estimated by sorting the offsets in ascending order and taking the value which included 68% of the objects in the bin. These values, reported in Table 3, range from 13 arcsec for the inner 10 arcmin of the PSPC field to 53 arcsec for the 50 – 60 arcmin ring.

Since the positional accuracy of radio catalogs decreases with flux, we investigated the possibility that a one arcminute cross-correlation radius might not be large enough at lower radio fluxes and/or large PSPC center offsets. We therefore cross-correlated WGACAT with the GB6 and PMN radio catalogs with a 1.5 arcmin radius. Total positional errors were derived by summing in quadrature the X-ray and radio uncertainties, the latter obtained from the GB6 catalog and from the PMN radio fluxes via the formulae given in the PMN papers. The significance of the match was quantified by the ratio between X-ray/radio offset and combined positional error. (Note that 1.5 arcmin is roughly equal to twice the combined X-ray and radio uncertainty of a source with PSPC offset ~ 30 arcmin and radio flux ~ 50 mJy.)

The results are as follows: for the WGACAT/PMN correlation, the number of X-ray/radio matches using a correlation radius of 1.5 arcmin increases by 40%. Dividing the WGACAT sample in an inner (PSPC offset ≤ 30 arcmin) and outer (PSPC offset > 30 arcmin) region, there is a 38% increase in the inner region and a 45% increase in the outer region. In the inner region most of the increase is due to “spurious” associations, which we define for the purpose of this experiment as those matches with ratio between offset and positional error > 2 . Of the 144 new sources, 104 are spurious, with a net increase of “good” sources $\sim 12\%$. In the outer region, of the 81 new sources, only 13 are spurious, so the number of good sources increases by $\sim 38\%$. This simply reflects the fact that WGACAT sources with larger offsets have larger positional uncertainties and “real” matches can have X-ray/radio offsets larger than one arcmin. For the WGACAT/GB6 correlation, the results were slightly different: the increase is only 25%, practically independent of WGACAT offset. The net increase of “good” matches is only $\sim 4\%$ in the inner region and $\sim 21\%$ in the outer one. That is, as the GB6 positions are better than the PMN ones, increasing the

correlation radius has a bigger effect on the WGACAT/PMN “real” matches than it has on the WGACAT/GB6 matches.

As a result of this experiment, we then added to the WGACAT/PMN candidate list the 29 unclassified sources obtained from the 1.5 arcmin correlation and having PSPC offsets ≤ 30 arcmin, ratio between X-ray/radio offset and positional error ≤ 2 , $|b| > 10^\circ$ and $\delta < 0^\circ$. (Note that these WGACAT/PMN additional candidates all have relatively small radio fluxes within a factor 2 of the PMN completeness limit.) By comparison, only 5 of the additional GB6 sources with PSPC offset ≤ 30 arcmin derived from the correlation with the larger radius had entries in the NORTH20CM catalog but all of them had $\alpha_r > 0.7$. This is easily explained: all these sources had relatively large positional errors and therefore relatively small radio fluxes ($F(6\text{ cm}) \sim 20 - 30$ mJy). Therefore, only steep-spectrum radio sources could have a 20 cm flux > 100 mJy, the limit of the NORTH20CM catalog.

In summary, based on the positional accuracy of both WGACAT and the radio catalogs used to construct our candidate list, we expect our final sample to be complete in terms of radio/X-ray correlations to the radio flux limit for center offsets $\lesssim 30$ arcmin. At present, these make up about 60% of our sources. At larger offsets, our completeness limit will be at somewhat higher radio fluxes.

We have already mentioned the possibility that some of the X-ray/radio associations are simply chance coincidences. From the number counts of flat-spectrum radio sources (Condon 1984), we estimate that only about 20 ± 4 objects in our sample are spurious X-ray/radio sources. Most of these will be singled out because of their large value of the ratio between X-ray/radio offset and positional error.

3. Source Classification

The definition of the blazar class has varied since the 1978 Pittsburgh conference, where the terminology was first suggested. The original definition of the class (cf. Angel & Stockman 1980) emphasized the dominance of a highly polarized, variable, nonthermal continuum over other properties. But in the last twenty years, the definition of the class as a whole, as well as various subclasses, has varied, partly as a result of observational selection. A variety of names (e.g., HPQ or highly polarized quasar; OVV or optically violent variable) have been applied to some objects, usually based upon finding extreme values of one or more of the signal properties of the blazar class (§ 1). A more commonly used set of subclasses are based upon the character of the optical spectrum: FSRQ (flat-spectrum radio quasar, for objects with emission-line dominated spectra) and BL Lac (nearly lineless objects).

Other authors have restricted the term “blazar” to those with emission-line spectra.

Further sub-divisions have been invented to describe objects found as a result of X-ray or radio surveys, or with certain broadband spectral shapes (e.g., X-ray selected BL Lacs or XBL, radio selected BL Lacs or RBL, low-energy peaked BL Lacs or LBL, high-energy peaked BL Lacs or HBL; see Padovani & Giommi 1995a and Urry & Padovani 1995). While the latter two are at least based upon a strictly defined spectral shape (see §6.2), all point out the difficulties inherent in defining the properties of a class based upon single-band surveys which cover fairly small ranges of flux in their survey band. Since the blazar population spans over seven decades of luminosity in the radio, optical and X-ray band, and over four decades in its ratio of X-ray to radio luminosity, single-band surveys are unable to representatively sample the blazar population, particularly when the dynamic range of fluxes being surveyed (i.e. F_{max}/F_{lim}) is less than 100.

The result is a confusing array of nicknames which are utilized with abandon in today’s literature. The physical meaning of many of these divisions is not at all clear. For example, much has been written about the temporary appearance of broad H α with $W_\lambda \approx 6 \text{ \AA}$, in the spectrum of BL Lac (Vermeulen et al. 1995). Similar occurrences have been noted in other objects, including 0846+513 (Arp et al. 1979), 0537–441 (Peterson et al. 1976), and 0215+015 (Boisse & Bergeron 1988). Indeed, the recent results of Sambruna et al. (1996) and Scarpa & Falomo (1997) suggest that the separation between BL Lac and FSRQ may be rather ill defined and perhaps of questionable physical meaning. And while it is true that the properties of BL Lacs found in radio surveys (which mostly have values of $\alpha_{rx} \gtrsim 0.8$) are considerably different from those found in X-ray surveys (which mostly have lower values of α_{rx}), the explanation for this difference is controversial, and has been the subject of some debate in the literature (e.g., Padovani & Giommi 1995a; Fossati et al. 1997; Georganopoulos & Marscher 1997).

A variety of deeper, multiwavelength surveys for blazars (of which DXRBS is one) are currently underway. The X-ray based surveys, DXRBS (this paper), REX (Wolter et al. 1997; Maccacaro et al., in preparation), HQS/RASS (Nass et al. 1996), RC (Kock et al. 1996), RGB (Laurent-Muehleisen et al. 1997), and RASS/NVSS (Giommi, Menna & Padovani, in preparation) take as their starting point either the pointed ROSAT database (REX, DXRBS) or the all-sky survey (HQS/RASS, RGB, RC, RASS/NVSS), and make up their candidate list via cross-correlations with radio survey lists or other properties. The radio-based surveys emerging from the FIRST project take the radio-selected FIRST sample as their starting point, and use variability, polarization and optical colors to select candidates (Gregg et al. 1996; Laurent-Muehleisen et al. in prep). These projects are complementary, using different techniques to sample different regions of parameter space.

These surveys will both sample the parameter space available to blazars more deeply and fill the holes left by previous, disjoint selection techniques. As they do so, we will gain the first complete picture of the range of properties encompassed by the blazar class. Given the confusing array of names currently in use (which may or may not be physically meaningful), these surveys (once completed) will need to resystematize the blazar definition, as well as those of its subclasses. However, neither this survey nor any of the other new X-ray or radio-based surveys can yet undertake the task of resystematizing the classification of flat-spectrum radio sources, as the identification of their samples are all incomplete. To do so at this time would risk not only confusion, but the real possibility of missing a population still extant within the unidentified objects.

For the present paper, we will adopt a form of the FSRQ-BL Lac dichotomy, basing our classifications solely upon the optical spectrum. We will apply the term “blazars” to both BL Lacs and FSRQs, since recent evidence (Fugmann 1988; Impey, Lawrence & Tapia 1991; Kühr & Schmidt 1990; Jannuzi et al. 1993, 1994) has shown that the properties outlined in § 1 are shared by both FSRQs and BL Lacs. We adopt the modified form of the BL Lac definition advocated by Marchã et al. (1996; see their Fig. 6) to classify BL Lacs and radio galaxies.

Their starting point is that the line luminosity seems to be independent of the observed continuum in blazars (see Koratkar et al. 1998 for an example of this behavior in 3C 279). It then follows that the Ca H & K break contrast, a measure of the presence of non-thermal continuum in a galaxy [defined by $C = (f_+ - f_-)/f_+$, where f_+ and f_- are, respectively, the flux redward and blueward of the Ca break], and equivalent width W_λ will be correlated (the lower C , i.e., the higher the non-thermal contribution, the lower W_λ). Thus, changing the viewing angle and/or the luminosity of the BL Lac relative to that of the host galaxy will move an object on a diagonal trajectory in the contrast – equivalent width plane. Marchã et al. (1996) showed convincingly that objects in a triangular area limited by contrast $C = 0.4$ (breaks with $C \sim 0.5$ are typical of elliptical galaxies; Dressler & Schectman 1987) and the diagonal line shown in Figure 1 (which assumed the line and galaxian continuum emission of 3C 371 as its starting points and a smoothly decreasing AGN contribution) should still be called BL Lacs. Note that this expands upon the “classical” definition used by previous authors (Stickel et al. 1991; Stocke et al. 1991; Perlman et al. 1996a) of equivalent width $W_\lambda < 5(1+z) \text{ \AA}$ for all emission lines and Ca H & K break strength $C < 0.25$. The fuzziness of the previously used criterion is further illustrated by the occasional observation of broad H α lines in the spectra of several famous BL Lacs (among them Mkn 501 and BL Lac; see, for example Vermeulen et al. 1995). Objects which fall outside the traditional definition of the BL Lac class, but within the Marchã et al. definition which we adopt, will be discussed individually in § 4, and we will return to the subject in § 7 when selection

effects are discussed.

Thus, objects which meet the Marchã et al. criteria are classified herein as BL Lac objects. Objects with higher-equivalent-width emission lines which are still narrow (FWHM $\lesssim 1000 - 2000$ km/s), or stronger Ca H & K breaks, are classified as radio galaxies, and are discussed individually in § 4, and as a group in § 7. All flat radio spectrum objects with higher equivalent widths and broad emission lines (FWHM $\gtrsim 1000 - 2000$ km/s) are classified as FSRQs. It is important to note that this classification is being applied without regard to any other characteristic, such as redshift, presence or lack thereof of a stellar continuum, or physical extent. As a result, a number of objects which have been called broad-line radio galaxies by other authors are included as FSRQs within the previously-identified portion of our sample. We return to this last topic in § 7.

Due to the many commonalities shared by all blazars, we believe that a unified approach to these enigmatic objects is more helpful in helping us understand them, similar to that taken for radio galaxies by Baum, Zirbel & O’Dea (1995) and Zirbel & Baum (1995). Therefore, while we will use the classical definition to classify sources here (in order to ensure easy compatibility with past studies), it is our goal in future works to consider the equivalent width and luminosity of emission lines simply as additional variables in the analysis.

4. Sample Identification

In order to identify a candidate object as either a BL Lac, FSRQ or radio galaxy, an optical spectrum is required. To pinpoint the optical counterpart we used, where available, positions from either the NVSS or our ATCA survey (both of which have errors $\lesssim 3''$ relative to the Digitized Sky Survey; note that the figure we use is significantly larger than typically quoted for NVSS and ATCA detections with $F > 50$ mJy due to the non-planarity in the sky survey plates and the slight inconsistencies between the coordinate systems of each; see, e.g., Irwin, Maddox & McMahon 1994; Drinkwater et al. 1995) to obtain finders from the Digitized Sky Survey (using Skyview, McGlynn & Scollick 1996). For some sources which did not have NVSS positions before the time of optical observations, arcsecond positions from the Texas survey (Douglas et al. 1996) and NED (typically based on VLA data) were used. Magnitudes for all X-ray/radio sources with counterparts on the POSS and UKST plates which comprise the Digitized Sky Survey were obtained from the Cambridge APM and Edinburgh COSMOS projects (Irwin et al. 1994; Drinkwater et al. 1995), except where a blend of two or more sources were observed, in which case a magnitude was estimated by eye. All X-ray/radio sources without counterparts on the

survey plates were imaged at either the KPNO 0.9m or the CTIO 0.9m telescopes. This allowed identification of all optical counterparts to $R = 23$.

Spectroscopic observations were conducted at the KPNO 2.1 m, MMT, Lick 3 m, ESO 2.2 m and 3.6 m, and CTIO 1.5 m telescopes. One object, WGAJ0449.4–4349, was observed by M. Ruiz at the CTIO 4 m telescope in January 1996; Dr. Ruiz has kindly allowed us to publish these data herein. In Table 1, we list all telescope runs (including, for completeness, the MMT and Lick runs, which were obtained for other projects, but during which a few DXRBS blazars were observed) and relevant details of the observing setup, such as approximate wavelength range and resolution. In Table 2, we list the details of the observations. Due to poor weather during the KPNO run (2 mostly cloudy nights out of 3) the data from this run are of lower quality than the ESO data. With the exception of the CTIO 4m and MMT observations, spectra were generally not taken at parallactic angle (mostly due to the difficulty of changing the position angle of the slit at the KPNO 2.1m, CTIO 1.5m and ESO 2.2m telescopes).

The spectra were reduced using standard IRAF routines. Data were overscan and bias-subtracted, and flatfielded using programs in the IRAF package *noao.imred.ccdred*, and spectra were extracted, wavelength-calibrated and flux-calibrated using programs in the package *noao.twodspec*. Cosmic rays were removed in the 1 and 2-dimensional data by hand.

A dereddening correction was applied to the data using the IRAF routine *noao.onedspec.dered* and assuming Galactic values of extinction derived from 21-cm measurements (Stark et al. 1992; Shafer et al., private communication).

We recorded the central wavelength, equivalent width, full-width at half-maximum, and flux in each spectral line. Those data will be given and analyzed in future papers. Except where noted, where only a single emission line was observed, it was assumed to be Mg II $\lambda 2798$ Å. Seven of 22 newly identified BL Lacs lack recognizable spectral features. These objects are not included in the redshift distributions discussed in § 5, and we have not computed luminosities for them. Higher signal-to-noise spectroscopic observations are required to obtain redshifts for these objects.

4.1. Identifications and Efficiency

In Figure 2, we show the spectra of the optical counterparts to 85 of 97 observed X-ray/radio sources. All spectra have been smoothed with Gaussians of width 3 pixels. Twelve spectra are not shown, either because (1) too few photons were observed to allow a

reliable classification to be made (6 sources), (2) the optical survey plate did not contain enough information to distinguish whether the counterpart was a bright star near the radio position or a fainter extragalactic object at the radio position (5 objects), or (3) because a lower-quality radio position was used (1 object). In this last case (WG AJ1022.1+4126), the object is also very close to a third-magnitude star, SAO 43310, making spectroscopic observations difficult.

Positional information for all 85 sources for which we announce identifications herein are given in Table 3, including information from WGACAT, the PMN and Green Bank surveys, the NVSS and our ATCA survey. A number of sources were serendipitously observed by ROSAT on more than one occasion; for completeness, we give WGACAT positions for all observations of DXRBS sources.

Of the 85 newly identified sources, 59 are FSRQs, and 22 are BL Lacs. Hence, our technique is $\sim 95\%$ efficient at selecting blazars, where we define the efficiency as the fraction of objects which turn out to be blazars in a given survey *after* selection criteria have been applied. Three of 85 objects are radio galaxies, with CaII breaks stronger than typical BL Lacs (but see § 7.1); while one quasar, which was observed before we had information on its spectral index, turned out to have $\alpha_r > 0.7$. Classifications, redshifts and observational details for these sources are given in Table 4. The 0.1-2.0 keV X-ray fluxes given in Table 4 are not corrected for Galactic absorption; however, the 1 keV X-ray fluxes given therein are unabsorbed. Note that both the 0.1-2.0 keV and 1 keV X-ray fluxes have been derived from ROSAT count rates using the observed hardness ratio and assuming Galactic N_H . These numbers may change somewhat when a more thorough analysis of the X-ray spectrum is done (this is in progress). For objects observed more than once by ROSAT, we give in Table 4 the count rates and X-ray fluxes found for each observation. For objects which we classify as either radio galaxies or BL Lacs, we give the equivalent width of the strongest emission line and Ca break strength in Table 5; these values have been also been displayed in Figure 1.

Previous X-ray and radio surveys can claim efficiencies which are nearly comparable to ours. For example, the efficiency of the Slew Survey at identifying HBLs within the well-known $(\alpha_{\text{ox}}, \alpha_{\text{ro}})$ box (Perlman et al. 1996a) is 80–90%, and the fraction of BL Lacs and FSRQs within the flat-spectrum subset of the 1 Jy survey is nearly 90% (260/298) for a dividing line at $\alpha_r = 0.5$, but goes below 80% (284/364) for a dividing line at $\alpha_r = 0.7$ (Stickel et al. 1994; see also § 7). However, each of these survey techniques were insensitive to large portions of the blazar population (§ 3). The combination of high sensitivity in both the X-ray and radio bands plus a two-band survey method gives DXRBS significant advantages over these previous survey methods.

4.2. Comments on Individual Sources

WGAJ0043.3–2638. Since being selected for the DXRBS sample, this source was observed by both Cristiani et al. (1995) and Wolter et al. (1998), both of whom identify it as a broad-emission line AGN at $z = 1.002$. Both this redshift and the redshift we list in Table 3 ($z = 0.451$) have problems reproducing some of the features found in both spectra. For example, if the object is at $z = 1.002$, it is difficult to explain the likely emission line at 4050 \AA , which we have classified as Mg II at $z = 0.451$. Further observations are needed to determine the correct redshift of this object. The rest-frame equivalent width of the 4050 \AA emission line is 9.6 \AA (if $z = 0.451$) or 7.0 \AA (if $z = 1.002$), only slightly above the dividing line between BL Lac and FSRQ. Therefore, even though the line is clearly broad (FWHM=3800 km/s), this object is similar to objects such as Mkn 501 and BL Lac which share this property and must be classified as a BL Lac.

WGAJ0100.1–3337. The single emission line, which we classify as Mg II at $z = 0.875$, is clearly broad (FWHM=2900 km/s) but its equivalent width is close to the BL Lac/FSRQ dividing line ($W_\lambda = 9.8 \text{ \AA}$ rest-frame). We classify this object as a BL Lac, similarly to WGAJ0043.3–2638 (see above discussion).

WGAJ0204.8+1514. This source, also known as 4C +15.05, has a radio flux > 3 Jy, and was also previously observed by Stickel et al. (1996), who classified the source as an AGN at $z = 0.833$ based upon the identification of two lines as OII $\lambda 3727$ and Ne I $\lambda 3833$. These lines are also present in our spectrum, as are four other lines (Figure 2). However, the redshift claimed by Stickel et al. (1996) is likely incorrect, as all six lines cannot be accounted for if the redshift is $z = 0.833$. We believe that a better fit is obtained with a redshift $z = 0.405$. This object is also the likely counterpart of the EGRET source 2EG0204+1514 (Thompson et al. 1995; Mattox et al. 1997).

WGAJ0210.0–1004. This object, at $z = 1.976$, is $\sim 2'$ from MS0207.4–1016, identified by Stocke et al. (1991) as a radio-quiet QSO ($F(6 \text{ cm}) < 0.3 \text{ mJy}$ at 3σ) at $z = 1.970$. A 6cm VLA survey done during the EMSS project showed that there are two fairly strong radio sources which likely would be in the PMN beam (Stocke, private communication). The stronger source, with a flux of 133 mJy, is at the position of WGAJ0210.0–1004; however, there is another 70 mJy source at a position which is not consistent with either WGAJ0210.0–1004 or MS0207.4–1016. Even with this reduced 6 cm flux, WGAJ0210.0–1004 is still a flat spectrum source ($\alpha_r = 0.58$). There is no question about the correctness of either X-ray source identification, since WGACAT lists a 0.01 ct/s X-ray source at a position consistent with MS0207.4–1016 (in addition to WGAJ0210.0–1004). It is possible, however, that X-ray emission from both sources may have contributed to the EMSS X-ray flux. What is particularly interesting is that these

two objects are at essentially the same redshift, and are therefore likely associated with one another in a group or cluster of galaxies, since the projected separation between them is 1.6 Mpc.

WGAJ0245.2+1047. This object is difficult to classify because of the large equivalent width of its H α emission line (19.1 Å rest-frame). However, when combined with its low Ca H & K break strength ($C = 0.26$) it rests securely in the BL Lac area of the (W_λ, C) plane as defined by Marchã et al. (1996). We therefore classify this object as a BL Lac.

WGAJ0313.9+4115. The H α emission line in this object’s spectrum is not very broad, exhibiting FWHM = 1780 km/s. The rest-frame equivalent width of this line is close to the BL Lac/FSRQ dividing line (13.0 Å rest-frame). The Ca II break strength is 0.38, close to the BL Lac/radio galaxy border we are using. We have classified this object as a BL Lac object, but we note that the 1σ errors on our measurement of C are not small enough to exclude the alternate classification as a radio galaxy (Figure 1). A higher signal-to-noise spectrum of this object is clearly necessary to confirm its nature.

WGAJ0340.8–1814. The H α emission line in the spectrum of this object has a rest-frame equivalent width of 16.0 Å, and its Ca II break strength is $C = 0.40$. Thus it is right on the borderline of the BL Lac region of the (W_λ, C) plane. We have classified this object as a radio galaxy; however, a higher signal-to-noise spectrum is clearly necessary to confirm its nature.

WGAJ0421.5+1433. Our spectra show no clear lines; however, due to its low signal-to-noise (~ 7), the 2σ upper limits that can be placed on its break strength ($C < 0.30$) and equivalent width of emission lines ($W_\lambda < 8.2$ Å) are not very stringent. They are adequate, however, to allow us to classify this object as a BL Lac. Better observations of this source are clearly necessary.

WGAJ0428.8-3805. This object has no detectable emission lines in its spectrum (2σ upper limit = 0.7 Å), and a weak Ca break ($C = 0.32$). We classify it as a BL Lac object using the Marchã et al. (1996) criteria.

WGAJ0449.4–4349. This bright BL Lac object was observed as a target by ROSAT; however, until now it was unidentified. Due to its nonserendipitous observation by ROSAT, we will not include it in computations of the luminosity function. We include it here as it was identified during our observing campaign and there will probably be no other opportunity to discuss it.

WGAJ0500.0–3040. We have termed this object a radio galaxy despite the fact that all of its emission lines have equivalent widths greater than 5 Å (some are as large as

70 Å), since all are relatively narrow (FWHM $\sim 1000 - 2000$ km/s). However, there is no detectable 4000 Å break in its spectrum, which points to an unusually strong non-thermal contribution.

WGAJ0513.8+0156. The Ca II break strength ($C = 0.34$) and lack of emission lines (2σ upper limit on $W_\lambda = 1.3$ Å) allow us to classify this object as a BL Lac object. However, the low signal-to-noise of its spectrum blueward of the Ca II break results in a relatively large 1σ error on its break strength, large enough so that we cannot exclude the alternate classification as a radio galaxy (Figure 1). A higher signal-to-noise spectrum of this source is required to confirm its nature.

WGAJ0558.1+5328. The H α emission line in this object’s spectrum is not very broad, exhibiting FWHM = 2100 km/s. The equivalent width of this line is close to the BL Lac/FSRQ dividing line (9.8 Å). The Ca II break strength is 0.29. We classify this object as a BL Lac. However, the low signal-to-noise of its spectrum, particularly blueward of the Ca II break (~ 5 compared to $\sim 12 - 15$ redward of the break) do not quite allow us to exclude the alternate (radio galaxy) classification. A higher signal-to-noise spectrum would clarify this question.

WGAJ0624.7–3230. The emission line and absorption line redshifts of this object are somewhat different ($z_{abs} = 0.252$ and $z_{em} = 0.275$). Therefore it is likely that the galactic emission in the spectrum is due to a foreground galaxy superposed upon the radio source. The sole emission line has a rest-frame equivalent width of 8.5 Å; slightly over the BL Lac/FSRQ dividing line, but the line is narrow (FWHM = 900 km/s). We are classifying this object as a BL Lac because of its small equivalent-width emission line and low Ca H & K break contrast ($C = 0.22$).

WGAJ0656.3–2403. There is a possible emission feature in the spectrum of this object at 3845 Å. It is unclear whether this is a real emission line, noise, or a cosmic ray due to the noisiness of the spectrum in this range. The lack of other emission lines in the spectrum and high noise level in the blue make it somewhat doubtful that this feature is truly an emission line. However, if it is due to Mg II emission, the redshift of this object would be $z = 0.371$, and it would be narrow (FWHM = 500 km/s). We classify this object as a BL Lac due to the likely lineless nature of its spectrum, though we note that if the 3845 Å feature is indeed an emission line it exceeds by more than a factor of four the traditional BL Lac/FSRQ dividing line (rest-frame $W_\lambda = 24.5$ Å).

WGAJ0724.3–0715. Despite its faintness, the H α emission line in the spectrum of this object is quite broad (rest-frame $W_\lambda = 30.3$ Å, FWHM = 4000 km/s). We therefore classify it as an FSRQ.

WGAJ0744.8+2920. This object was identified independently by Gregg et al. (1996) as part of the FIRST bright QSO sample, and by Wolter et al. (1998). We confirm both identifications and redshifts; however, a comparison of our spectrum with that given by Wolter et al. reveals a large deficit in the blue in our spectrum. This is most likely due to a combination of instrumental and weather related factors.

WGAJ0816.0–0736. We tentatively classify this object as a BL Lac due to its lack of emission lines and low break strength ($C = 0.37$). However, due to the low signal-to-noise of its spectrum blueward of the Ca II break (~ 4 compared to ~ 20 at $> 5000 \text{ \AA}$), we cannot exclude the alternative (radio galaxy) classification due to the large 1σ error on C (0.18). A higher signal-to-noise spectrum is required to clarify its nature.

WGAJ0900.2–2817. A second spectrum of this object, with much wider wavelength coverage, was obtained in May 1997 at the ESO 2.2m. That spectrum (which will be published in a later paper) confirms the identification of the single line as Mg II $\lambda 2798$.

WGAJ1057.7–7724. The fairly low signal-to-noise spectrum we have ($S/N \sim 7$) places 2σ limits on C and W_λ which are sufficient to classify this object as a BL Lac. A higher signal-to-noise spectrum is required to obtain a redshift.

WGAJ1222.6+2934. The fairly low signal-to-noise spectrum we have ($S/N \sim 6$) places 2σ limits on C and W_λ which are sufficient to classify this object as a BL Lac. A higher signal-to-noise spectrum is required to obtain a redshift.

WGAJ1525.3+4201. This source was listed as a BL Lac candidate by Ruscica et al. (1996). However, our spectrum shows strong, broad lines, and we identify this object as a quasar at $z = 1.189$.

WGAJ2317.9–4213. This object is most likely a radio galaxy based upon its strong Ca II break ($C = 0.52$). It is probably associated with a group of galaxies at the same redshift found by the Las Campanas Redshift Survey (Schechtman et al. 1996).

WGAJ2322.0+2114. This object was also observed by Wolter et al. (1998). We confirm both their identification and redshift.

4.3. Previously Identified Sources

Previously known serendipitous sources were selected by cross-correlating WGACAT with a variety of optical and radio catalogs, including the Verón-Cetty & Verón (1996) and Hewitt & Burbidge (1993) quasar catalogs, the 1 Jy (Stickel et al. 1994) and S4 (Stickel

& Kühr 1994) radio catalogs, and the BL Lac catalog of Padovani & Giommi (1995b). Also, the classification of non-AGN sources (which is important to select the unclassified objects) was done as described in White et al. (1995). In some cases classifications were also double-checked in the NASA Extragalactic Database (NED) or taken from very recent papers. All objects broad-line radio galaxies (BLRGs) have been included with the FSRQ class (see §3). The adopted cross-correlation radii were the same as those used for the selection of our candidates (§ 2). Selection criteria identical to those described in §2 were applied to the previously known objects. Potential mis-identifications through chance coincidences of previously known AGN which fulfill our selection criteria were addressed by shifting the X-ray positions by one degree at a time several times, and repeating the cross-correlations between WGACAT and the AGN catalogs. The number of spurious X-ray/optical associations was zero, which implies a negligible (2σ upper limit $\sim 4\%$) contamination by spurious sources.

Ninety-seven previously known objects were thus found, of which 11 are BL Lacs and 76 are FSRQs. The remaining ten objects are Narrow Line Radio Galaxies (NLRGs) with $\alpha_r \leq 0.7$. Details of these 97 objects are given in Table 6. The mean X-ray/optical offset for these sources is $\simeq 22$ arcsec, while the median one is $\simeq 17$ arcsec, in agreement with the estimated errors on the positions of the WGA sources (§ 2). Since no preselection was done on WGACAT for these objects (with the exception of excluding regions at $|b| < 10^\circ$ and within 5° of the LMC, SMC and M31), these objects will qualify for our complete sample, and will be discussed along with the newly-identified sources in §§5-7.

4.4. Sample Properties

In this subsection we utilize the data given in Tables 4 and 6 to calculate basic parameters such as X-ray and radio luminosities. The distributions of these parameters will be analyzed in upcoming sections. In Figure 3, we plot the redshift distribution of DXRBS FSRQs opposite that of the 1 Jy and S4 samples. In Figure 4, we plot the redshift distribution of DXRBS BL Lacs opposite the Slew and 1 Jy samples. In Figure 5, we have plotted the X-ray and radio luminosities of all the FSRQs in our sample, as well as those of the 1 Jy and S4 samples. A similar plot is given in Figure 6 for the BL Lacs, with the comparison samples being the 1 Jy, Slew and EMSS samples. The apparent deficit of objects at the very highest luminosities is a result of the smaller area of sky covered by DXRBS compared to, e.g., the Slew and 1 Jy samples. The 1 keV X-ray luminosities plotted in Figs. 5 and 6 have been K -corrected and de-absorbed using the X-ray spectral indices derived from the WGACAT hardness ratios as detailed in Padovani & Giommi

(1996). Where an object was observed more than once by ROSAT, the X-ray luminosity plotted represents the average luminosity.

When complete, the DXRBS blazar sample will include more than 300 blazars, considerably larger than any previous complete sample of blazars. Combining the objects for which we have announced identifications in this paper with previously identified objects, the sample is now over 50% identified. All further analysis in this paper will be done using all identified objects with redshifts (including both newly and previously identified objects).

5. Redshift Distribution

The distribution of redshifts among the DXRBS FSRQs identified so far (Figure 3) is quite similar to that of the 1 Jy and S4 samples. Not much more can be said at present. A more thorough comparison will have to await completion of our survey and the convolution of the redshift distribution with the WGACAT sky coverage. As has already been mentioned by Hook et al. (1996), selecting flat-spectrum sources is an efficient way of finding high-redshift, radio-loud quasars. We would therefore expect that the majority of the FSRQs would be at high redshifts ($z > 1$), a suspicion which the data confirm. The mean redshift of our FSRQ sample is $z \sim 1.2$, and the high-redshift tail extends to $z \sim 4$. Our redshift distribution cannot, however, be directly compared to that of Hook et al. (1996) because those authors required that the sources be particularly “red,” a criterion we do not impose.

While a significant fraction (7 of 33) of the BL Lacs so far included in our sample still lack redshifts, it is apparent that the redshift distribution for the DXRBS BL Lacs (Figure 4) is dominated by objects at $z < 0.4$, and therefore more similar to that of the Slew Survey (Perlman et al. 1996a; or the EMSS survey: Stocke et al. 1991) than the 1 Jy sample (Stickel et al. 1991), which is less peaked at low redshifts and has a much more prominent high- z tail than either the DXRBS or Slew Survey samples. As above, a direct comparison between these distributions is not possible at present, given also the different survey methods and selection criteria. We only mention here that the difference between the DXRBS and 1 Jy redshift distributions appears to be striking considering that the radio flux limit of DXRBS is a factor 20 lower so that if anything, one would expect a *higher* fraction of high- z sources, rather than the dearth of high- z sources that we observe. The flatter distribution of the 1 Jy sample might be related to the fact that it misses some low redshift objects hidden within bright hosts (which might be misidentified as radio galaxies; see §7) and might also be contaminated by misidentified quasars at high redshifts (e.g., 1 Jy 1308+326), as suggested by Marchã & Browne (1995) and Perlman et al. (1996b). Some

1 Jy BL Lacs might be gravitationally lensed if superposed by chance onto a lower-redshift galaxy (as originally suggested by Ostriker & Vietri 1985). This last possibility now appears quite likely from the results of Stocke & Rector (1997), which show that the 1 Jy BL Lacs have a $2.5 - 3\sigma$ excess of Mg II absorbers along their sight lines.

6. A More Complete Picture of the Blazar Class

DXRBS' unique combination of a dual X-ray/radio survey method and high sensitivity has opened up important, large new regions of parameter space for both blazar sub-classes, within which a large fraction of our sample (nearly 50%) lie. This section is devoted to discussing these discoveries and their impact upon our understanding of the blazar class.

6.1. FSRQs

An examination of Figure 5 shows that the FSRQs in the DXRBS sample cover a much wider range of parameter space than those in the two previously existing complete samples of FSRQs, the 1 Jy and S4 samples (radio data for these samples were taken from Stickel et al. 1994 and Stickel & Kühn 1994, while X-ray data for these objects were taken from the multifrequency AGN database of Padovani et al. (1997b; and references therein); it should be noted that the deeper S5 sample is $\sim 25\%$ unidentified and half of the objects lack redshifts, as noted in Stickel & Kühn 1996). We have quantified these differences by 1-dimensional and 2-dimensional Kolmogorov-Smirnov (K-S) tests. The 2-dimensional K-S test reveals that the differences in the (L_X, L_R) plane coverage between the DXRBS and 1 Jy and S4 samples are significant: the probability that the 1 Jy and DXRBS samples could emerge from the same parent population is 0.2%, where as the probability that the S4 and DXRBS samples could emerge from the same parent population is 2.2%. Given the fainter flux limits of DXRBS, this is expected.

One-dimensional K-S tests reveal that largest difference is in the radio luminosity. The probability that the 1 Jy and DXRBS radio luminosity distributions could emerge from the same parent population is $< 0.1\%$, and the probability that the S4 and DXRBS radio luminosity distributions could emerge from the same parent population is 0.7%. The mean of the DXRBS L_R distribution is different from that of both the S4 and 1 Jy at greater than 99.9% significance. The situation is somewhat different for the X-ray luminosity distribution. The probability that the 1 keV luminosity distribution of the 1 Jy and DXRBS sample could emerge from the same parent population is 15%, i.e. our results are

inconsistent with them emerging from a different parent population. The result is similar for the S4 (23% probability). Also, the mean of the DXRBS sample’s X-ray luminosity differs from that of both the 1 Jy and S4 samples’ only at the 93 and 92% level respectively. Note, however, that X-ray data are available only for $\sim 53\%$ and 66% of the S4 and 1 Jy FSRQs respectively, so their X-ray luminosity distributions are likely to be skewed towards the most luminous X-ray sources.

Inspection of Figure 5 reveals that the differences lie in two areas: at low luminosities (particularly low radio luminosities) and high ratios of L_X/L_R . The former regime could not be surveyed well by previous surveys due to their considerably higher flux limits. It is therefore not surprising that, as shown in Figure 5, the 1 Jy and S4 samples together have only twelve objects at radio luminosities $L_R < 10^{33.5} \text{ erg s}^{-1}$ ($\sim 3\%$), and none at $L_R < 10^{32.5} \text{ erg s}^{-1}$. The fraction of low-luminosity objects is much higher in the DXRBS sample (Fig. 5), which, while still incomplete, already contains over twice as many objects (28; or $\sim 20\%$) with $L_R < 10^{33.5} \text{ erg s}^{-1}$, six of which are at $L_R < 10^{32.5} \text{ erg s}^{-1}$. The DXRBS sample is therefore the very first sample of blazars to contain statistically significant numbers of blazars at low luminosities, approaching what should be the lower end of the FSRQ luminosity function according to unified schemes, i.e. $\sim 10^{31.5} \text{ erg s}^{-1} \text{ Hz}^{-1}$ (Urry & Padovani 1995).

The discovery of a large population of FSRQs with ratios of X-ray to radio luminosity $L_X/L_R > 10^{-6}$ ($\alpha_{\text{rx}} < 0.78$), values more similar to HBLs, is more startling, as few such objects were known in previous complete samples (there are nine such objects in the 1 Jy and S4 combined; see Fig. 5). The finding of a large population of “HBL-type” FSRQs contradicts the prediction of Sambruna et al. (1996) that, based upon the similarities in the optical-X-ray broadband spectral characteristics of LBLs and FSRQs, there should be no HBL-type FSRQs. Padovani, Giommi & Fiore (1997b) were the first to notice that about 17% of all radio quasars with radio/optical/X-ray data (previous to DXRBS) fell in the region of the $(\alpha_{\text{ox}}, \alpha_{\text{ro}})$ plane typical of HBLs (or X-ray selected BL Lacs) and called them “HBL-like” quasars.

We term these objects “HFSRQs”, or high-energy peaked FSRQs; this terminology stresses their apparent similarity to the HBLs. These objects comprise $\sim 25\%$ (32/135) of the DXRBS sample of FSRQs so far. However they probably comprise a somewhat larger proportion of the DXRBS FSRQ population as a whole, as $\sim 40\%$ (25/59) of the newly-identified FSRQs are HFSRQs. Padovani et al. (1997b) have proposed that the X-ray band in these objects, unlike in lower L_X/L_R FSRQs, in which inverse Compton emission prevails (Padovani, Giommi & Fiore 1997a), is dominated by synchrotron emission (see also Sambruna 1997), as the X-ray spectra of the previously-observed HFSRQs in their

database were as steep as those of HBLs (Perlman et al. 1996b; Sambruna et al. 1996; Padovani & Giommi 1996). As the DXRBS sample contains a larger, more representative sample of HFSRQs than could be gleaned from previously identified samples, we will revisit this assertion and address the properties of the HFSRQ subclass in depth in a future paper (Perlman & Padovani, in prep). However, the data herein allow us the first measure of the prevalence of such objects and their proportion among FSRQs in a well defined sample, as well as the first opportunity to speculate upon their relationship to the FSRQ subclass as a whole.

In order to examine the differences between the HFSRQs and lower L_X/L_R objects, we have performed 1-dimensional K-S tests on the radio and X-ray luminosity distributions on the subsamples of DXRBS FSRQs with L_X/L_R greater and less than 10^{-6} . These tests reveal that the probability that the X-ray luminosity distribution of the two subsamples could emerge from the same parent population is 41% (i.e. consistent with having been drawn from the same parent population), while the probability that the radio luminosity distribution of the two subsamples could emerge from the same parent population is $\sim 0.01\%$. The same story is told by the mean X-ray and radio luminosities: The mean radio luminosities differ by 0.75 in the log and the significance of the difference is $> 99.99\%$, where as the difference in the X-ray luminosities is only 0.18, and is not statistically significant ($P = 77\%$). This trend can also be seen on Figure 5. There is only one HFSRQ at luminosities $L_R > 10^{35} \text{ erg s}^{-1} \text{ Hz}^{-1}$, compared to over two dozen lower- L_X/L_R objects. And a careful examination of the figure reveals that the lower- L_X/L_R objects are much more strongly clustered at high radio luminosities than are the HFSRQs. The fraction of HFSRQs also increases as radio luminosity decreases. These trends are similar to (but not as marked) as what is seen for BL Lacs (Urry & Padovani 1995; see also below).

6.2. BL Lacs

The BL Lac objects found within DXRBS fall mostly in the range $10^{-7.5} \lesssim L_X/L_R \lesssim 10^{-5.5}$. Only a few objects are found at higher values of L_X/L_R , as expected given our radio flux limits (§ 2.1). A large fraction of the BL Lacs so far in our sample are at $L_X/L_R < 10^{-6.5}$, the region of Figure 6 populated by LBLs. In this region of parameter space (to the left of the left-most dashed line in Figure 6), DXRBS includes objects up to two orders of magnitude fainter than the 1 Jy survey. Most of these objects are radio galaxies (which are discussed in more detail in §7), but three are clearly BL Lacs. As with the FSRQs, this is expected given our much fainter flux limits. This comment can also be made for objects in the range $10^{-6.5} \lesssim L_X/L_R \lesssim 10^{-5.5}$, between the two dashed

lines in Figure 6 – of which all but one object is classified herein as a BL Lac.

About 50% of the BL Lacs so far in our sample fall in the range $10^{-6.5} \lesssim L_X/L_R \lesssim 10^{-5.5}$ ($0.72 \lesssim \alpha_{\text{rx}} \lesssim 0.85$), and are “intermediate” BL Lacs, objects with spectral shapes intermediate between the X-ray bright and radio-bright varieties of BL Lacs (Padovani & Giommi 1995a). Similar objects have also been found in two ROSAT All-Sky Survey-based samples (Kock et al. 1996, Nass et al. 1996), as well as the *Einstein* Slew Survey sample (Perlman et al. 1996a). For comparison, we have plotted the $(\alpha_{\text{ox}}, \alpha_{\text{ro}})$ values for members of these three ROSAT-based surveys (DXRBS, HQS/RASS and RC) in Figure 7. Since redshift information for the ROSAT-based samples is still incomplete, it is difficult to compare them on the (L_X, L_R) plane. It is important to note that the optical magnitudes used to derive the effective spectral indices at present include the galaxy contribution; this explains the somewhat extreme objects in the lower right corner of the diagram, all BL Lacs and radio galaxies at relatively low redshifts. If only the non-thermal flux were used, these objects would move towards the other objects along lines parallel to the dashed lines in Fig. 7.

As can be seen from Figure 7, each of these surveys covers a slightly different region of the $(\alpha_{\text{ox}}, \alpha_{\text{ro}})$ plane. The HQS/RASS survey of Nass et al. (1996) is dominated by objects at $\alpha_{\text{rx}} < 0.72$ (the left-most diagonal line plotted in Figure 7), i.e. HBLs, but does include a significant fraction of these intermediate objects (8 of 34). Its makeup is thus similar to the Slew Survey sample (Perlman et al. 1996a), which contains 5 transition objects and 5 LBLs ($\alpha_{\text{rx}} > 0.85$, the right-most line plotted in Figure 7) among a sample of 66 (Figure 6; note that the diagonal lines thereon plotted represent the same values of α_{rx}). By comparison, objects from the RC survey of Kock et al. (1996) are more heavily concentrated (6 of 13) at intermediate values of α_{rx} , although another 6 are HBLs. The fraction of intermediate BL Lacs among the DXRBS sample (15 of 32) is comparable to that in the RC sample. However, as shown in Figure 7, the DXRBS intermediate BL Lacs are concentrated at lower values of α_{ro} than those in either the HQS/RASS or RC samples. The large majority of the remainder (12 of 32) of the DXRBS BL Lacs are LBLs, and only a few objects (5 of 32) are HBLs.

These differences are no doubt due to the differing flux limits of the surveys. The similarities of the HQS/RASS and Slew Survey samples are no surprise given their low radio flux limits (a few mJy) and coverage of mostly X-ray bright objects. By comparison, the RC sample covers a range of X-ray fluxes similar to the HQS/RASS sample, but does not go as deep as DXRBS (by a factor ~ 10), while its radio flux limit, at ~ 40 mJy, is similar to ours. Finally, both the HQS/RASS and RC survey groups observed only objects with optical counterparts on sky survey plates, a restriction not found in DXRBS. An

examination of Figure 7 reveals that these facts naturally translate to the $(\alpha_{\text{ox}}, \alpha_{\text{ro}})$ plane.

What is most important in Figures 6 and 7 is that once again the advantages of newer, deeper surveys which cover large dynamic ranges of fluxes in more than one survey band is shown. Only these very recent surveys (and particularly DXRBS, which already contains more intermediate BL Lacs than the HQS/RASS and RC samples combined) have revealed a large population of BL Lacs with $0.72 < \alpha_{\text{rx}} < 0.85$; they went largely undetected in the 1 Jy and EMSS surveys because of the single-band nature and small dynamic range covered by those surveys (Stickel et al. 1994, Stocke et al. 1991, 1997). The exact population fraction of these “intermediate” BL Lacs is not yet known, as a bivariate luminosity function has yet to be computed for the BL Lac class. Our results do not allow us to comment significantly on the relative proportion of HBLs and LBLs among BL Lacs (e.g., Padovani & Giommi 1995a; Urry & Padovani 1995), since we are sensitive to high L_X/L_R objects only at high X-ray fluxes.

7. Selection Effects

Several effects may bias samples of blazars, causing them to miss objects which fall within their survey area and flux limits. Many, but not all, are intimately tied up with the question of classification (§ 3). We will attempt to discuss each of these effects in turn. They include the the Browne & Marchã (1993; BM) effect, lack of consistent (or consistently applied) identification criteria in some samples, and the effect of continuum variability on spectral indices. Tied up with the second topic is the question of whether all broad-line, flat-spectrum objects should be classified as FSRQs, or whether objects in which the continua are dominated by galactic light should be referred to as BLRG.

It is safe to say that there is probably no survey which is completely immune from selection effects. The impact of selection effects upon most previous surveys is not known, but must be understood to make progress towards better understanding the AGN phenomenon. The BM (1993) effect has caused Perlman et al. (1996b) and Stocke et al. (1997) to reconsider the makeup of the original Morris et al. (1991) complete sample of EMSS BL Lacs, adding three BL Lacs to the C-EMSS sample after an exhaustive perusal of the available X-ray, radio and optical data, followed by further ROSAT HRI observations and optical spectroscopy. These two papers represent the only serious attempts to reformulate existing samples of blazars to minimize selection effects. Other existing samples should be re-considered in similar fashion.

7.1. The Browne & Marchã Effect

The BM effect causes low-luminosity blazars (particularly BL Lacs) to be missed in surveys because the apparent luminosity of the non-thermal nuclear source does not exceed that of the host galaxy by a large factor. X-ray and radio-faint surveys are the most heavily affected. The effect probably is more severe for LBLs than HBLs, since galaxies hosting a relatively weak non-thermal source of the LBL type (where the peak of the synchrotron emission is at energies lower than 4000 \AA) might not qualify as a BL Lac simply because its nonthermal emission at 4000 \AA is already much reduced compared to its peak in the IR, and not strong enough to produce a Ca II H & K break less than 25%. Yet an HBL-type object with identical radio characteristics (flux, spectral shape, polarization, etc.) would be much more likely to be classified as a BL Lac since its synchrotron emission at 4000 \AA is much stronger and still growing.

We may gauge the impact of the BM effect upon our sample by considering the likely properties of such objects (low-luminosity blazars hidden within bright galaxies). In such a case, the optical spectrum would resemble that of a radio galaxy, either with broad, narrow, or no emission lines whatsoever (a similar argument, although for BL Lacs only, was given in Laurent-Muehleisen et al. 1997). We have attempted to eliminate this ambiguity for broad-lined sources by grouping all broad-line radio galaxies with the FSRQs (but see §7.2 below). It therefore remains for us to consider the narrow-lined objects which remain in our sample.

Three of our first 85 IDs (WGAJ0340.8–1814, WGAJ0500.1–3040, WGAJ2317.9–4213) meet this description and have herein been described as radio galaxies. A few other objects which we have tentatively identified as BL Lacs (Table 5) may fall into this classification when higher signal-to-noise spectra are taken (these have been individually discussed in §4.2). Ten of the previously identified sources also fall into this category as NLRGs. But given that these objects exhibit flat-spectrum radio sources, some of these objects may house low-luminosity blazars. This is particularly true of the ten previously identified sources, for which the NLRG classifications (taken from the literature) were made by older standards (usually – but not always – the classical definition mentioned in §3). Further observations should be made to further probe their nature.

We have plotted these objects in Figures 6 and 7. Inspection of Figure 6 reveals that these NLRGs are less luminous than BL Lacs on average, but not the least luminous objects in our sample. This result is consistent with the predictions made by Browne & Marchã (1993) and Marchã & Browne (1995). Perhaps more interesting is the fact that the large majority (10 of 13) of these NLRGs lie within the LBL region of the $(\alpha_{\text{ox}}, \alpha_{\text{ro}})$ plot (Figure 7). This verifies our suspicion (above) that, since the synchrotron continuum produced by

LBLs most often peaks in the near-to-mid infrared, and is already decreasing in the optical, the BM effect is stronger among LBLs than HBLs. Also noteworthy is the fact that the majority of these radio galaxies – 7 of 13 – are at low values of α_{ro} and high values of α_{ox} . As with the BL Lacs which occupy this region of Figure 7, these objects are all at low z and therefore the optical fluxes are largely contaminated by the host galaxy.

In addition to these objects, a large fraction of the newly-identified BL Lacs in our sample (10 of 22; see Table 5) have been so classified only by virtue of our usage of the expanded Marchã et al. (1996) definition of the BL Lac class. These objects would not have been classified as BL Lacs under earlier, more restrictive definitions of the class (Stickel et al. 1991, Stocke et al. 1991, Perlman et al. 1996a), though they might have received some mention under such standards. The large fraction of objects falling in this category confirms the predictions of Marchã & Browne (1995) for low-flux-limit X-ray surveys such as this. Similar results were also found in the RGB BL Lac Survey (Laurent-Muehleisen et al. 1997), as well as the 200 mJy sample (Marchã et al. 1996). Note that Marchã et al. showed that at least some of the objects outside the “classical” BL Lac region of the (C, W_λ) (but within the expanded Marchã et al. definition) also share the polarization properties of BL Lacs.

Returning to Figure 7, it is now important to point out that we suspect that the two ROSAT-based samples to which we compared the DXRBS BL Lacs in §6.2, those of Kock et al. (1996) and Nass et al. (1996), may contain a number ($\sim 20\%$, as in the EMSS; Stocke et al. 1997) of objects which could be classified as BL Lacs using the Marchã et al. (1996) redefinition of the BL Lac class. This is because both Kock et al. and Nass et al. used (somewhat unclearly defined) versions of the classical BL Lac-radio galaxy division to define their samples. It is also possible that these two samples may contain a few radio galaxies whose spectra should be more carefully scrutinized, as the regions of parameter space that they cover overlap significantly with the radio galaxies in our sample (Figure 7). Further evidence for this point can be seen in the recent findings of Laurent-Muehleisen et al. (1997, specifically their Fig. 3).

7.2. Inconsistent (or Inconsistently Applied) Identification Criteria

As we mentioned in § 3, there has not, to date, been either a single definition of the blazar class or of the BL Lac and FSRQ subclasses. The literature contains several examples of such inconsistencies. For example, as pointed out by Perlman et al. (1996b), the lack of a Ca II H & K break strength criterion in the 1 Jy, S4 and S5 samples of BL Lacs, has caused numerous objects to be misclassified as radio galaxies instead of BL Lacs

(see also Marchã & Browne 1995, 1996). It is therefore likely that a number of low- z objects may have been missed in this fashion.

Similarly, inspection of the spectra of 1 Jy BL Lacs (Stickel et al. 1993) reveals several which have emission lines considerably stronger than $W_\lambda = 5(1+z) \text{ \AA}$. While one may argue that some of these objects fall in the expanded region of the (H & K break strength, equivalent width) diagram that Marchã et al. (1996) allot to the BL Lacs, several, for example 1 Jy 1308+326, do not. The majority of these broad-line objects are at $z > 0.5$ and they may be the reason why the redshift distribution of the 1 Jy BL Lac sample is so dissimilar from the EMSS, Slew and DXRBS BL Lac redshift distribution. The variable nature of blazars makes this a particularly thorny problem to deal with. It is well known that several BL Lacs exhibit emission lines in their faint states (as we mentioned in § 3). Therefore it is entirely possible that the classification of a given object may be related to the state it was in when its classification spectrum was taken.

A third facet of this problem is the question of whether all flat-spectrum, broad-lined objects deserve to be called FSRQs. We believe this to be the case, based upon the general similarities of properties between BLRGs and FSRQs (e.g., Siebert et al. 1996). However we should note that the intrinsic power of the AGN affects how a source will be classified (see above). Others, however, have taken a different approach, and as a result some of the previously-identified objects which we list as FSRQs in Table 6 have been classified as BLRGs by other authors.

7.3. The Effect of Continuum Variability on Spectral Indices

Another possible bias, present in this as well as all other surveys which use spectral indices based upon nonsimultaneous data in their selection process, is due to variability. Existing X-ray surveys have made variability-based allowances for this effect, which likely decreases its impact greatly (see, e.g., Laurent-Muehleisen 1996; Perlman et al. 1996a). The magnitude of this effect upon existing samples which used radio-spectral index criteria has been addressed by Drinkwater et al. (1997), who utilize the variability statistics compiled by Stannard & Bentley (1977) to estimate that the number of sources which have average values of $\alpha_r < 0.5$ that would not be included in a survey based upon two radio fluxes measured at different frequencies at times separated by ~ 2 years, is $\sim 10\%$.

We have chosen to take a somewhat different approach to addressing this issue. The basis for this approach is not only that variability affects the measured spectral index when the data points in question are non-simultaneous, but also that the physical meaningfulness

of a cut at $\alpha_r = 0.5$, as opposed to, say, $\alpha_r = 0.7$ has never truly been tested. A factor of two variability between nonsimultaneous observations at 6 and 20 cm will change the observed radio spectral index by 0.58. In order to minimize the effect of non-simultaneous radio survey data upon our samples, we decided to expand the common definition of flat-spectrum radio sources to extend to $\alpha_r = 0.7$ (instead of 0.5). Selecting all sources with $\alpha_r \leq 1.1$ (that is, 0.5 plus 0.6 to include a factor of two variability) would considerably lower the efficiency of the technique, as the large majority of such steep-spectrum sources are radio galaxies (although some are radio-loud quasars, often called SSRQs, or steep-spectrum radio-loud quasars, which are thought to be oriented at intermediate angles between FR 2s and FSRQs). The compromise approach we adopted allows an intrinsically $\alpha_r = 0.5$ source to vary by $\sim 20\%$ between 20 cm and 6 cm survey observations. We believe the incompleteness due to missing sources which varied by larger amounts is small ($< 5\%$) given the distribution of instantaneous 3.6-6 cm spectral indices among core-dominated radio sources from our ATCA radio survey, and we will use the ATCA data to both estimate the contamination from truly steep-spectrum sources (and try to eliminate it) and test the significance and meaning of both our cutoff and the more traditional $\alpha_r = 0.5$ one.

It is important to note that the selection of sources with α_r as high as 0.7 makes our BL Lac sample virtually 100% complete. In fact, of the 180 confirmed BL Lacs with radio spectral index information in the multifrequency AGN database of Padovani et al. (1997b), only 5% have $\alpha_r > 0.7$ and all of these have X-ray-to-radio flux ratios much higher than those to which we are sensitive to. In other words, no BL Lac object should have been missed because of the α_r cut.

8. Conclusions

While the DXRBS sample is not yet completely identified (the objects discussed in this paper represent $\sim 60\%$ of our object list), this paper has detailed a number of interesting and exciting results from our deep survey. Most prominent among these results are:

1. A very high efficiency (95%) at finding FSRQs and BL Lacs once the list of radio-X-ray sources found by a cross-correlation of the ROSAT WGACAT with single-dish radio catalogs has been limited to serendipitous flat radio spectrum sources ($\alpha_r \leq 0.70$).
2. The DXRBS sample has vastly expanded coverage of the low luminosity end of the luminosity function both for BL Lacs and FSRQs, compared to all previous samples of blazars. Twenty-eight of 135 DXRBS FSRQs are at $L_R < 10^{33.5} \text{ erg s}^{-1} \text{ Hz}^{-1}$, compared to only 12 of 383 in the 1 Jy and S4 surveys combined. Among these 28 DXRBS objects, six

are at $L_R < 10^{32.5}$ erg s⁻¹ Hz⁻¹. These numbers are sure to increase as the remaining 40% of DXRBS objects (primarily optically faint) are identified.

For the BL Lacs, the increase is just as drastic, though restricted to objects with $L_X/L_R < 10^{-5.5}$ (i.e. LBL and intermediate BL Lacs). The DXRBS sample includes eight BL Lacs with $L_R < 10^{32}$ erg s⁻¹ Hz⁻¹ and $L_X/L_R < 10^{-5.5}$. While a few such objects are probably also included in the ROSAT based samples of Nass et al. (1996) and Kock et al. (1996), their prevalence in these samples is difficult to evaluate because of the large fraction of objects in those samples which lack redshifts. However it must be smaller given the higher X-ray flux limits of the Kock et al. and Nass et al. surveys, which are an order of magnitude higher than DXRBS. This is confirmed by the more recent work of Bade et al. (1997), who have just published redshifts for all but a few of the Nass et al. sample; they find very few objects in their sample at $L_X < 10^{26}$ erg s⁻¹ Hz⁻¹.

3. DXRBS has also filled large holes in our coverage of (L_X, L_R) parameter space, both for BL Lacs and FSRQs. The impact here is much more drastic for the FSRQs. Prior to DXRBS, only nine FSRQs within complete samples were known at values of $L_X/L_R > 10^{-6}$. Indeed, the continuity of LBL and FSRQ broad-band and X-ray spectral properties led Sambruna et al. (1996) to predict that no class of HBL-like FSRQs exists. Our results clearly refute this prediction. Thirty-two of the 135 (25%) DXRBS FSRQs so far identified fall in this category; the fraction is even larger (40%; 25 of 59) among the newly identified objects. These objects (whose numbers will surely increase as the remainder of the DXRBS sample is identified), which we term HFSRQs, exhibit clearly smaller (by nearly an order of magnitude) radio luminosities than lower L_X/L_R FSRQs. In the light of this finding, a re-examination of the broadband properties of FSRQs and indeed of the blazar class is in order. We intend to make this subject a priority in our future work.

For BL Lacs, DXRBS contains a large number of “intermediate” BL Lacs, objects with $10^{-6.5} < L_X/L_R < 10^{-5.5}$. Until very recently, this region of parameter space was almost completely unexplored. The *Einstein* Slew survey found the first such objects (Perlman et al. 1996a), and more recently two ROSAT based surveys (Kock et al. 1996, Nass et al. 1996) have found considerable numbers of such objects. However, due to the considerably fainter flux limit of DXRBS, our sample includes fainter objects in this region of parameter space than any previous sample.

EP acknowledges support from a USRA Visiting Scientist Fellowship while at Goddard Space Flight Center, and helpful discussions with G. Madejski and C. M. Urry. PP acknowledges financial support from MURST and ASI. PP and PG acknowledge S. Benetti and M. Turatto for their assistance at La Silla, and M. Della Valle and A. Fontana for their

help in preparing for the ESO observing run. RS and LJ acknowledge the support of NRC Regular and Senior Research Fellowships while at Goddard Space Flight Center. This work would have not been possible without the availability of the many radio, optical, and X-ray databases quoted in this paper, namely the NVSS, PMN, GB6, NORTH20CM, TEXAS, APM, COSMOS, WGACAT. We thank all the persons involved in the making of these databases for their effort. This research has made use of the BROWSE program developed by the ESA/*EXOSAT* Observatory and by NASA/HEASARC and of the NASA/IPAC Extragalactic Database (NED), which is operated by the Jet Propulsion Laboratory, California Institute of Technology, under contract with the National Aeronautics and Space Administration. The Australia Telescope Compact Array, a facility of the Australia Telescope National Facility, is funded by the Commonwealth of Australia for operation as a National Facility managed by CSIRO.

REFERENCES

- Angel, J. R. P., & Stockman, H. S., 1980 ARA&A 18, 321.
- Arp, H., Sargent, W. L. W., Willis, A. G., & Oosterbaan, C. E., 1979, ApJ 230, 68.
- Bade, N., et al. 1997, A & A submitted.
- Baum, S. A., Zirbel, E. L., & O’Dea, C. P., 1995, ApJ 451, 88.
- Blandford, R. D., & Rees, M. J., 1978, in Pittsburgh Conference on BL Lac Objects, ed. A. N. Wolfe, 328.
- Boisse, P., & Bergeron, J., 1988, A&A 192, 1.
- Browne, I. W. A., & Marchã, M. J. M., 1993, MNRAS 261, 795.
- Castander, F. J., Bower, R. G., Ellis, R. S., Aragon-Salamanca, A., Mason, K. O., Hasinger, G., McMahon, R. G., Carrera, F. J., Mittaz, J. P. D., Perez-Fournon, I., & Lehto, H. J., 1995, Nature 377, 39.
- Condon, J. J., 1984, ApJ 287, 461.
- Condon, J. J., Cotton, W. D., Griesen, E. W., & Yin, Q. F., Perley, R. A., Taylor, G. B., & Broderick, J. J., 1997, preprint (<http://www.nrao.edu>).
- Cristiani, S., et al., 1995, A&AS, 112, 347.
- Douglas, J. N., Bash, F. N., Bozayan, F. A., Torrence, G. W., & Wolfe, C., 1996, AJ, 111, 1945.
- Dressler, A., & Schectman, S. A., 1987, AJ 94, 899.

- Drinkwater, M. J., Barnes, D. G., & Ellison, S. L., 1995, PASA 13, 12.
- Drinkwater, M. J., Webster, R. L., Francis, P. J., Condon, J. J., Ellison, S. L., Jauncey, D. L., Lovell, J., Peterson, B. A., & Savage, A., 1997, MNRAS 284, 85.
- Fossati, G., Celotti, A., Ghisellini, G., & Maraschi, L., 1997, MNRAS 289, 136.
- Fugmann, W., 1988, A&A 205, 86.
- Georganopoulos, M., & Marscher, A. P., 1997, Astrophysics & Space Science, in press
- Gregg, M. D., Becker, R. H., White, R. L., Helfand, D. J., McMahon, R. G., & Hook, I. M., 1996, AJ 112, 407.
- Gregory, P. C., Scott, W. K., Douglas, K., & Condon, J. J., 1996, ApJS 103, 427.
- Griffith, M. R., & Wright, A. E., 1993, AJ 106, 1095.
- Hewitt, A., & Burbidge, G., 1993, ApJS, 87, 451
- Hook, I. M., McMahon, R. G., Irwin, M. J., Hazard, C., 1996, MNRAS 282, 1274.
- Impey, C. D., Lawrence, C. R., & Tapia, S., 1991, ApJ 375, 46.
- Irwin, M., Maddox, S. & McMahon, R., 1994, Spectrum 2, 14.
- Jannuzi, B. T., Smith, P. S., & Elston, R., 1994, ApJ 428, 130.
- Jannuzi, B. T., Smith, P. S., & Elston, R., 1993, ApJS 85, 265.
- Koratkar, A., Pian, E., Urry, C. M., & Pesce, J. E., 1998, ApJ, in press.
- Kock, A., Meisenheimer, K., Brinkmann, W., Neumann, M., Siebert, J., 1996, A & A 307, 475.
- Kühr, H., Schmidt, G. D., 1990, AJ 99, 1.
- Laurent-Muehleisen, S. A., 1996, PhD Thesis, Pennsylvania State University.
- Laurent-Muehleisen, S. A., Kollgaard, R. I., Ciardullo, R., Feigelson, E. D., Brinkmann, W., & Siebert, J., 1997, preprint (astro-ph/9711268)
- Marchã, M. J. M., & Browne, I. W. A., 1995, MNRAS 275, 951.
- Marchã, M. J. M., & Browne, I. W. A., 1996, MNRAS 279, 72.
- Marchã, M. J. M., Browne, I. W. A., Impey, C. D., & Smith, P. S., 1996, MNRAS 281, 425.
- Mattox, J. R., Schachter, J., Molnar, L., Hartman, R. C., & Patnaik, A. R., 1997, ApJ 481, 95.
- McGlynn, T., & Scollick, K., 1996, <http://skyview.gsfc.nasa.gov/skyview.html>
- Morris, S. L., Stocke, J. T., Gioia, I. M., Schild, R. E., Wolter, A., Maccacaro, T., & Della Ceca, R., 1991, ApJ 380, 49.

- Nass, P., Bade, N., Kollgaard, R. I., Laurent-Muehleisen, S. A., Reiners, D., & Voges, W., 1996, *A & A* 309, 419.
- Ostriker, J. P., and Vietri, M., 1985, *Nature* 318, 446.
- Padovani, P., 1997, in *Very High Energy Phenomena in the Universe*, Y. Giraud-Héraud, J. Trân Thanh Vân eds., Editions Frontieres, 7.
- Padovani, P., & Urry, C. M., 1990, *ApJ* 356, 75.
- Padovani, P., & Urry, C. M., 1991, *ApJ* 368, 373.
- Padovani, P., & Urry, C. M., 1992, *ApJ* 387, 449.
- Padovani, P., & Giommi, P., 1995a, *ApJ* 444, 567.
- Padovani, P., & Giommi, P., 1995b, *MNRAS*, 277, 1477.
- Padovani, P., & Giommi, P., 1996, *MNRAS*, 279, 526.
- Padovani, P., Giommi, P., & Fiore, F., 1997a, *MNRAS*, 284, 569.
- Padovani, P., Giommi, P., & Fiore, F., 1997b, in *From the Micro- to the Mega-Parsec*, A. Comastri, T. Venturi, M. Bellazzini eds., *Mem. Soc. Astr. It.*, 68, 147.
- Perlman, E. S., Schachter, J. F., & Stocke, J. T., in preparation.
- Perlman, E. S., Stocke, J. T., Schachter, J. F., Elvis, M., Ellingson, E., Urry, C. M., Potter, M., Impey, C. D., & Kolchinsky, P., 1996a, *ApJS* 104, 251.
- Perlman, E. S., Stocke, J. T., Wang, Q. D., & Morris, S. L., 1996b, *ApJ* 456, 451.
- Peterson, B. A., Jauncey, D. L., Wright, A., & Condon, J. J., 1976, *ApJL* 207, L5.
- Ruscica, C., Caccianiga, A., Maccacaro, T., & Wolter, A., 1996, in *Extragalactic Radio Sources*, R. Ekers, C. Fanti, L. Padrielli eds., 271.
- Sambruna, R. M., Maraschi, L., & Urry, C. M., 1996, *ApJ* 463, 444.
- Sambruna, R. M., 1997, *ApJ* 487, 536.
- Scarpa, R., & Falomo, R., 1997, *A&A* submitted.
- Schechtman, S. A. et al. 1996, *ApJ* 470, 172.
- Siebert, J., Brinkmann, W., Morganti, R., Tadhunter, C. N., Danziger, I. J., Fosbury, R. A. E., & di Serego Alighieri, S., 1996, *MNRAS*, 279, 1331
- Stannard, D., & Bentley, M., 1977, *MNRAS* 180, 703.
- Stark, A. A., Gammie, C. F., Wilson, R. W., Bally, J., Linke, R. A., Heiles, C., Hurwitz, M., 1992, *ApJS*, 79, 77.
- Stickel, M., Padovani, P., Urry, C. M., Fried, J. W., & Kühr, H., 1991, *ApJ* 374, 431.

- Stickel, M., & Kühr, H., 1994, *A&AS* 105, 67.
- Stickel, M., & Kühr, H., 1996, *A&AS* 115, 1.
- Stickel, M., Meisenheimer, K., & Kühr, H., 1994, *A&AS* 105, 211.
- Stickel, M., Rieke, G. H., Kühr, H., & Rieke, M. J., 1996, *ApJ* 468, 556.
- Stocke, J. T., Morris, S. L., Gioia, I. M., Maccacaro, T., Schild, R., Wolter, A., Fleming, T. A., 1991, *ApJS* 76, 813.
- Stocke, J. T., & Rector, 1997, *ApJ* 489, L17.
- Stocke, J. T., Rector, T. A., Perlman, E. S., & Gioia, I. M., 1997, in prep.
- Thompson, D. J., et al., 1995, *ApJS* 101, 259.
- Torra, J., & Turon, C., eds. 1985, *Scientific Aspects of the Input Catalogue Preparation*, Aussois, ESA-SP 234
- Urry, C. M., & Padovani, P., 1995, *PASP*, 107, 803
- Urry, C. M., Padovani, P., & Stickel, M., 1991, *ApJ* 382, 501.
- Vermeulen, R. C., Ogle, P. M., Tran, H. D., Browne, I. W. A., Cohen, M. H., Readhead, A. C. S., Taylor, G. B., & Goodrich, R. W., 1995, *ApJS* 452, L5.
- Verón-Cetty, M.-P., & Verón, P., 1996, *A Catalogue of Quasars and Active Nuclei*, 6th ed. ESO Scientific Report No. 13
- White, R. L., & Becker, R. H., 1992, *ApJS*, 79, 331.
- White, N. E., Giommi, P., & Angelini, L., 1995, <http://lheawww.gsfc.nasa.gov/~white/wgacat.html>
- Wolter, A., et al. 1997, *MNRAS* 284, 225.
- Wolter, A., Ruscica, C. & Caccianiga, A., 1998, *MNRAS* in press.
- Zirbel, E. L. & Baum, S. A., 1995, *ApJ* 448, 521.

Figure Captions

Figure 1. Ca II break strengths C and rest-frame emission line equivalent widths of radio galaxies and BL Lacs are shown. Quasars are not graphed here because they fall too far to the right to be included (as does one radio galaxy, WGAJ0500.1–3040, which, despite the extremely large equivalent width of several of its emission lines, is a narrow-line object, as described in §4). We have overplotted the traditional definition of the BL Lac class (dashed box) as used in Stickel et al. (1991), Stocke et al. (1991) and Perlman et al. (1996a), as well as the expanded definition of the BL Lac class advocated by Marchã et al. (1996) (the region in between the dot-dashed lines). Objects where both C and W_λ could be measured are shown as squares. Objects where one or both of these figures are upper limits are denoted by diamonds. All error bars shown are 1σ , and all upper limits shown are at the 2σ significance level.

Figure 2. Optical spectra of all 85 objects for which we announce identifications in this paper. All spectra have been dereddened and cleaned of cosmic rays as described in Section 3.

Figure 3. Redshift distribution for the DXRBS, S4, and 1 Jy samples of FSRQs (radio quasars with $\alpha_r \leq 0.7$).

Figure 4. Redshift distribution for the DXRBS, Slew, and 1 Jy samples of BL Lacs. The hatched areas represent lower limits. Redshift figures for 1 Jy BL Lacs have been taken from Stickel et al. (1994), while those for Slew BL Lacs have been taken from Perlman et al. (1996a), Bade et al. (1997), and Perlman, Schachter & Stocke (in preparation).

Figure 5. The X-ray and radio luminosities of FSRQs. Newly identified DXRBS FSRQs are shown as filled circles, while previously identified serendipitous DXRBS FSRQs are shown as filled squares. DXRBS objects identified as radio galaxies with broad emission lines are shown as crosses. The published complete samples of blazars (the 1 Jy [triangles] and S4 [squares]) cover the low-luminosity end very poorly: while still incomplete, the DXRBS blazar survey already includes higher numbers of faint FSRQs (over $3\times$ the number in the 1 Jy and S4 combined). One in 4 FSRQs have high ratios of X-ray to radio luminosity $L_X/L_R > 10^{-6}$ (to the right of the dashed line). Previous radio surveys included very few objects in this region. See sections 5 and 6 for discussion. Radio data for the S4 and 1 Jy sources from Stickel & Kühn (1994) and Stickel et al. (1994); X-ray data from the multifrequency AGN database of Padovani et al. (1997b) and references therein. Note that X-ray data are available only for $\sim 53\%$ and 66% of the S4 and 1 Jy FSRQs respectively.

Figure 6. The X-ray and radio luminosities of BL Lacs. Newly identified DXRBS BL Lacs are shown as filled circles, while previously identified serendipitous DXRBS BL Lacs

are shown as filled squares. DXRBS objects identified as radio galaxies with narrow or no emission lines are shown as crosses. The 1 Jy, Slew, and EMSS BL Lacs are represented by triangles, circles, and squares respectively. Crosses represent the NLRGs in our sample. While DXRBS does not include extremely high L_x/L_r BL Lacs such as those found in the *Einstein* Slew Survey, it can be seen that prior to DXRBS, region of the graph between $-6.5 \lesssim \log L_x/L_r \lesssim -5.5$ (denoted by two dashed lines) was very poorly populated, a consequence of the disparate survey methods used. The high sensitivity and combined selection method of DXRBS reveals the previous “zone of avoidance” in this graph to be illusory. See Sections 4 and 5 for discussion. Most of the data come from the original papers; additional radio and X-ray data are from the multifrequency AGN database of Padovani et al. (1997) and references therein.

Figure 7. The X-ray-optical (α_{ox}) and radio-optical (α_{ro}) effective spectral indices of the BL Lacs in the DXRBS sample compared to those in the samples of Koch et al. (1996) and Nass et al. (1996). Newly identified DXRBS BL Lacs are shown as filled circles, while previously identified serendipitous DXRBS BL Lacs are shown as filled squares. Empty circles represent the Nass et al.’s objects, while empty squares indicate the Koch et al.’s sources. Crosses represent the NLRGs in our sample. The two dashed lines denote the loci of points with $\log L_x/L_r = -6.5$ ($\alpha_{rx} \simeq 0.85$, upper line) and $\log L_x/L_r = -5.5$ ($\alpha_{rx} \simeq 0.72$, lower line). Each of the three surveys covers different areas of parameter space, as shown. The spectral indices α_{ox} and α_{ro} are defined in the usual way and calculated between the rest-frame frequencies of 5 GHz, 5000 Å, and 1 keV.

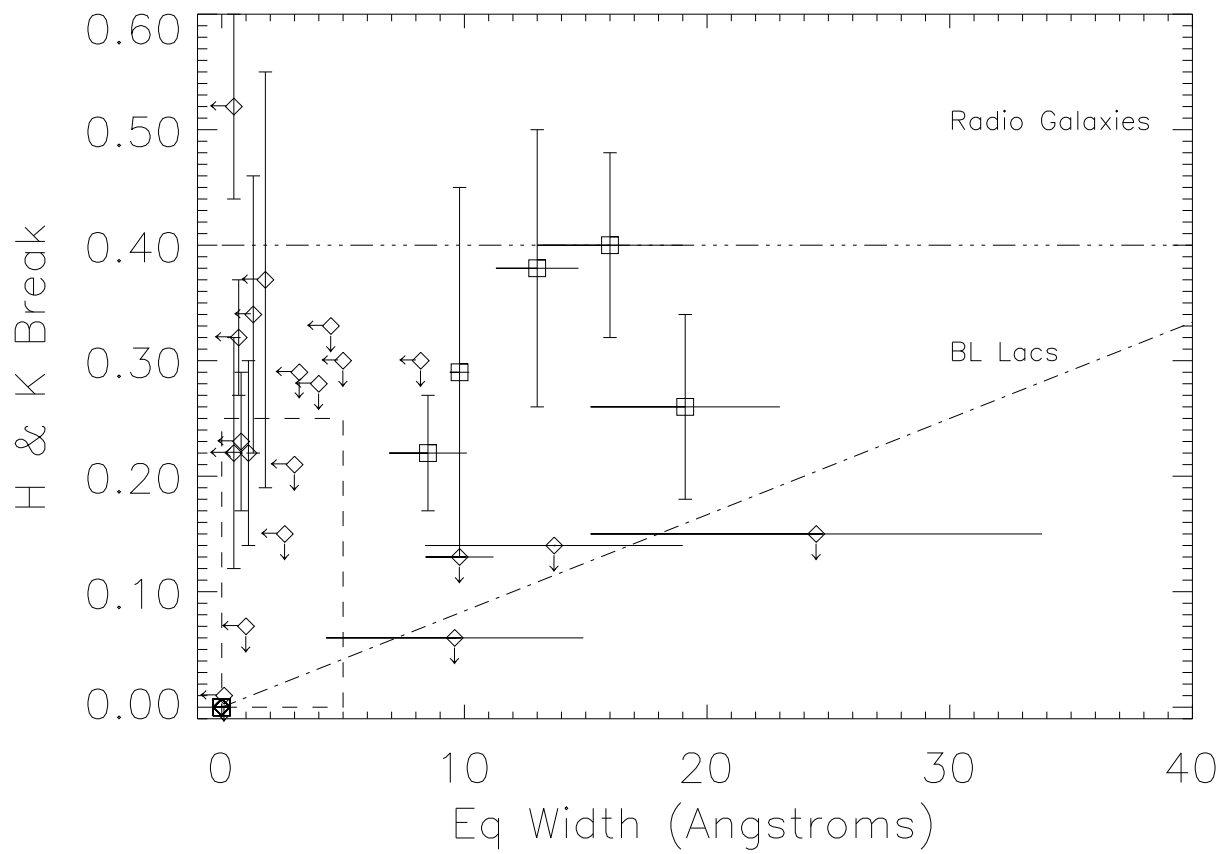
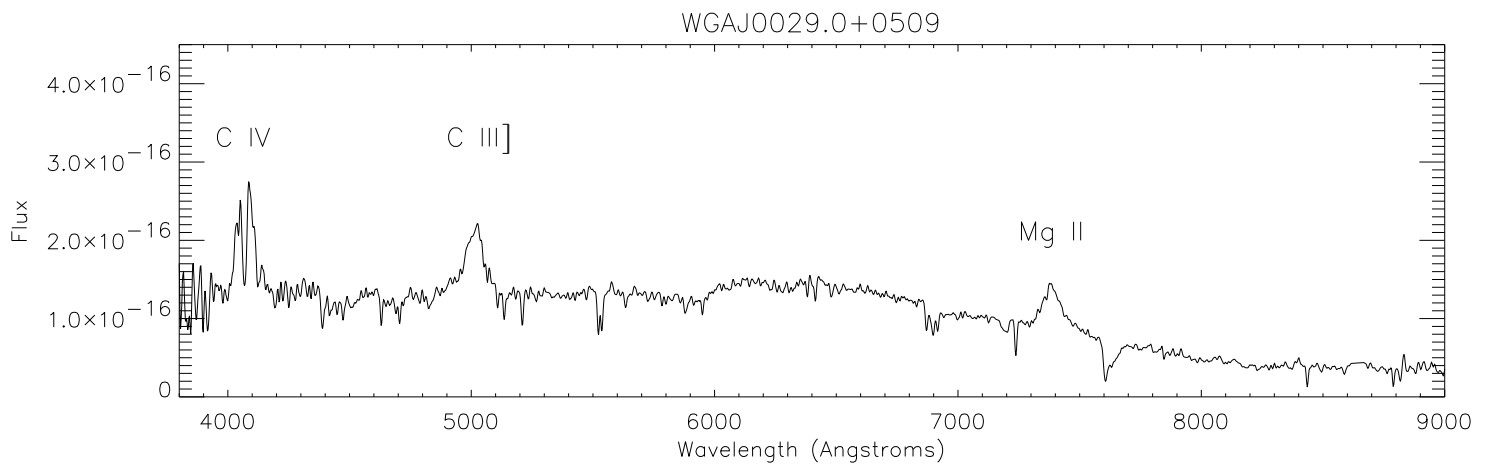
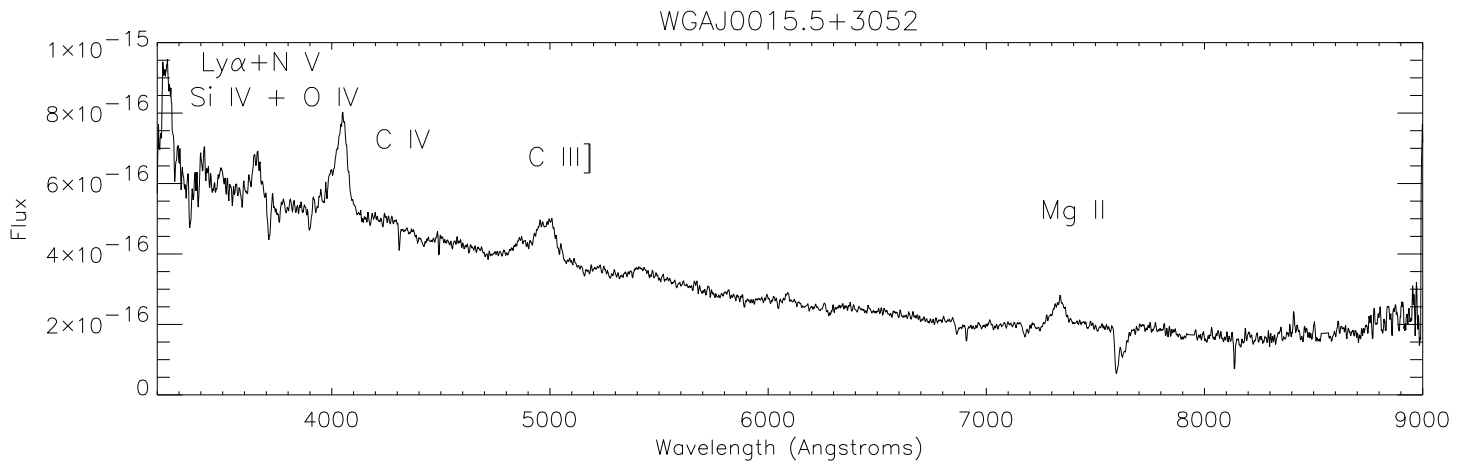
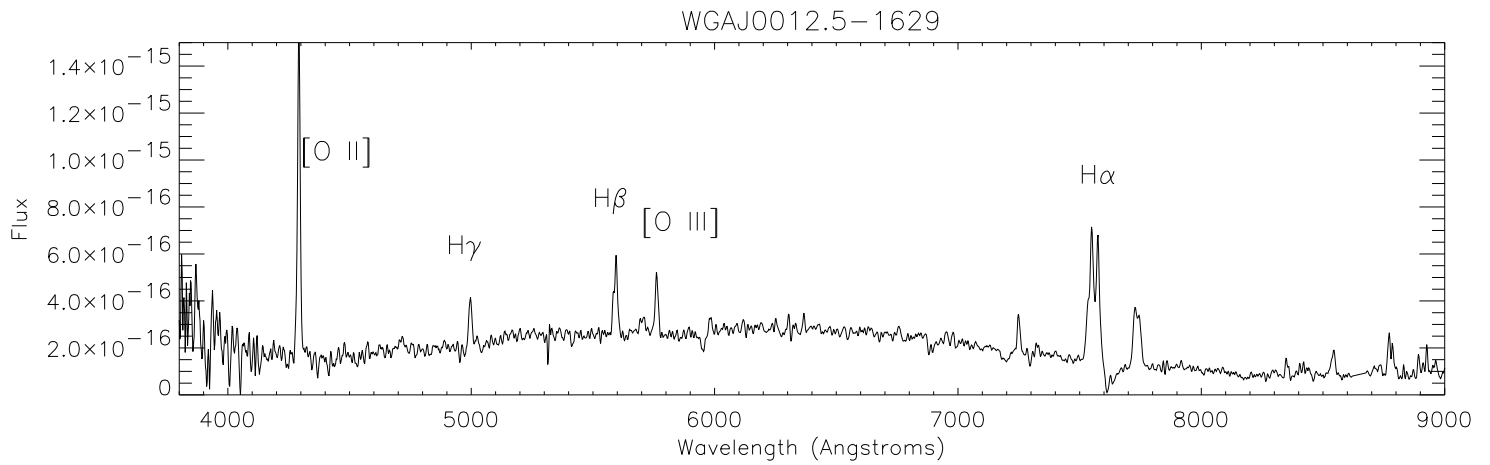
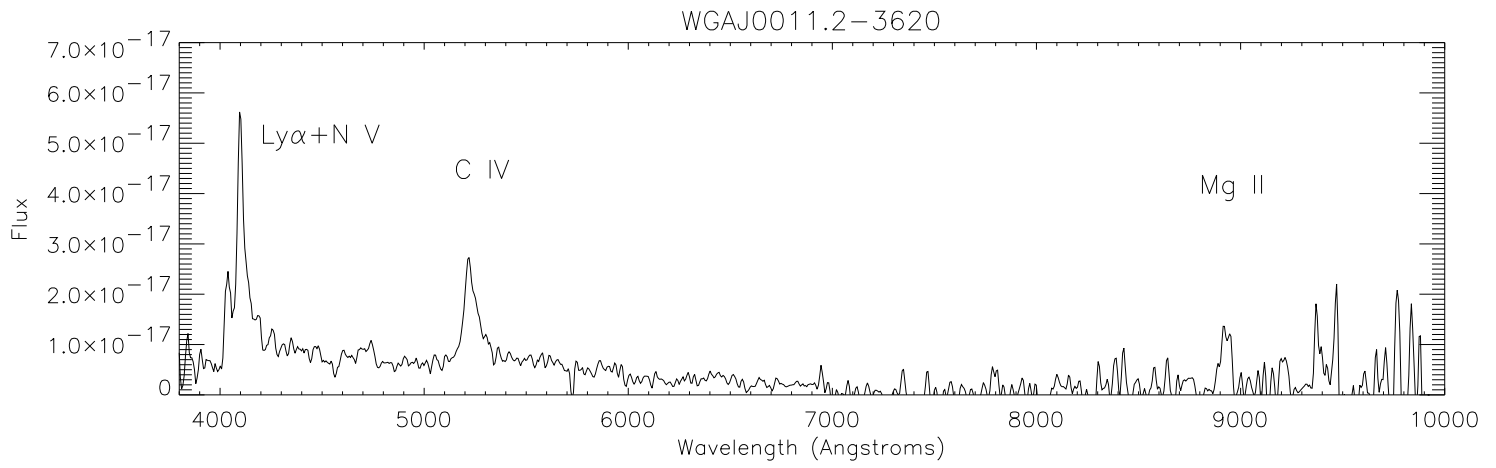
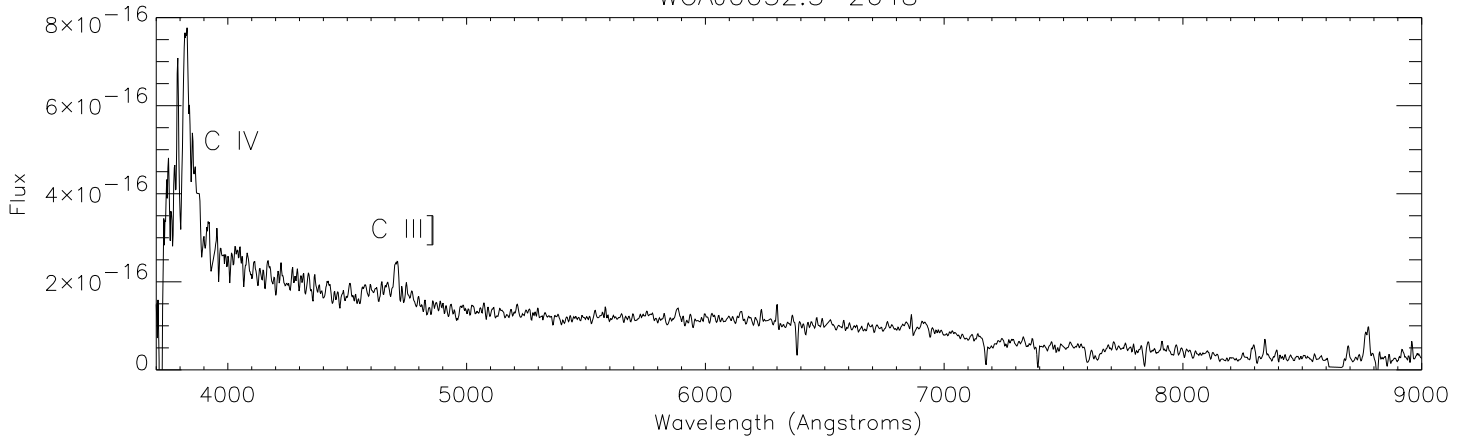


TABLE 1
OBSERVING RUN INFORMATION

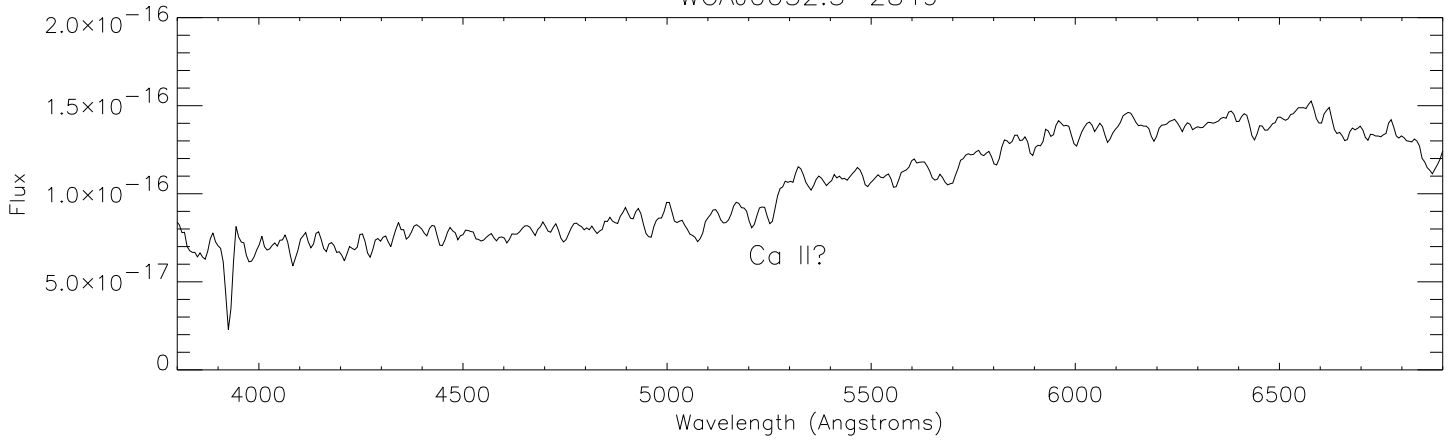
Telescope	Å/ pixel	Approx. Range(Å)
KPNO 2.1m	2.4	3700–9000
ESO 2.2m	5.2	2500–12000
ESO 3.6m	6.3	3700–6900 (B300 grism)
	6.3	6700–10000 (R300 grism)
CTIO 1.5m	5.4	3600–10000
CTIO 4.0m	1.2	3800–7300
MMT	2.0	3800-9000
Lick 3m	1.8	3700-8300



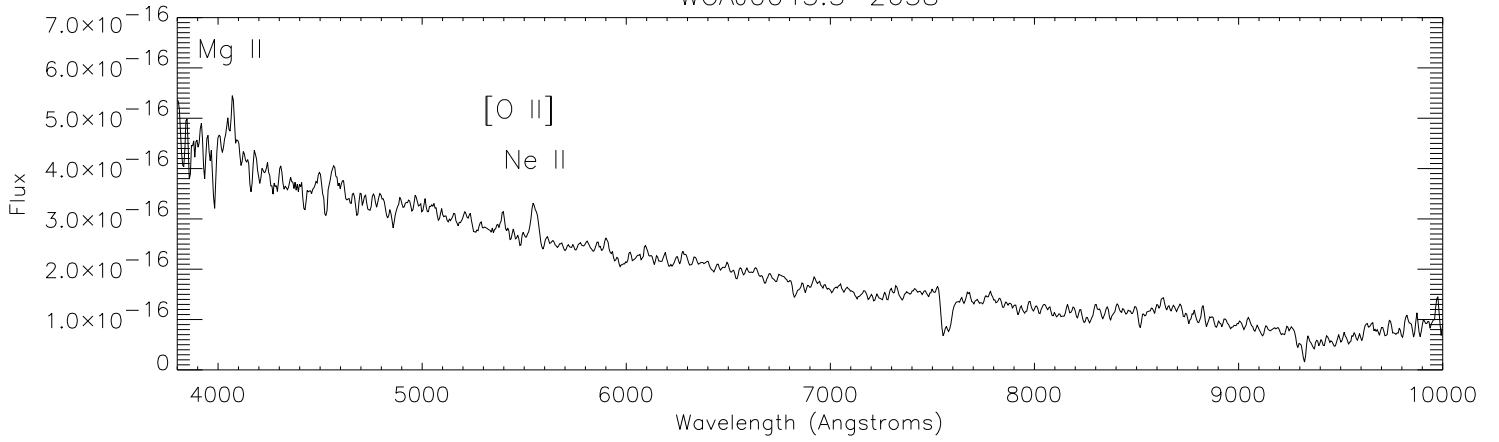
WGAJ0032.5-2648



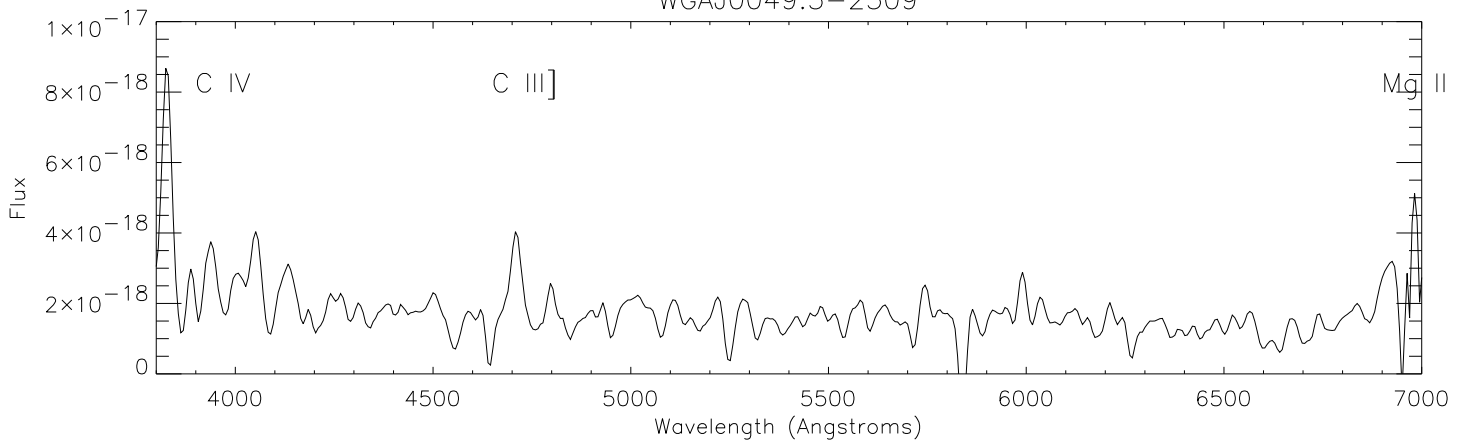
WGAJ0032.5-2849



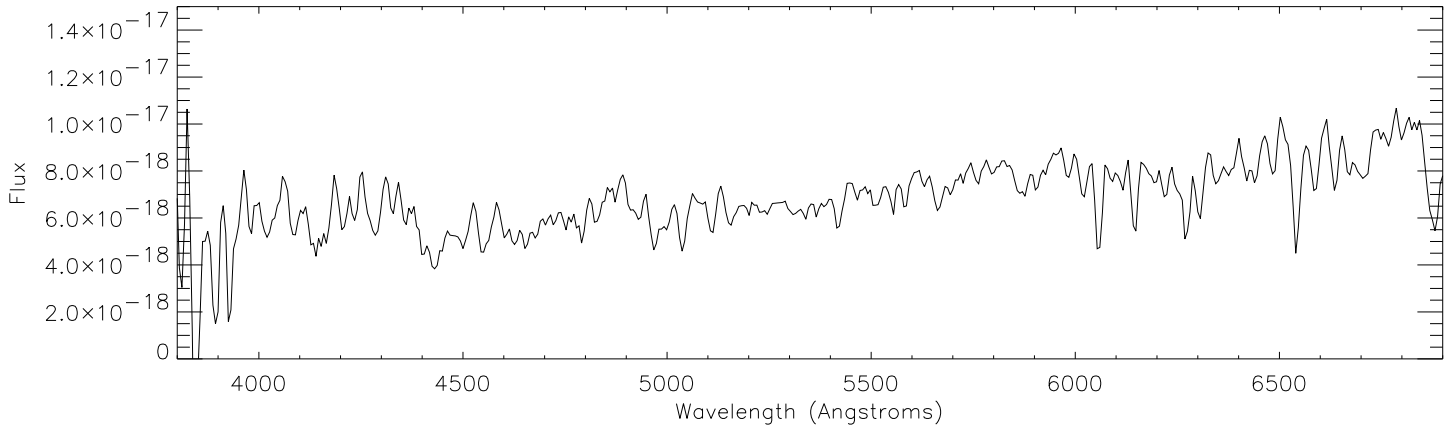
WGAJ0043.3-2638



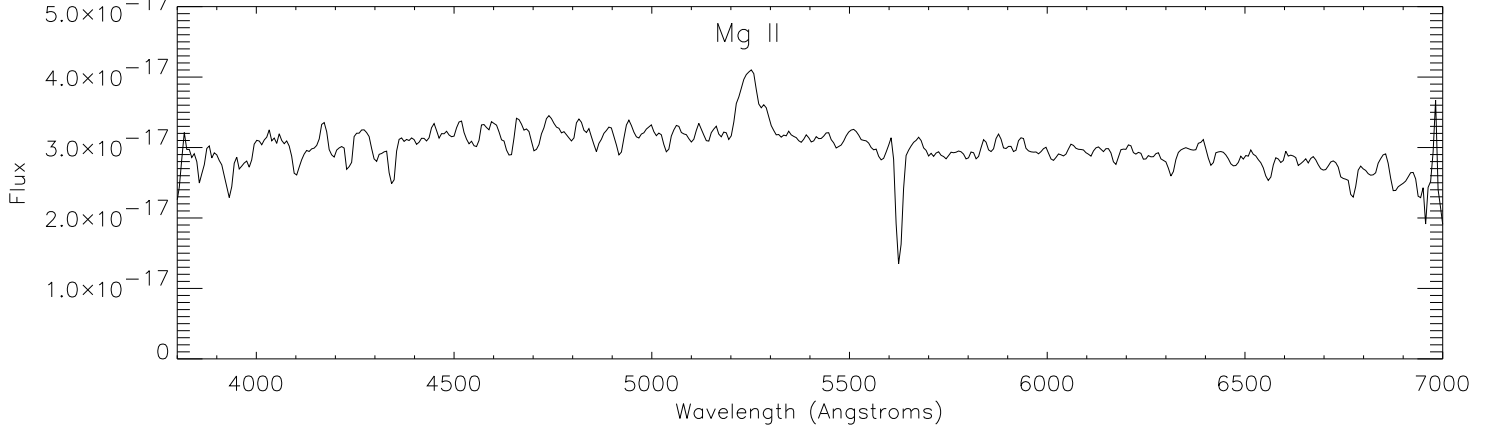
WGAJ0049.5-2509



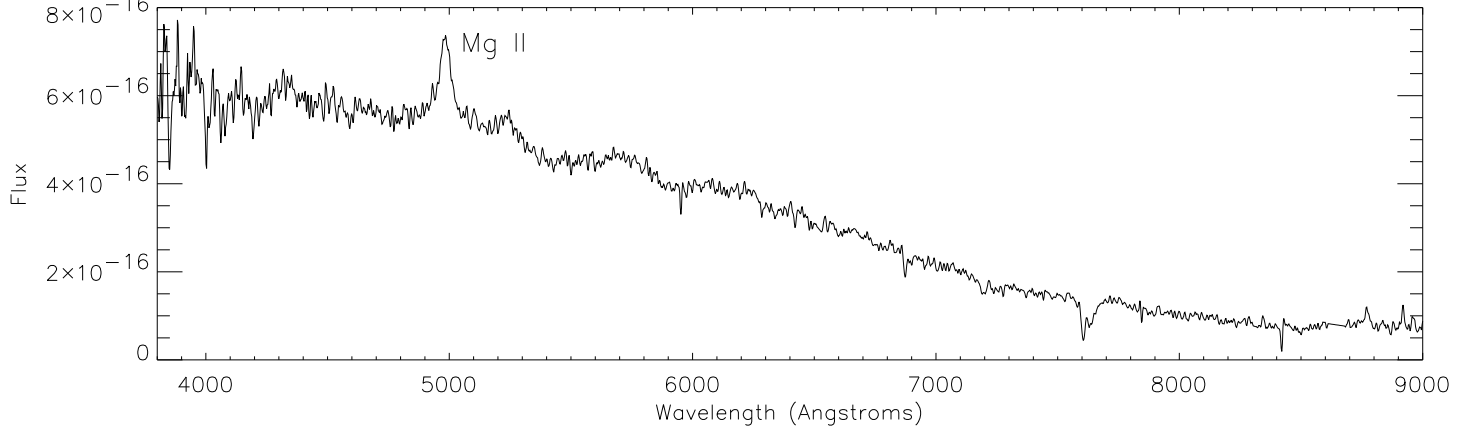
WGAJ0057.3-2212



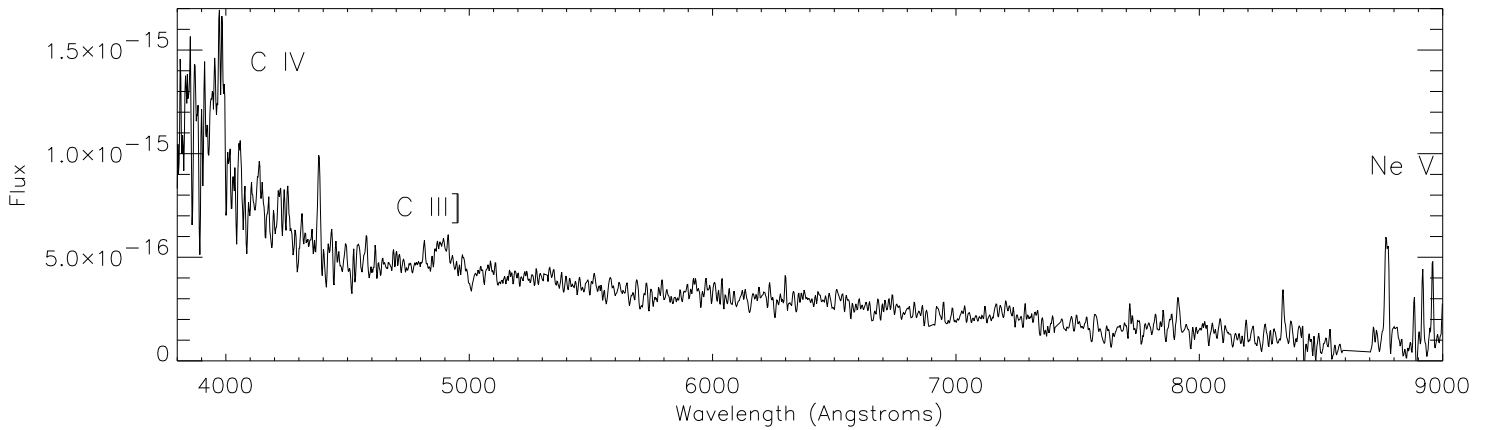
WGAJ0100.1-3337

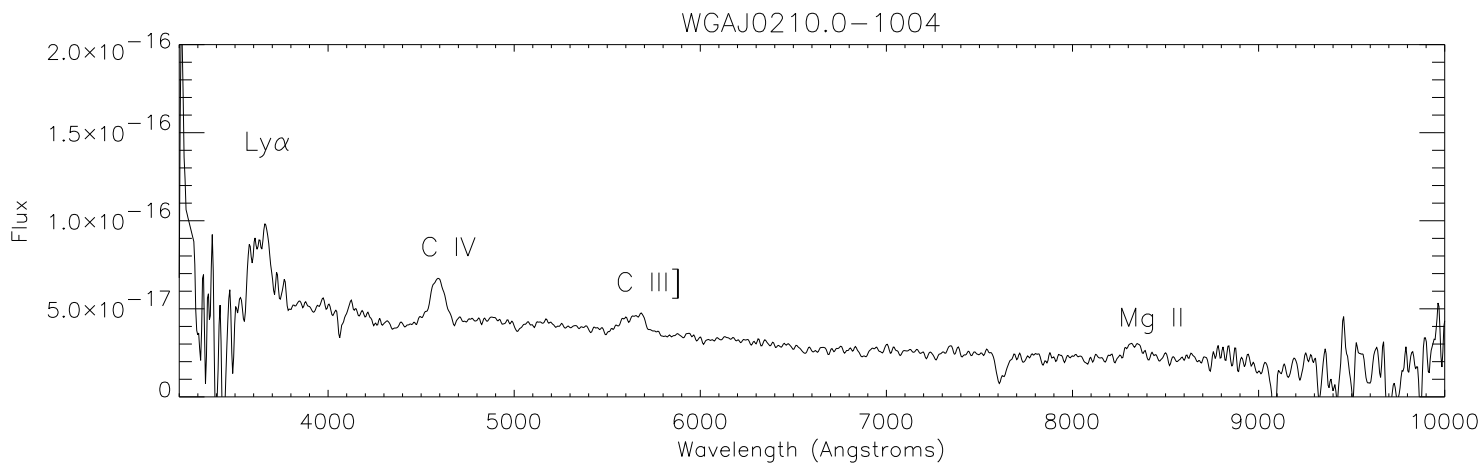
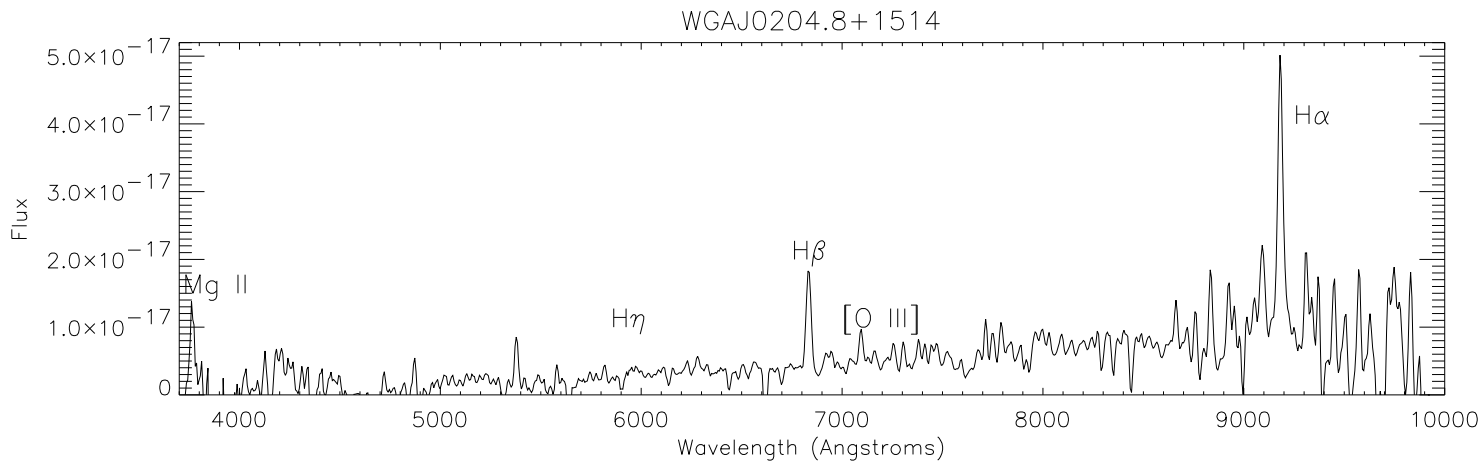
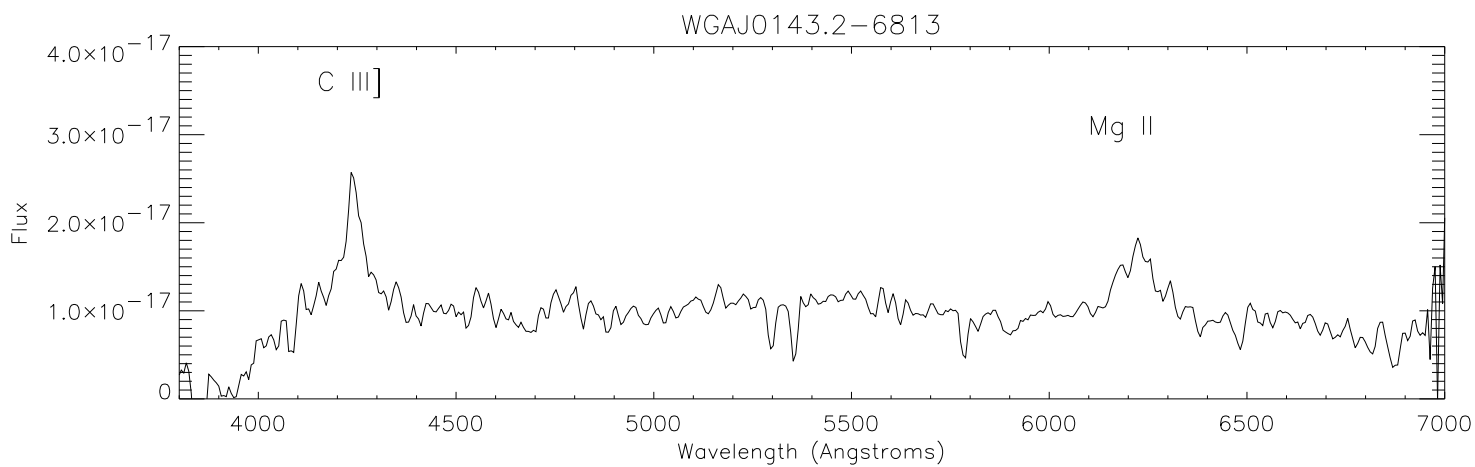
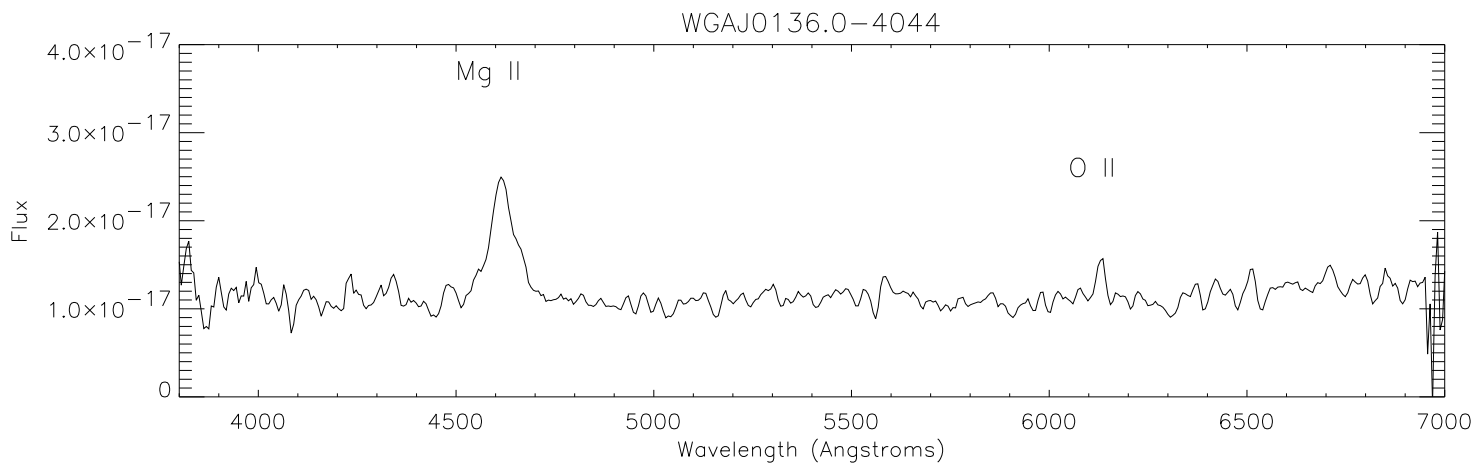


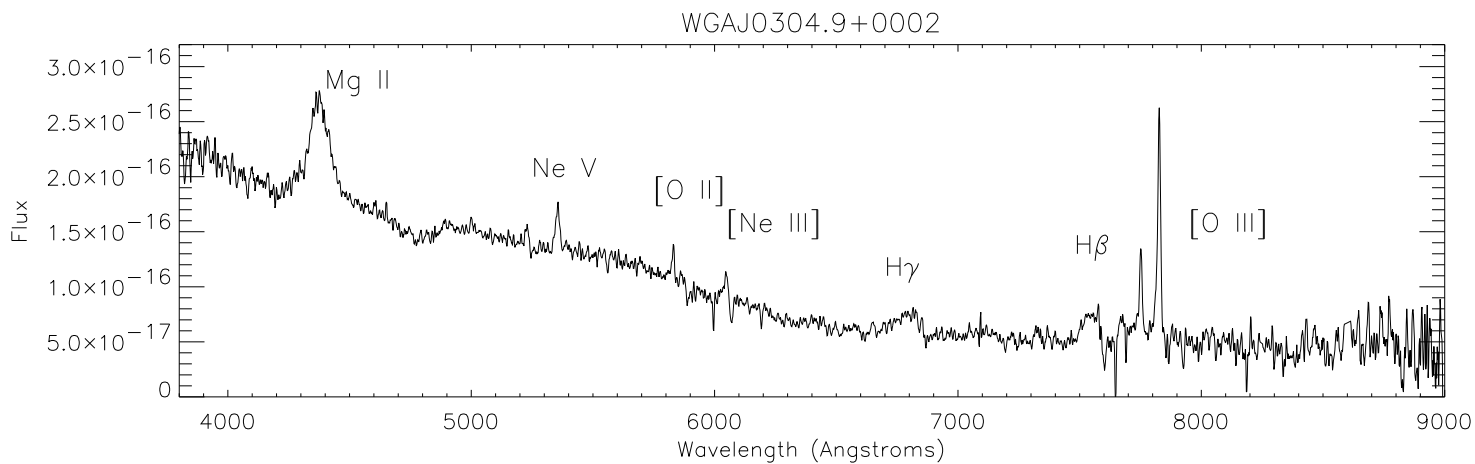
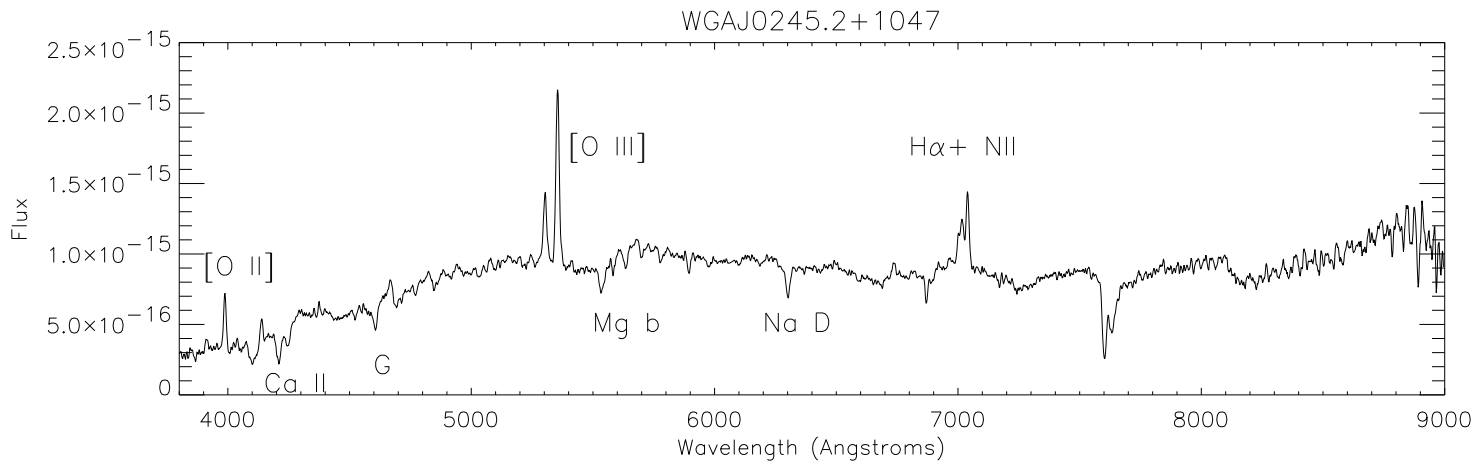
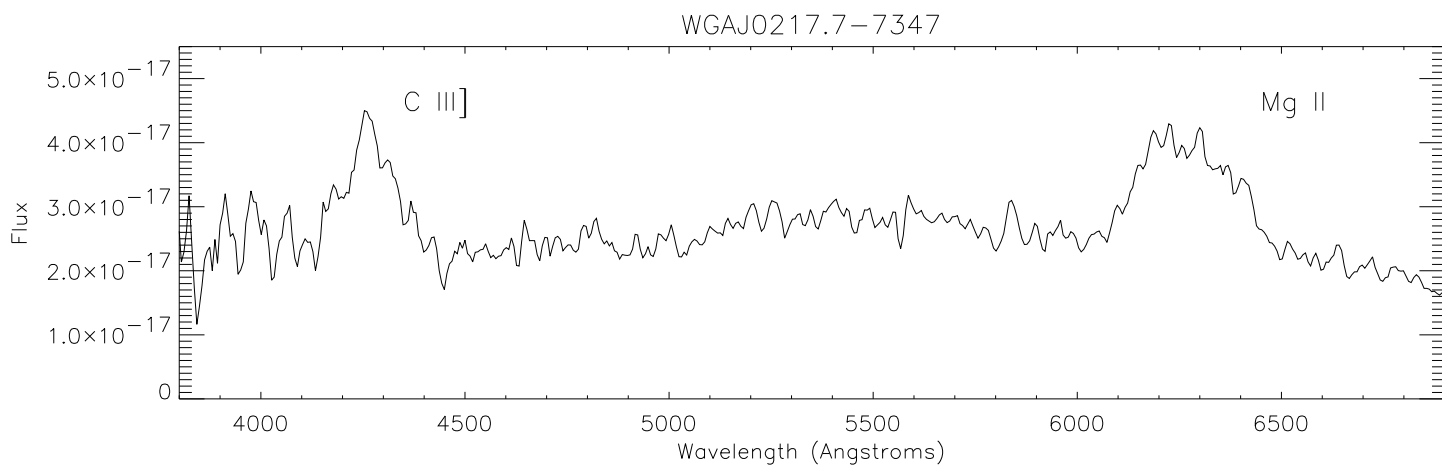
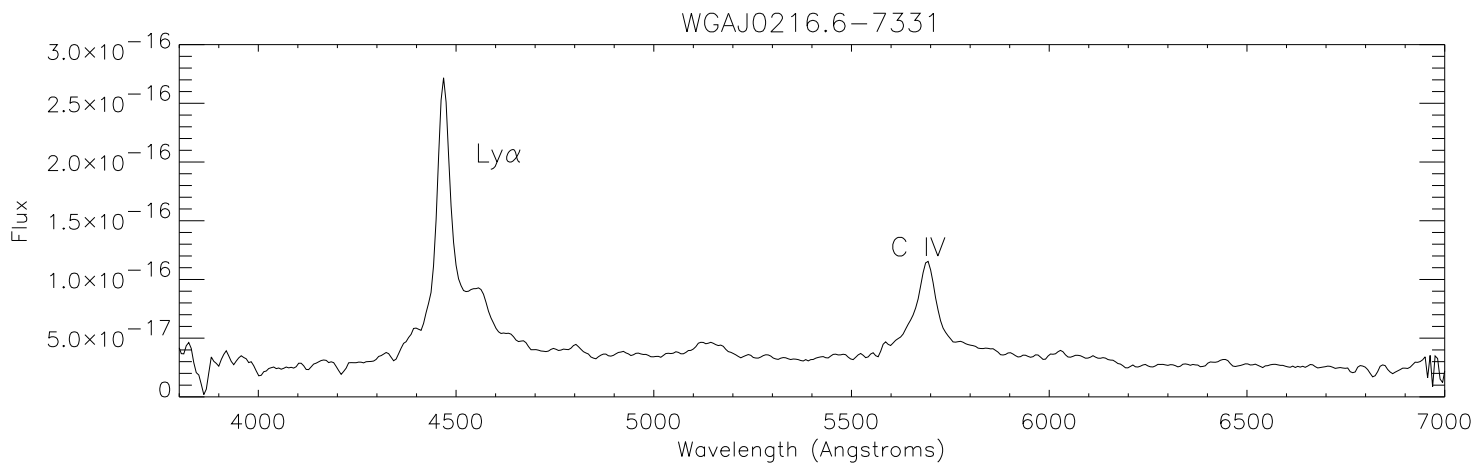
WGAJ0110.5-1647

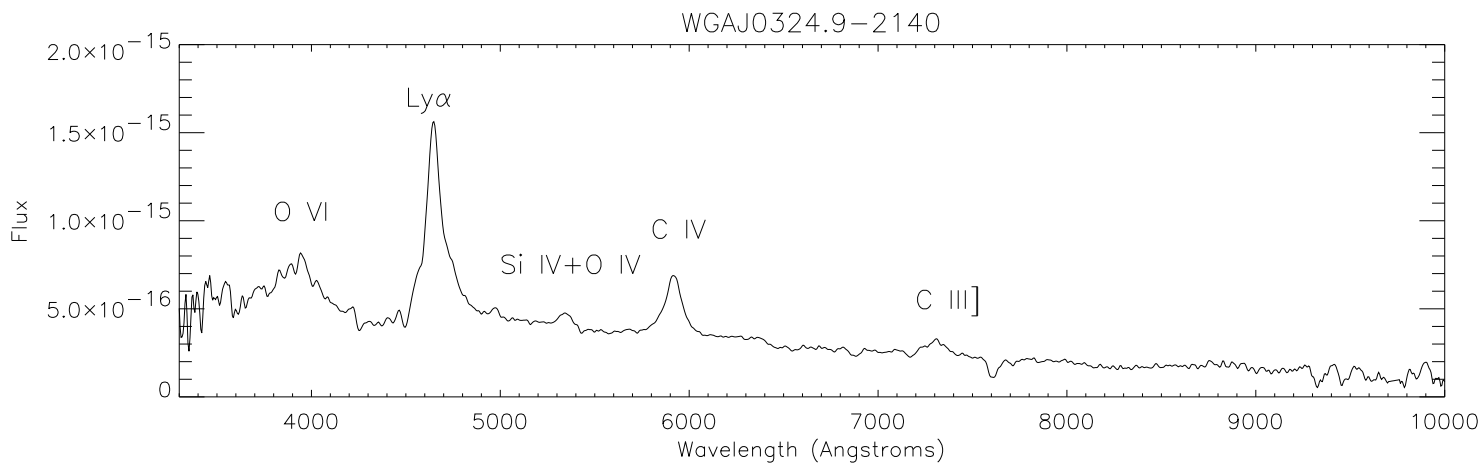
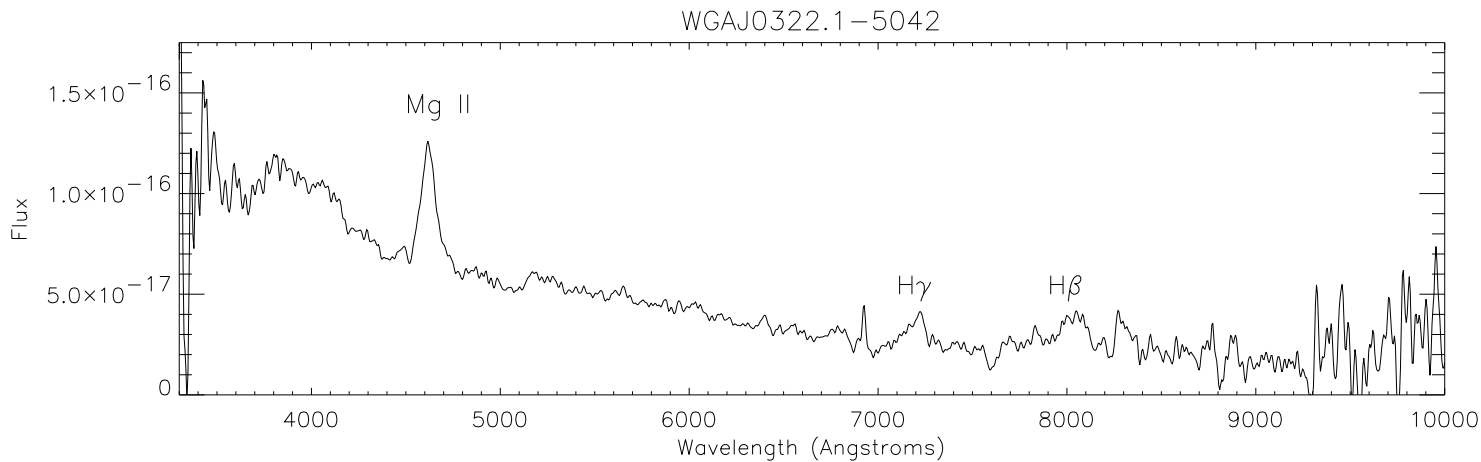
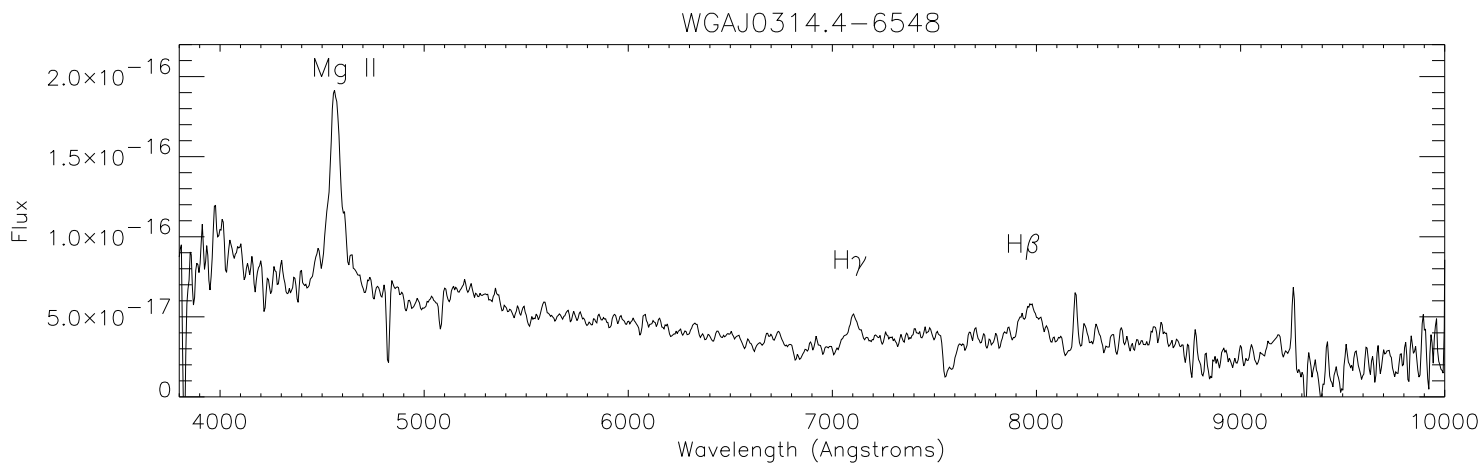
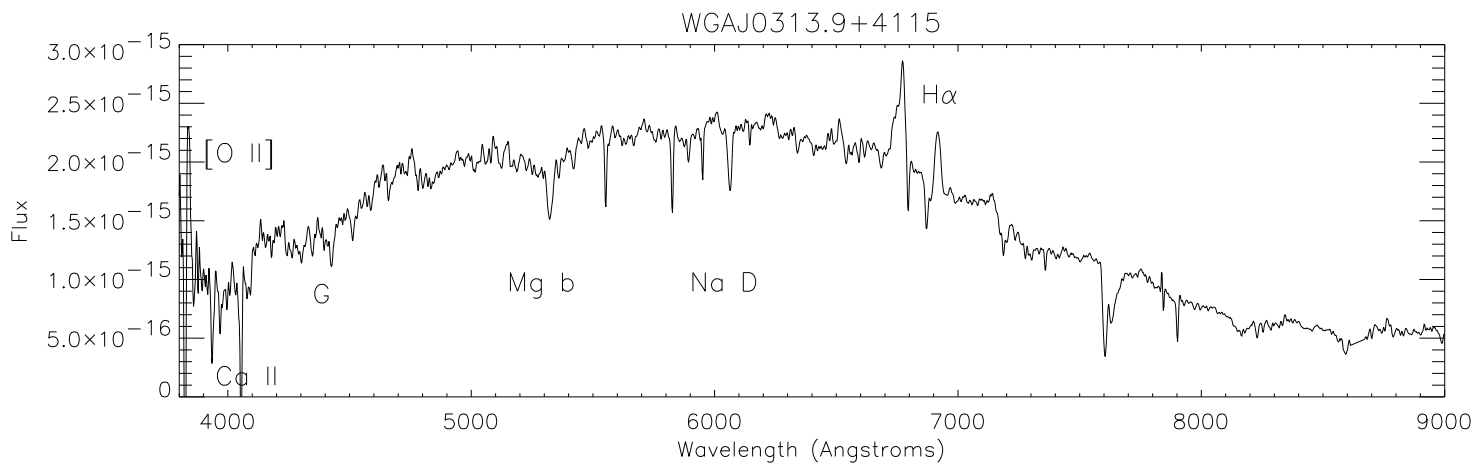


WGAJ0125.0+0146

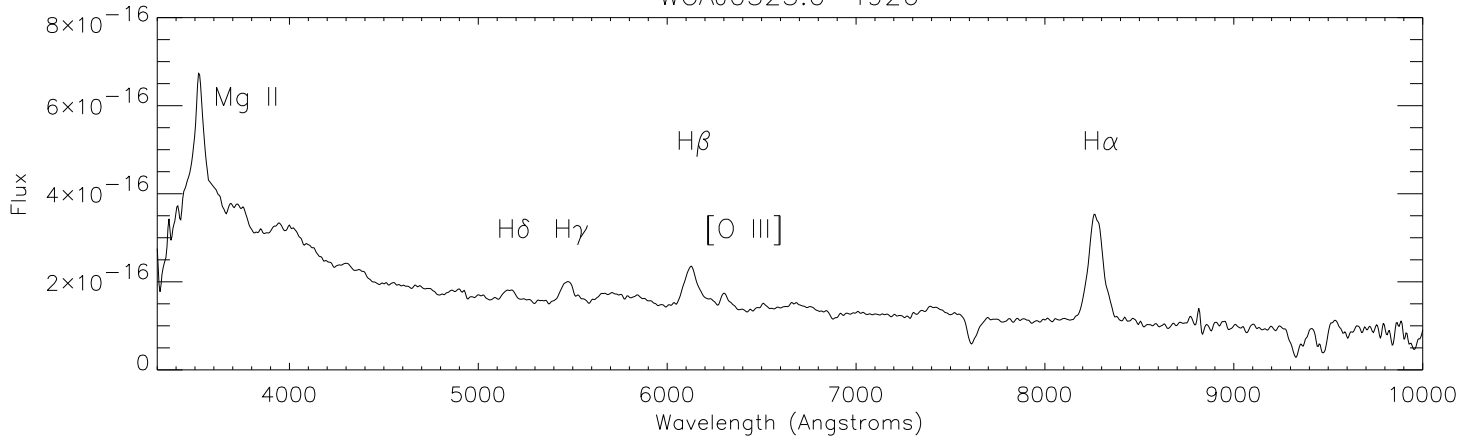




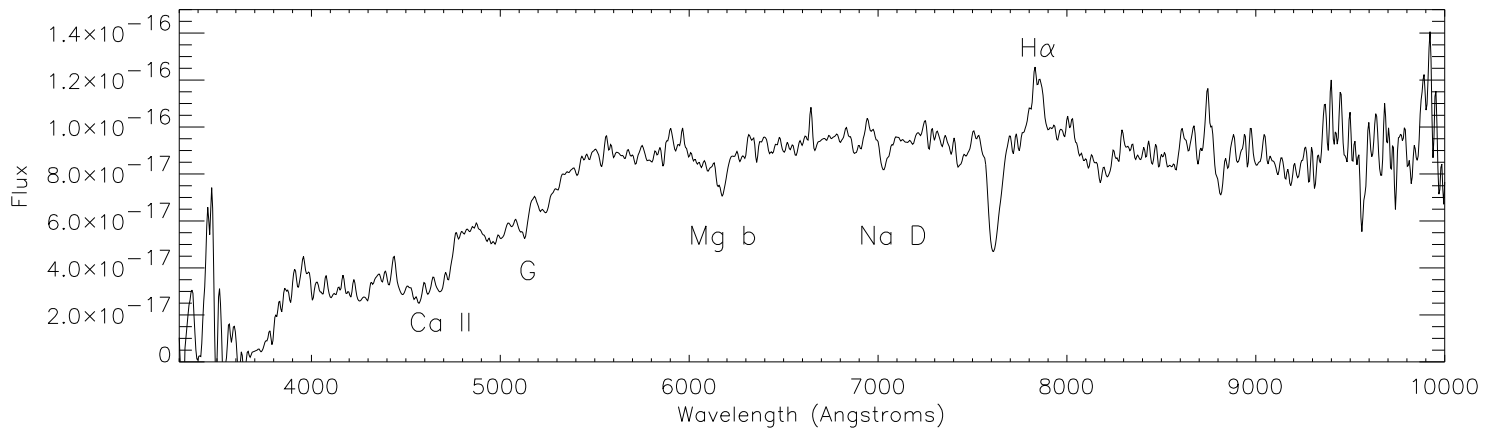




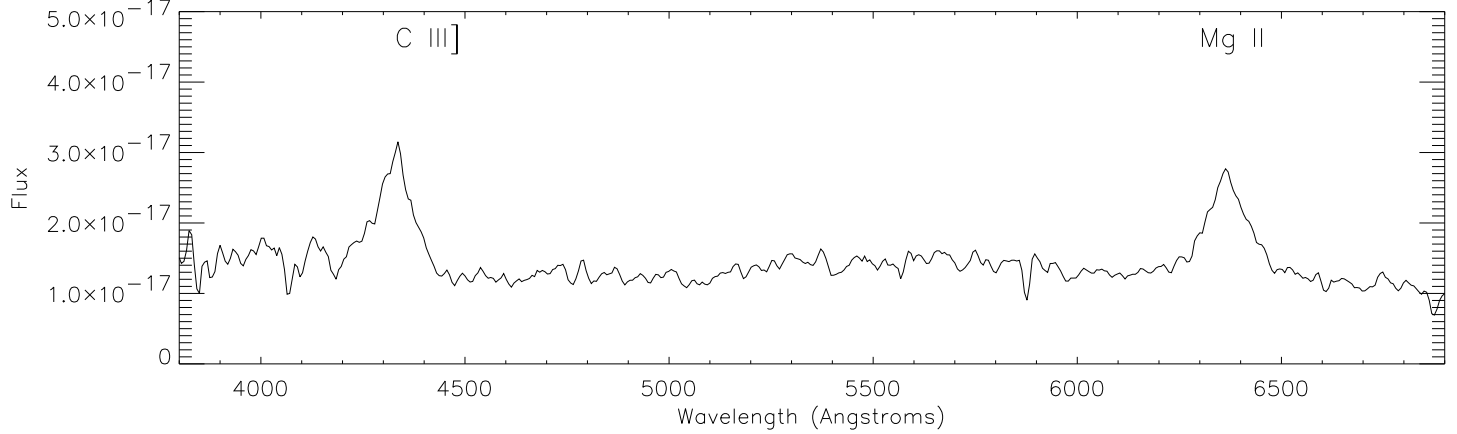
WGAJ0325.0-4926



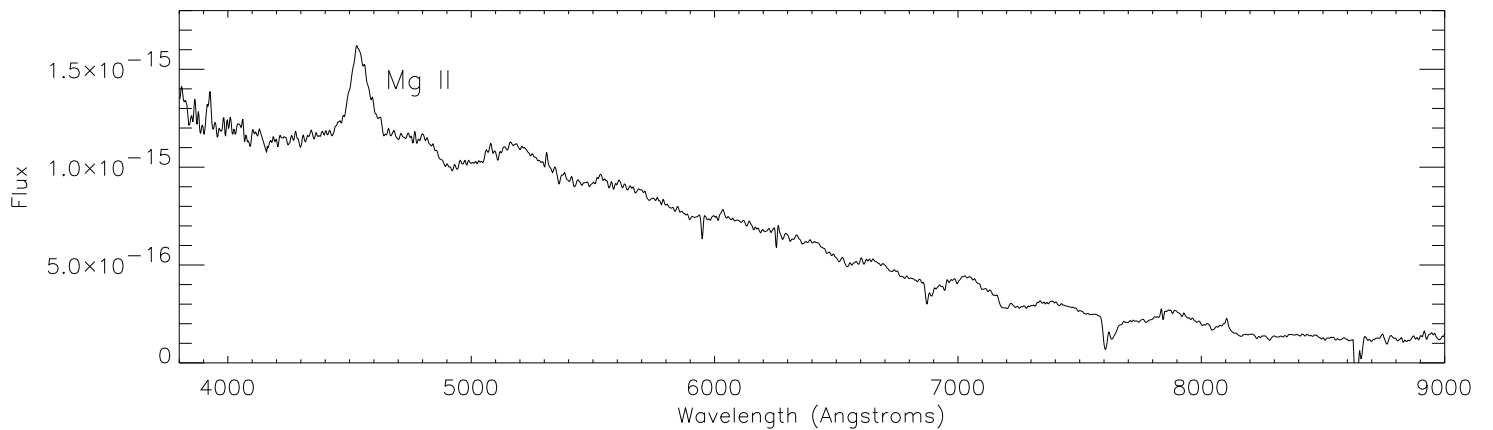
WGAJ0340.8-1814

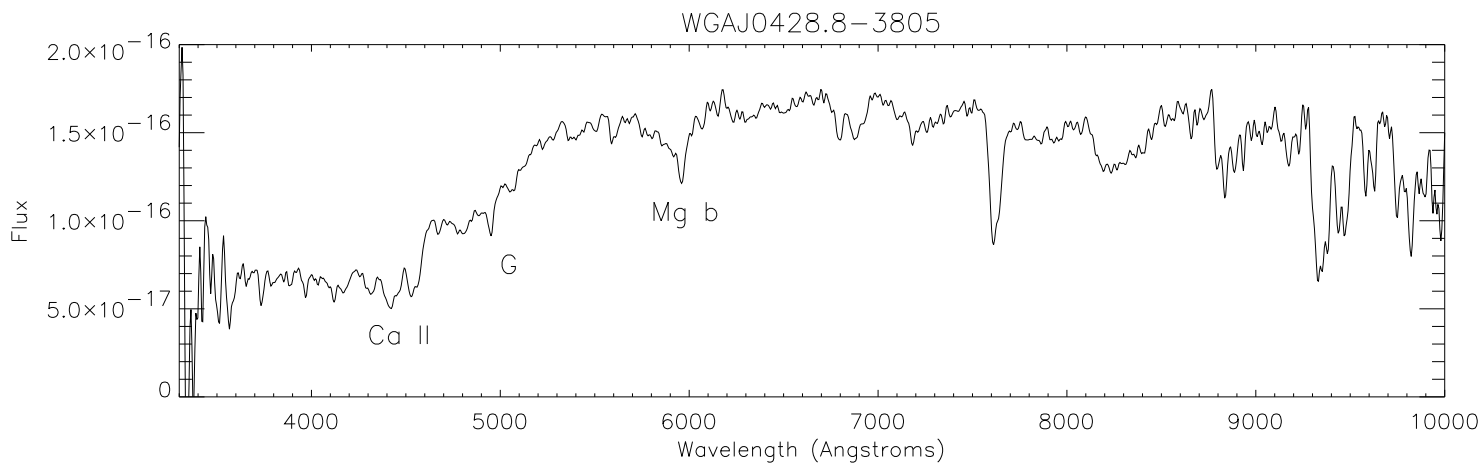
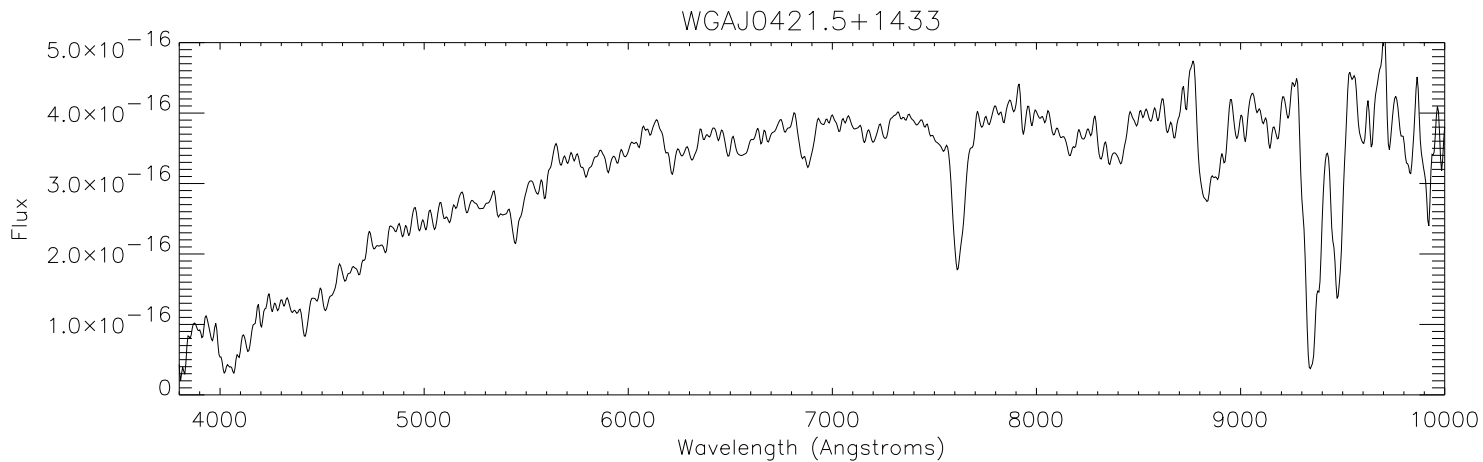
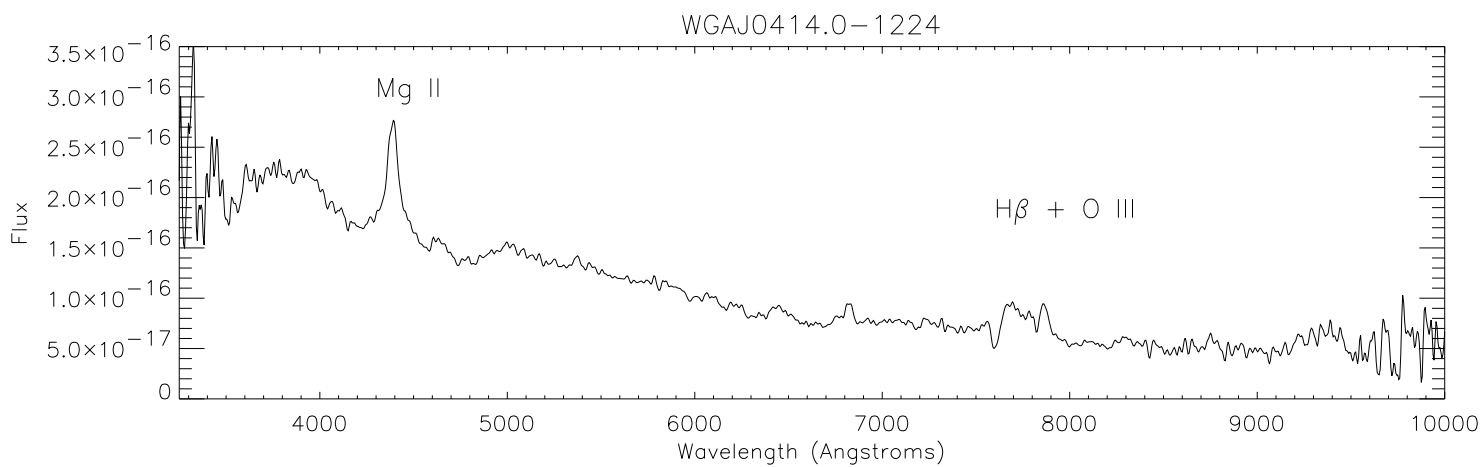
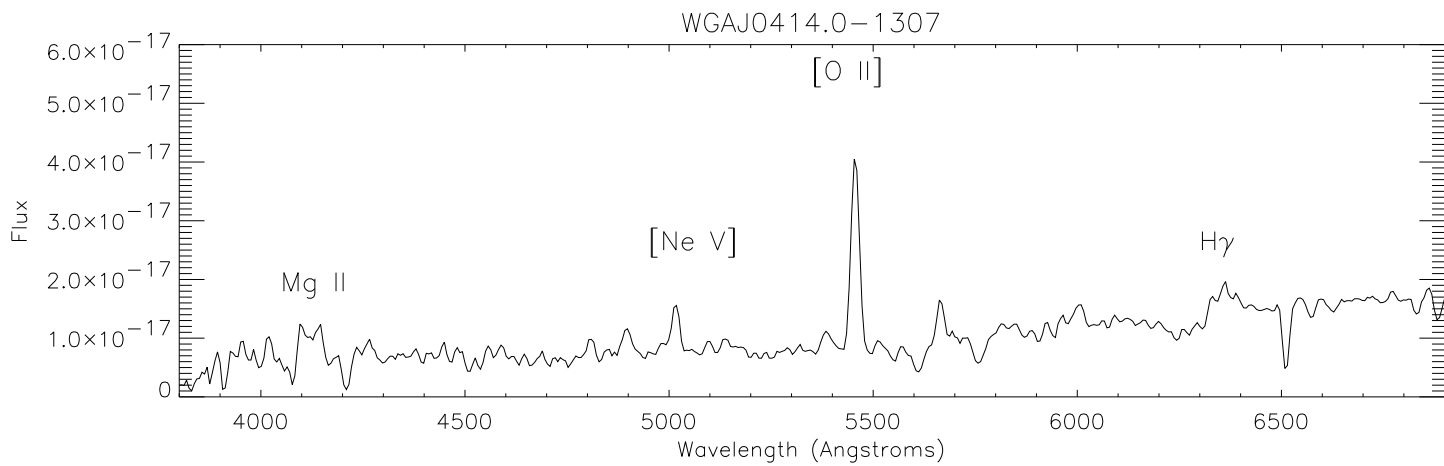


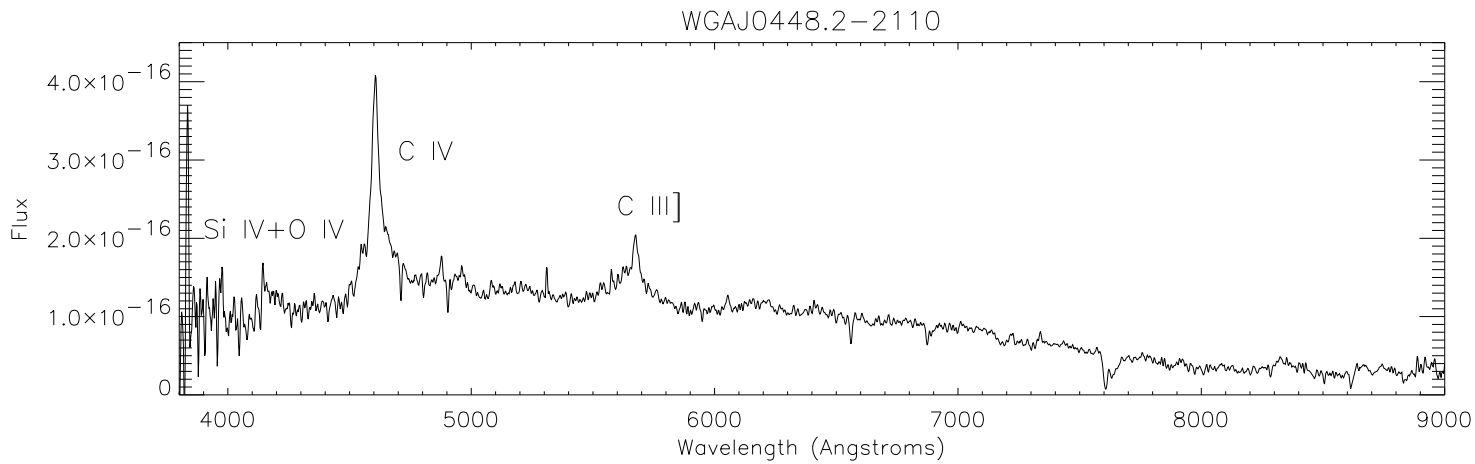
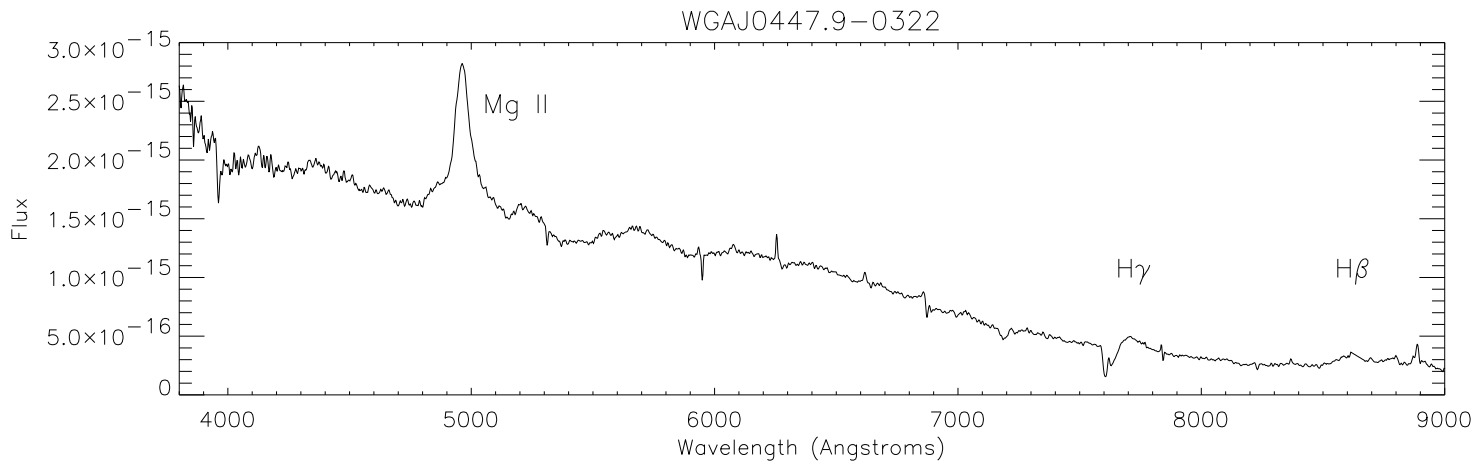
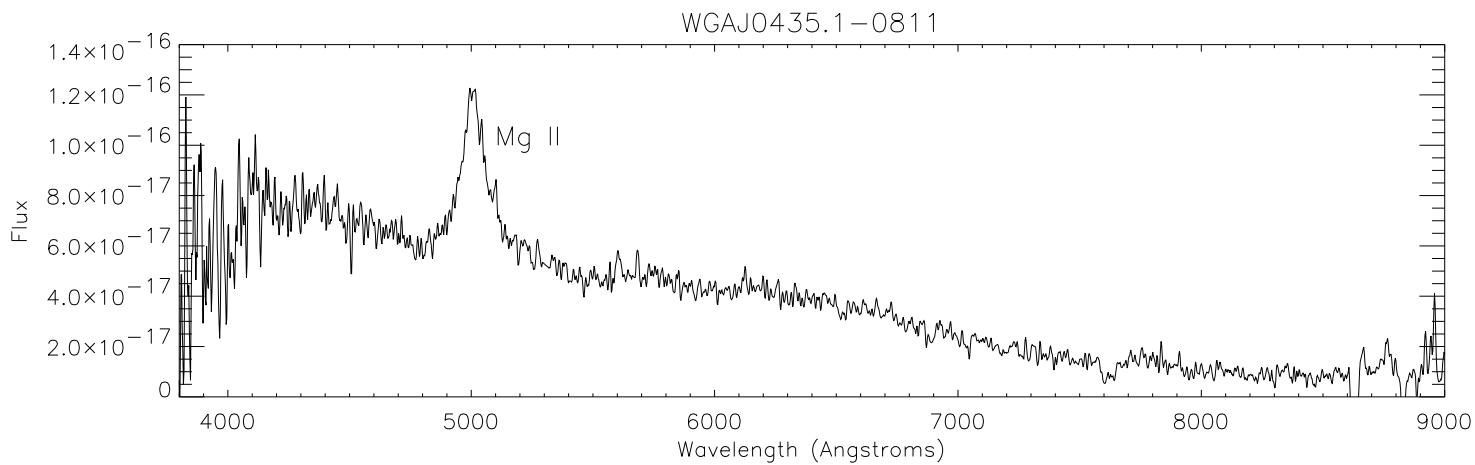
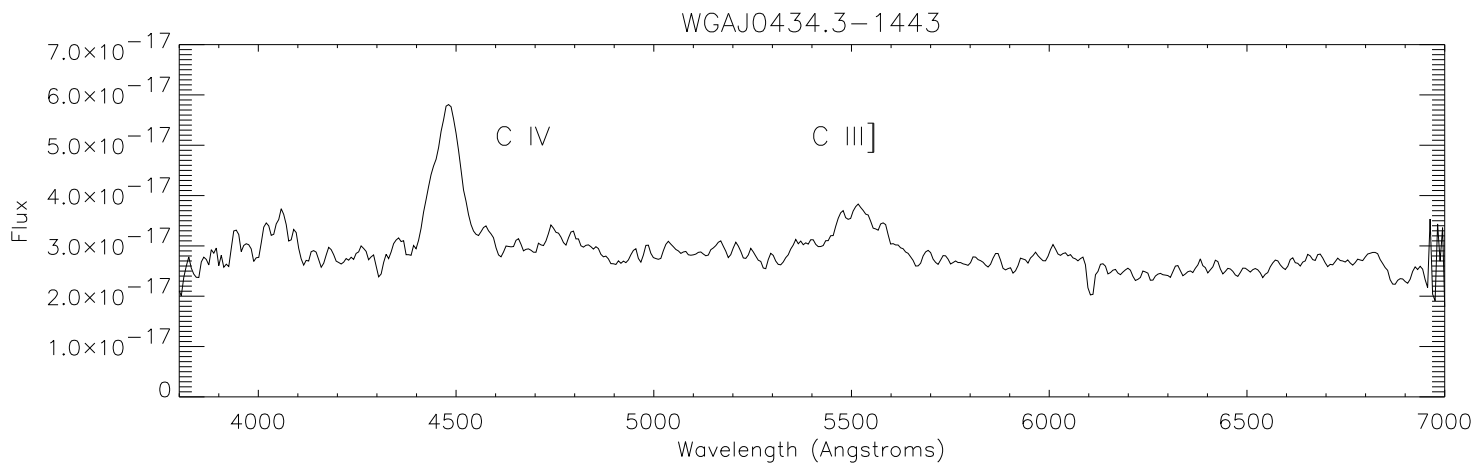
WGAJ0357.6-4158

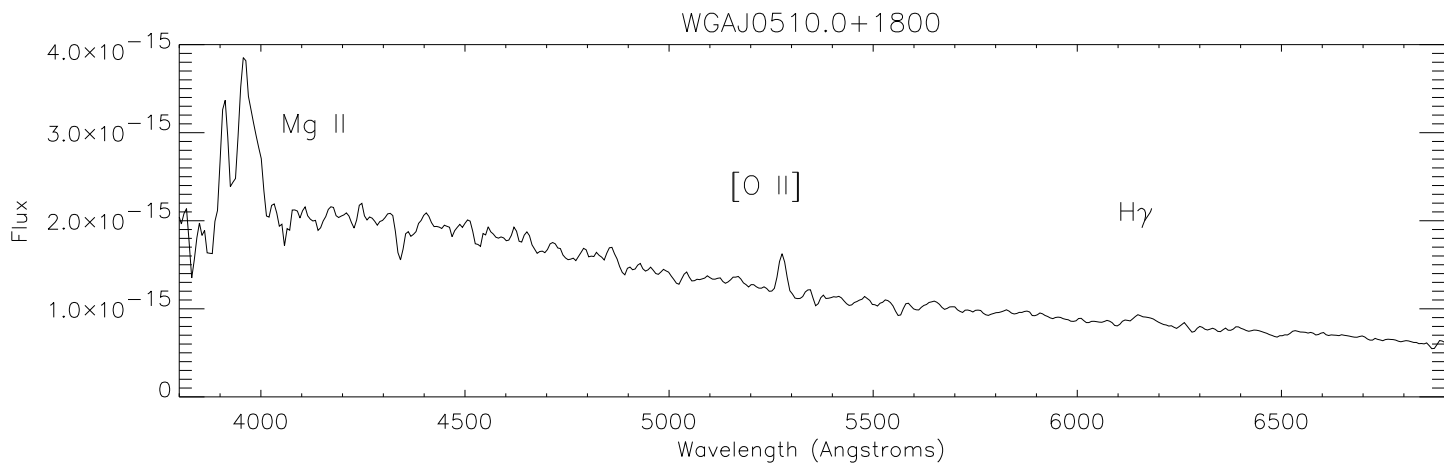
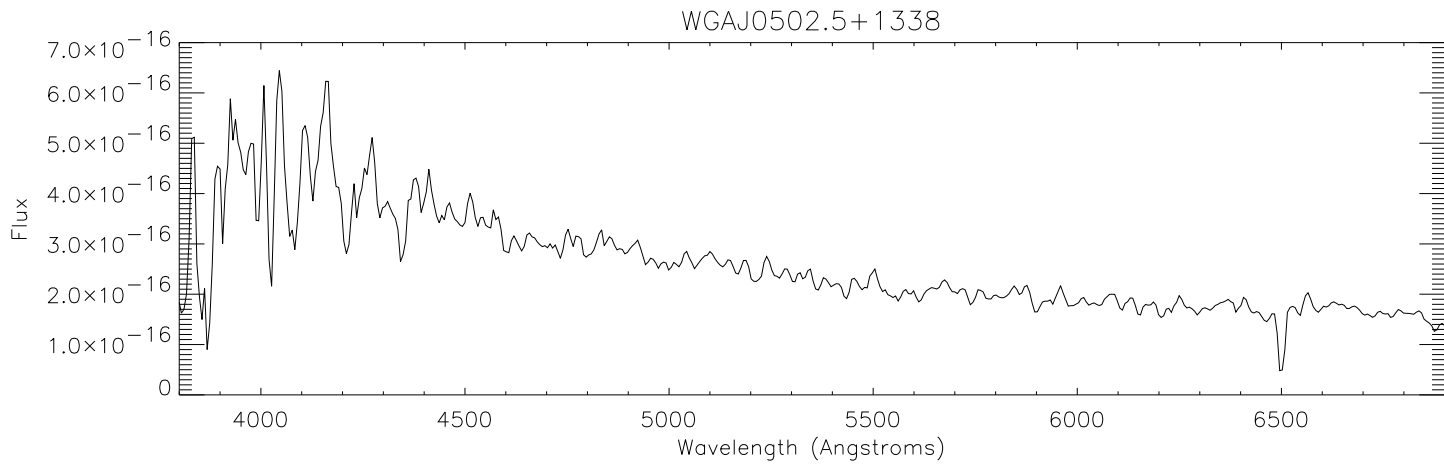
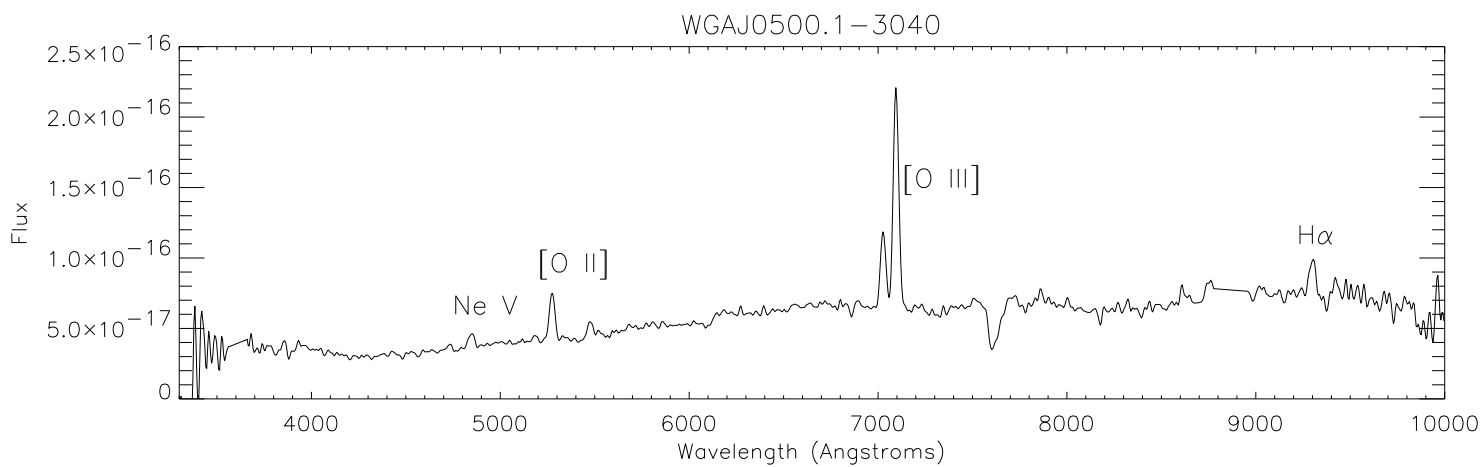
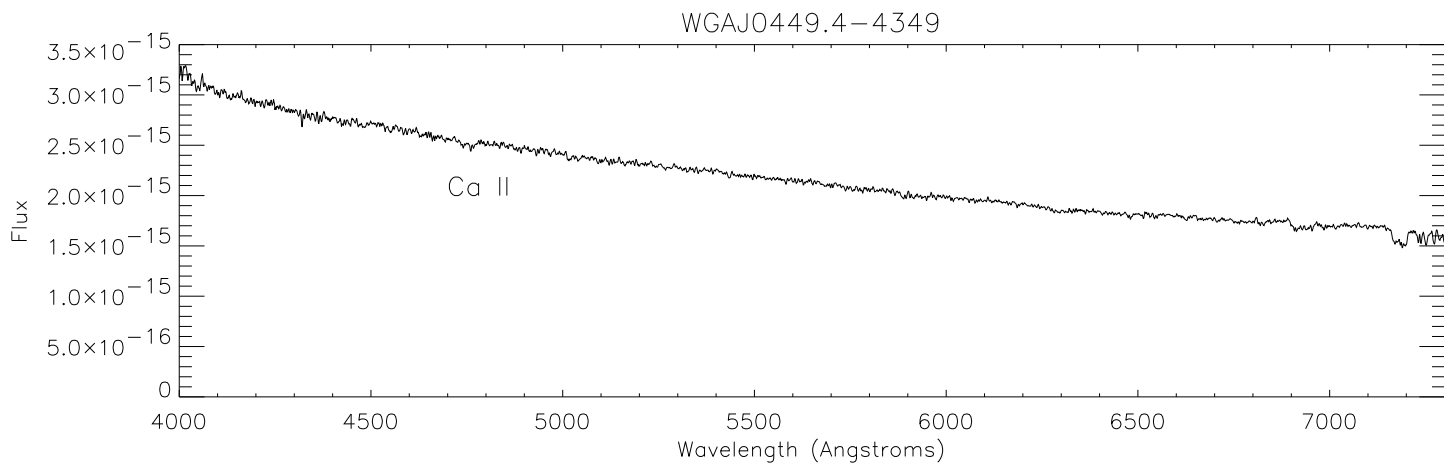


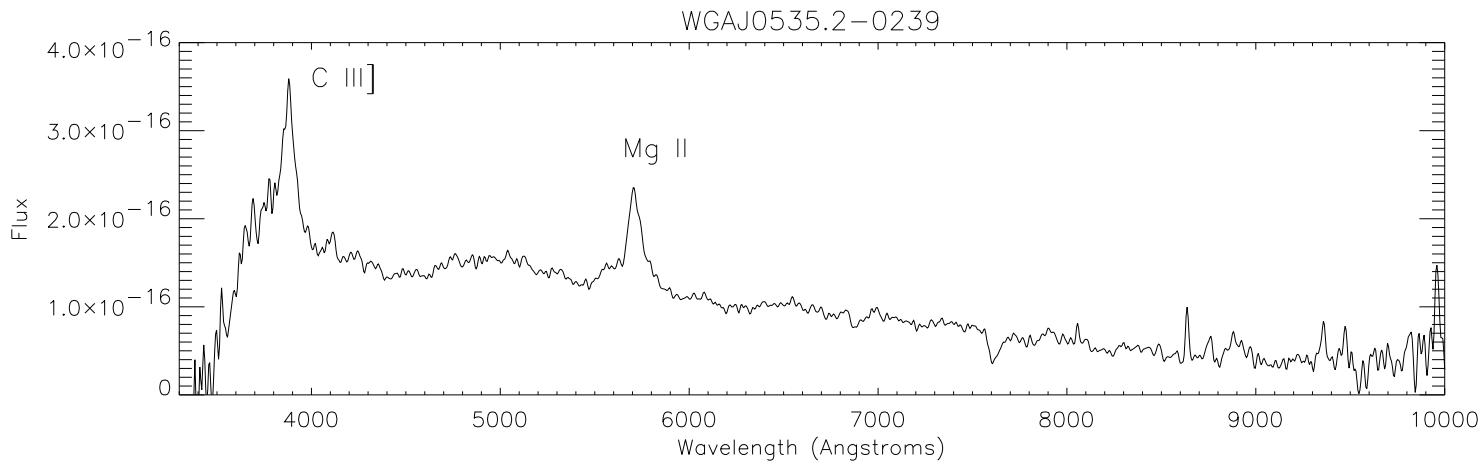
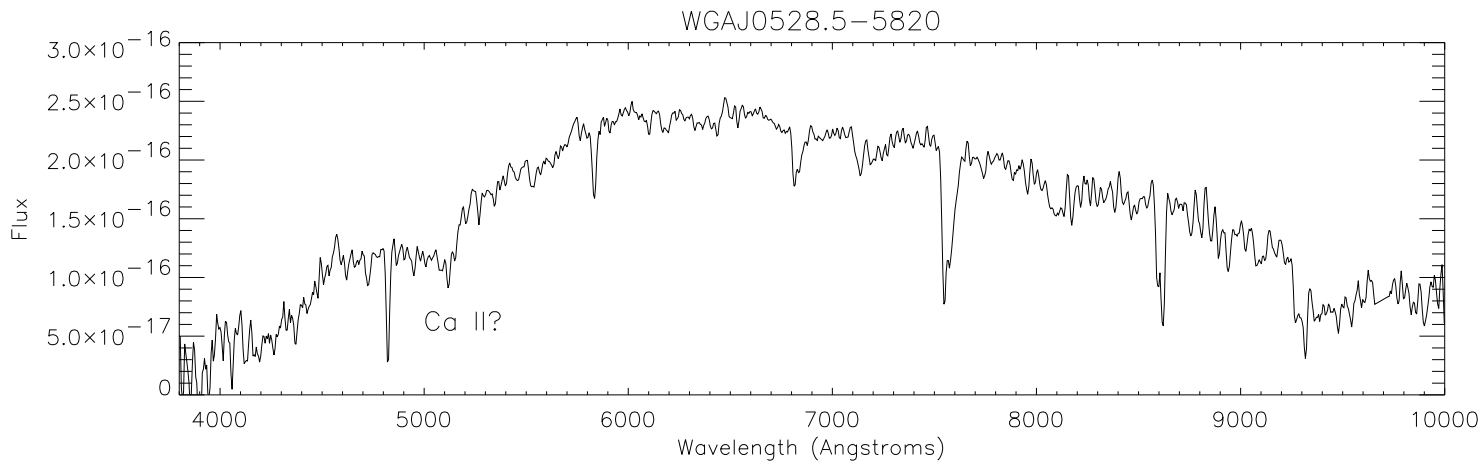
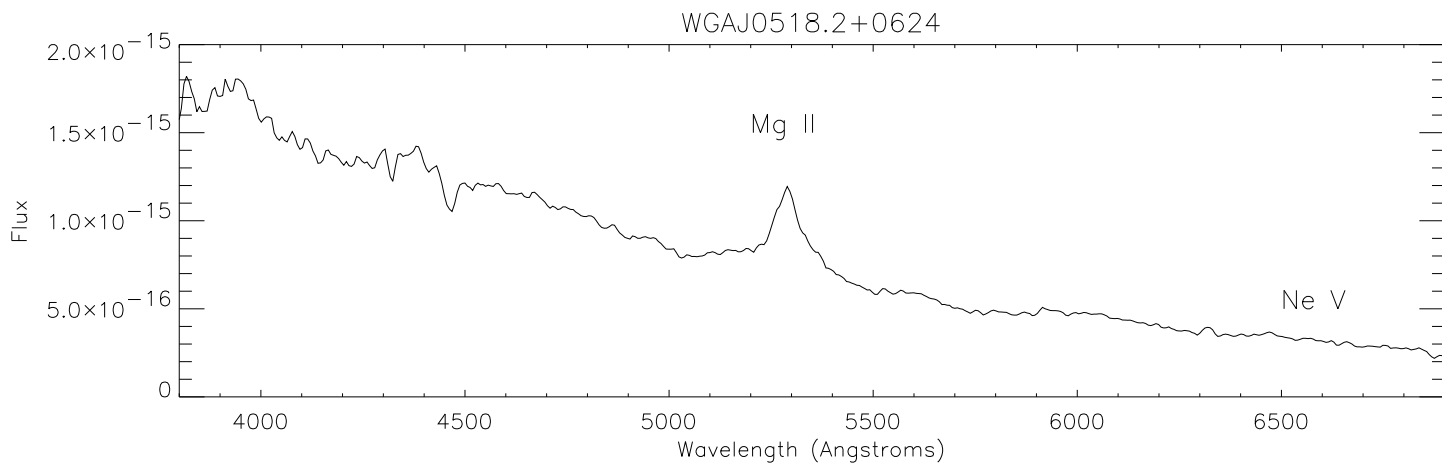
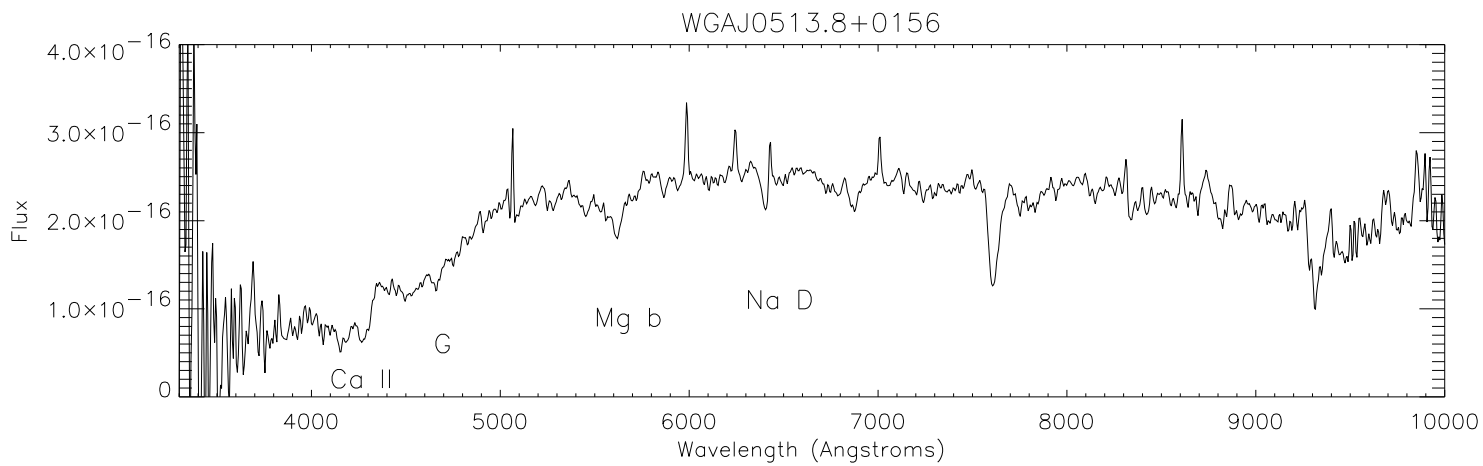
WGAJ0411.0-1637

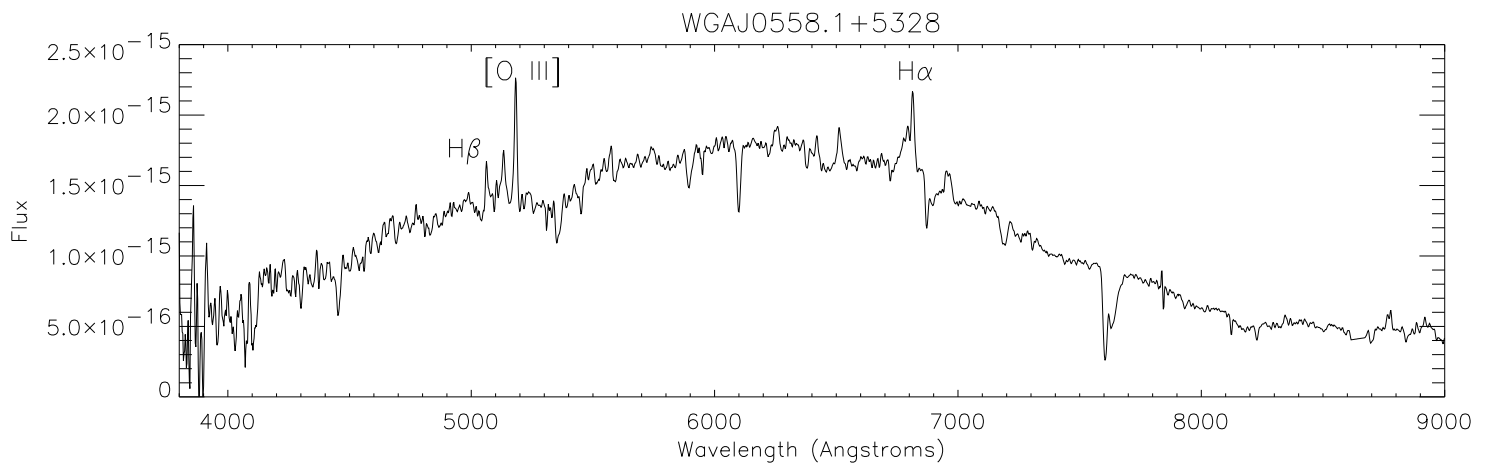
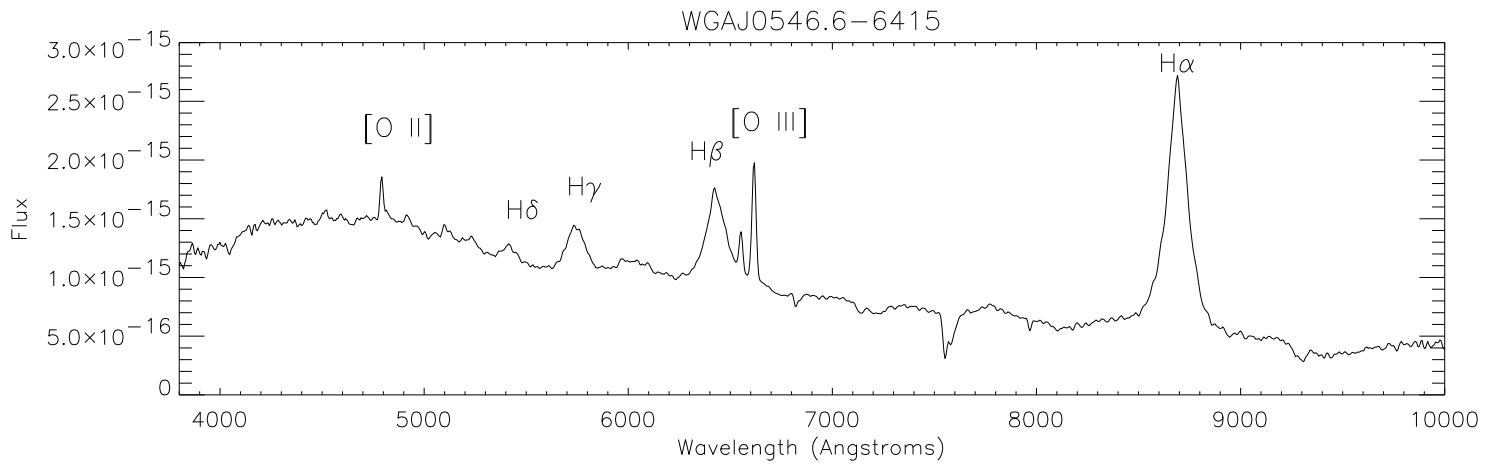
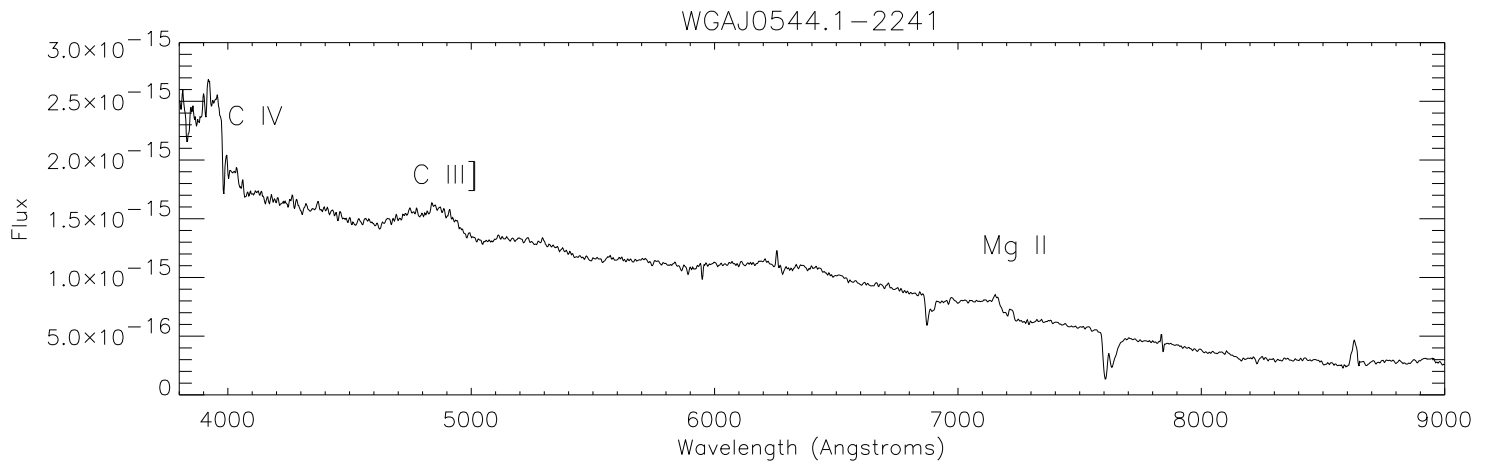
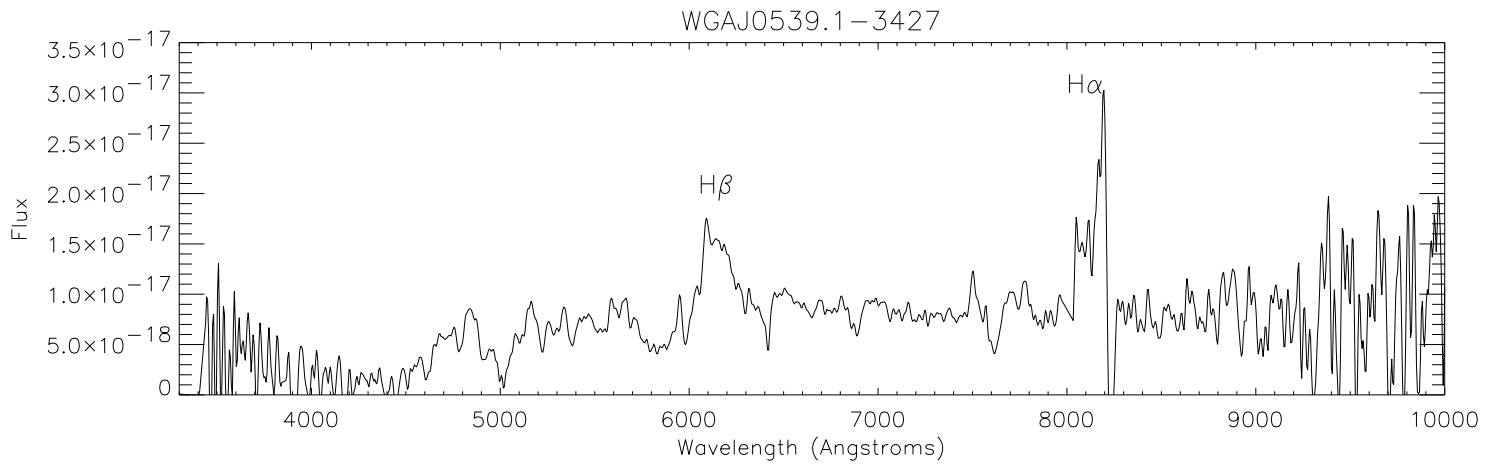


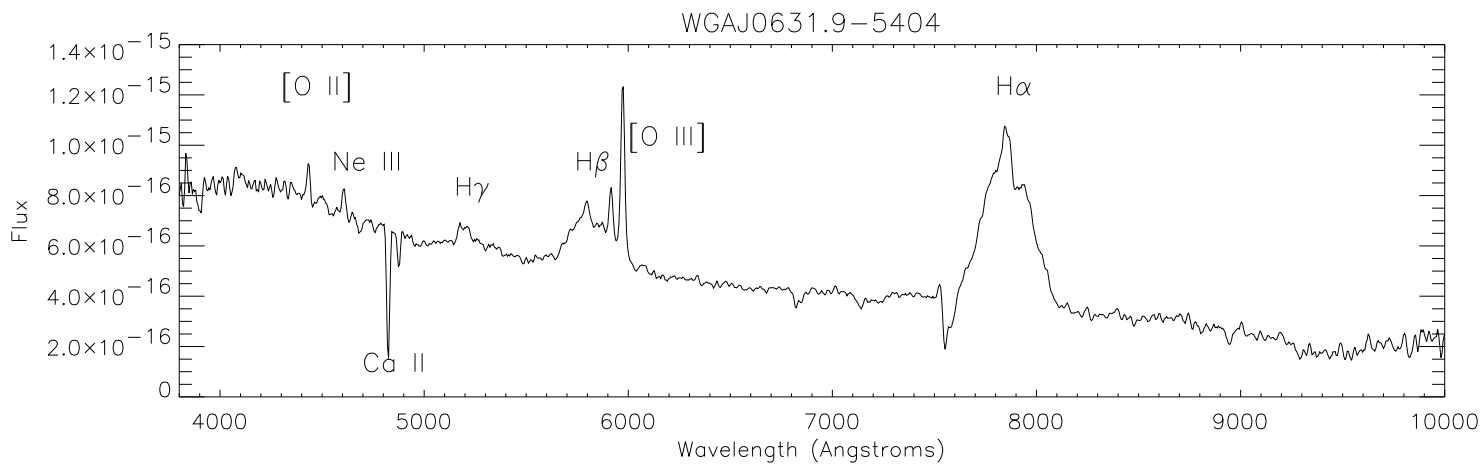
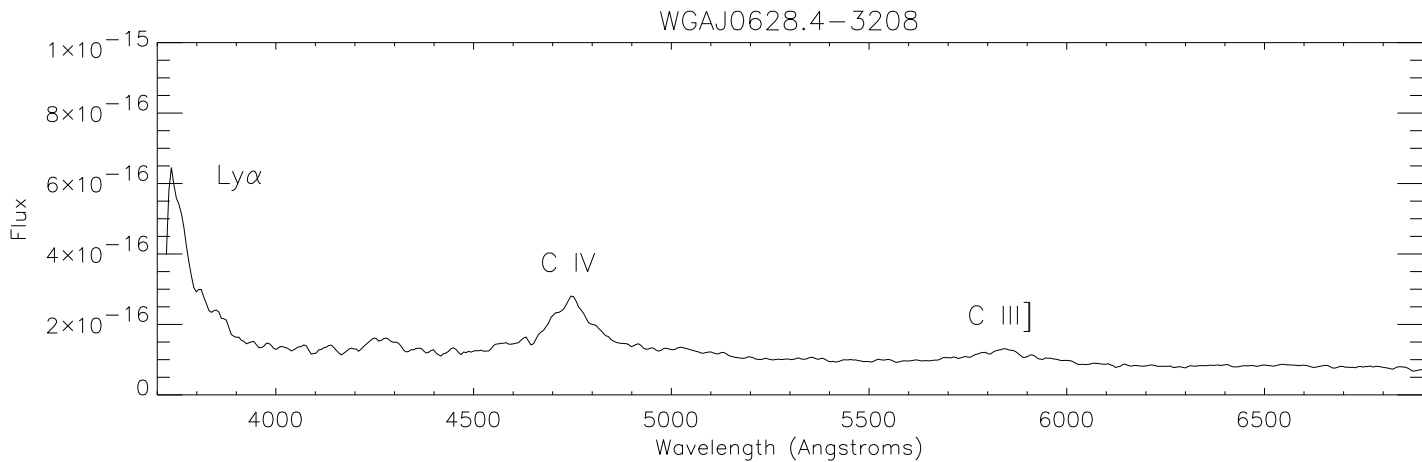
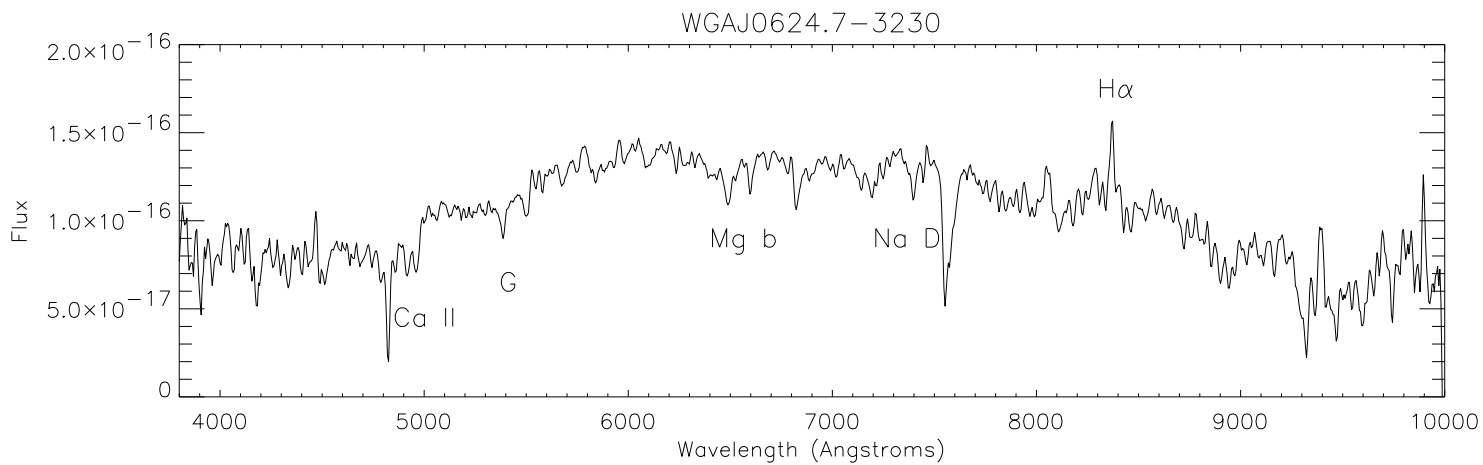
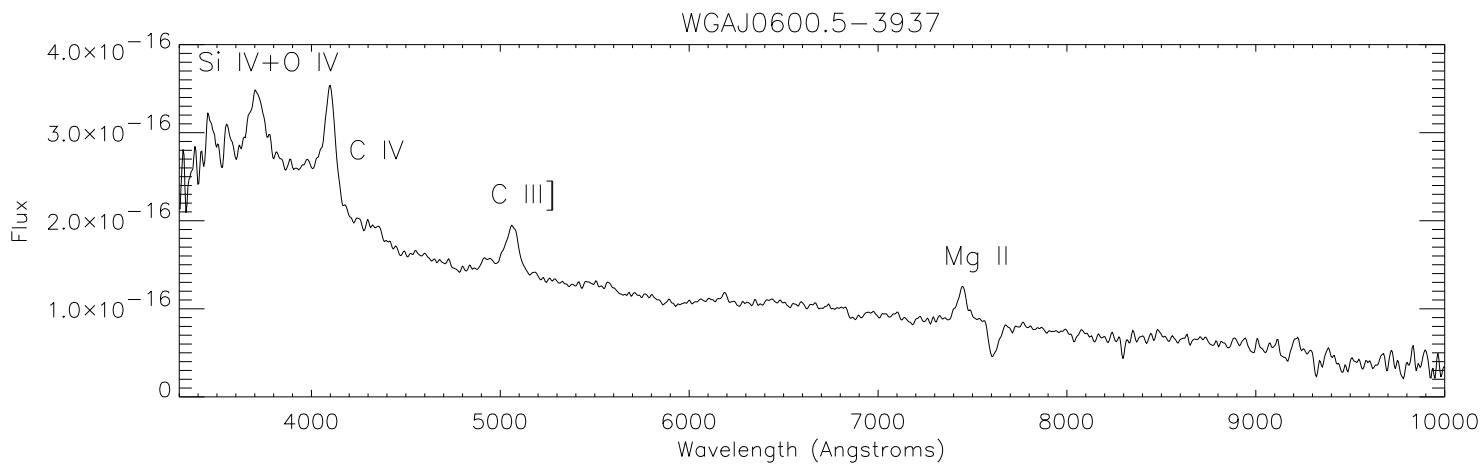


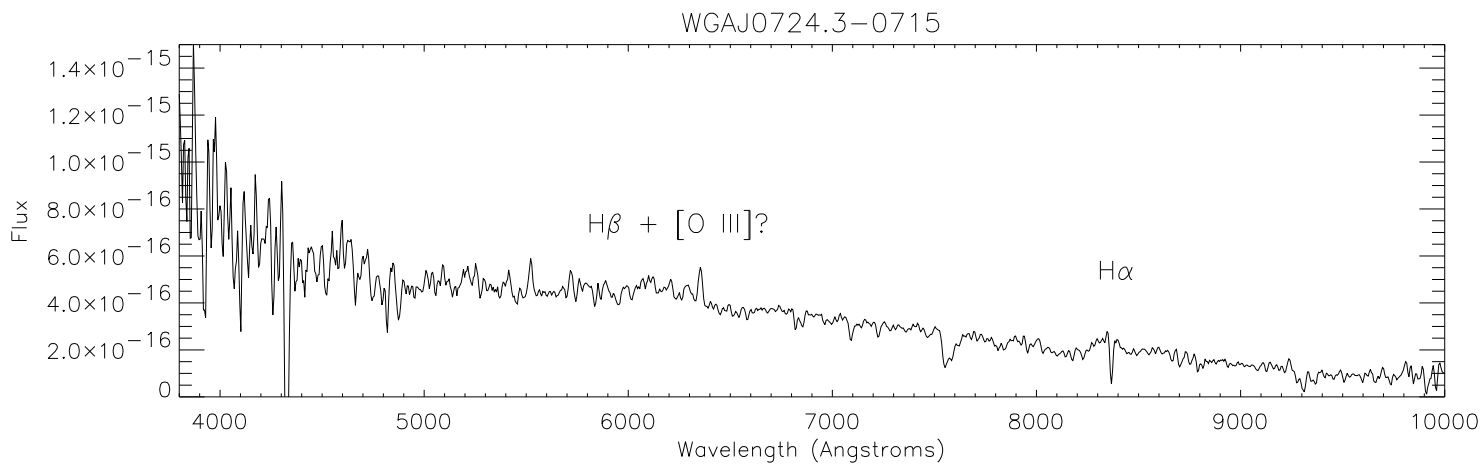
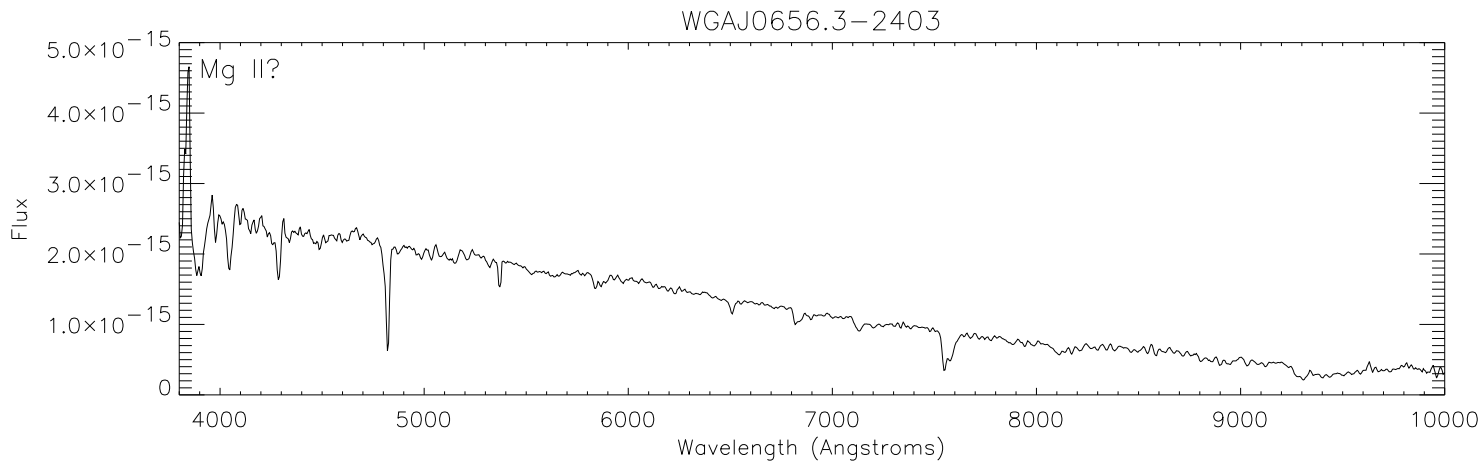
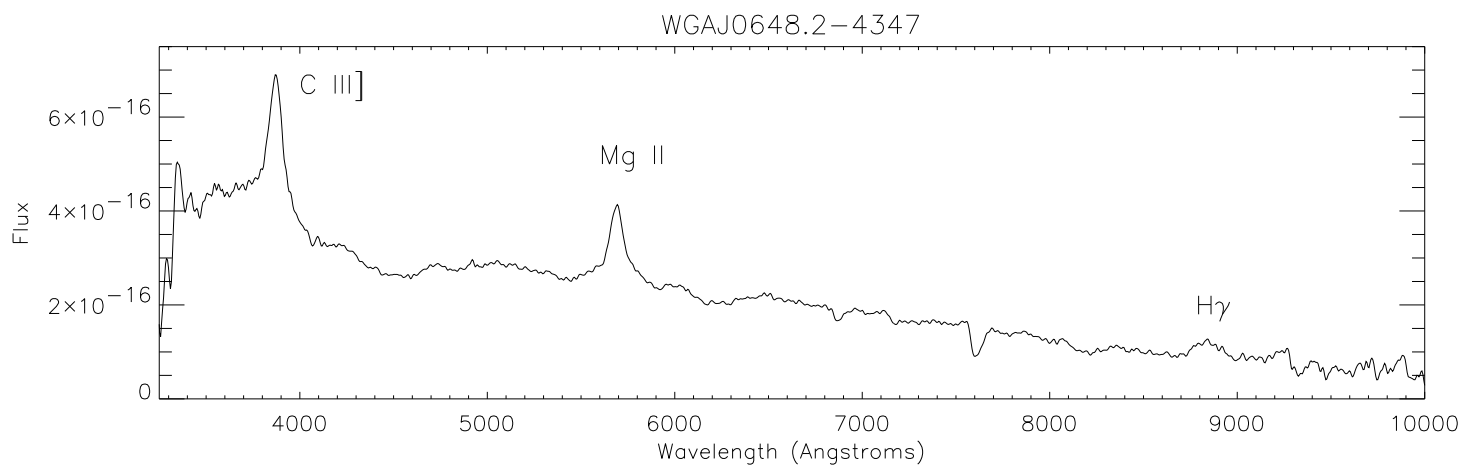
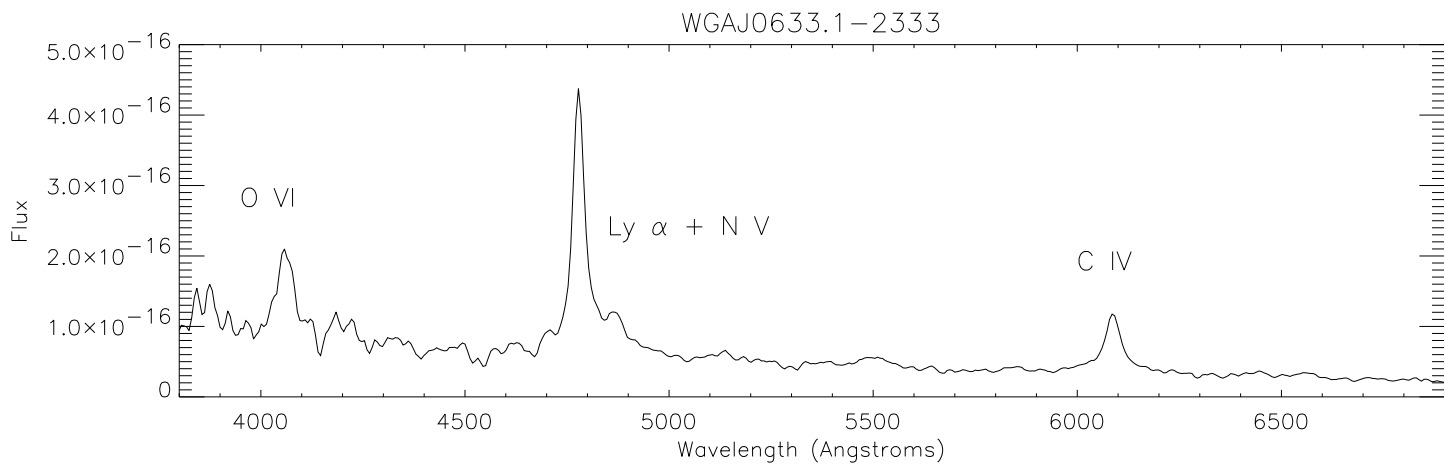


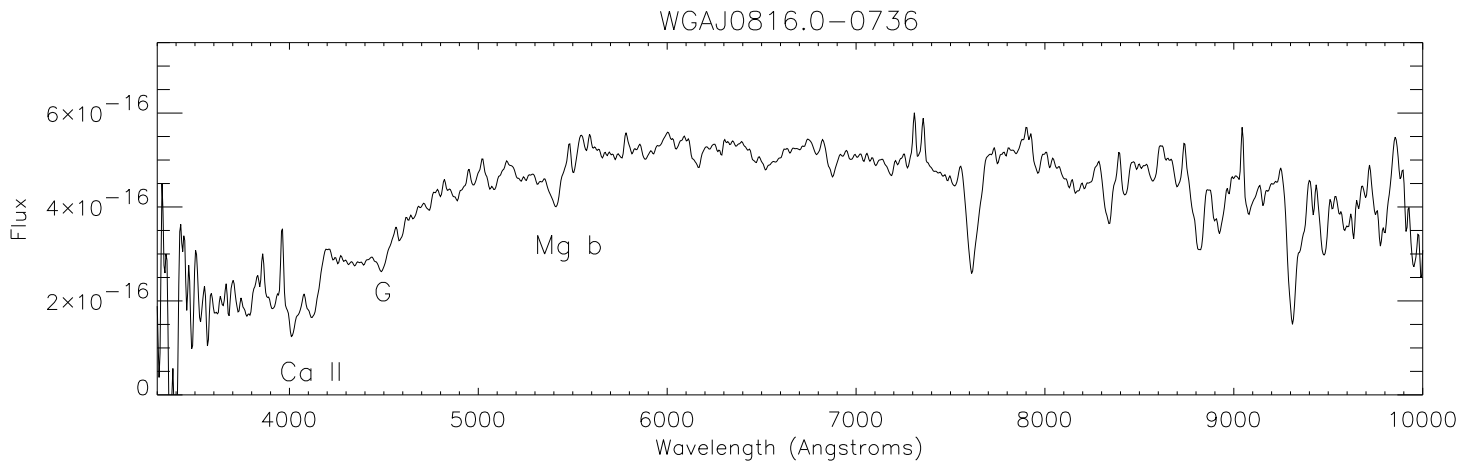
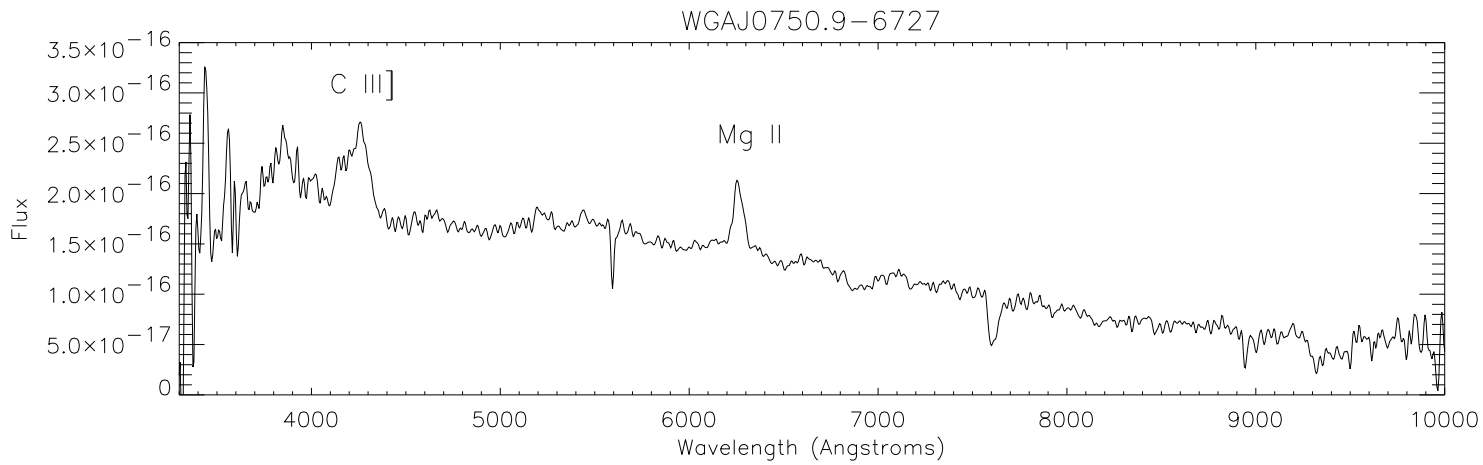
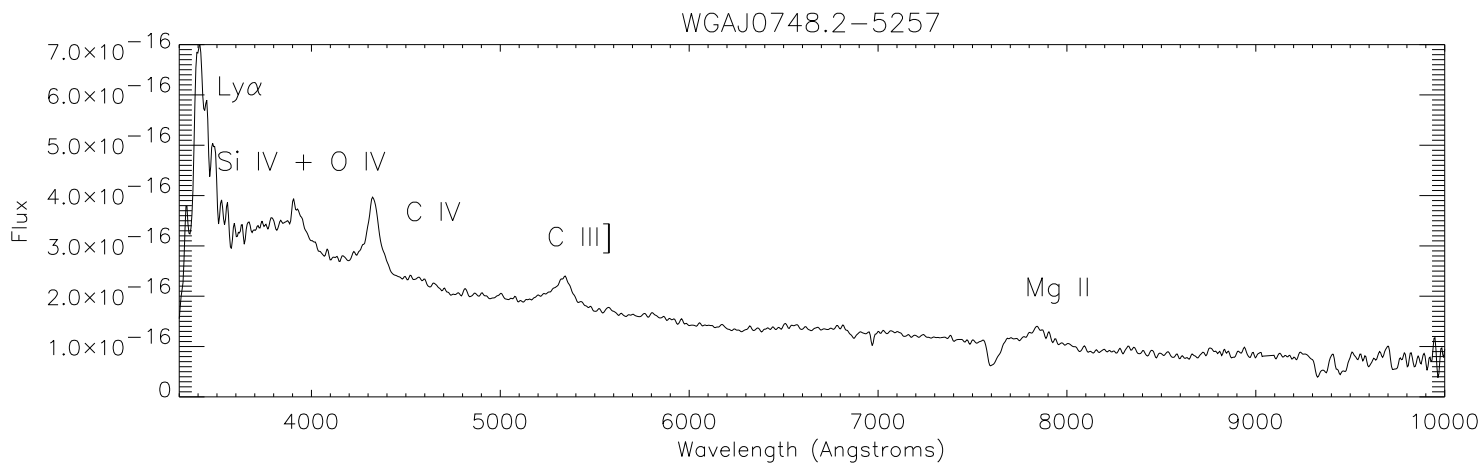
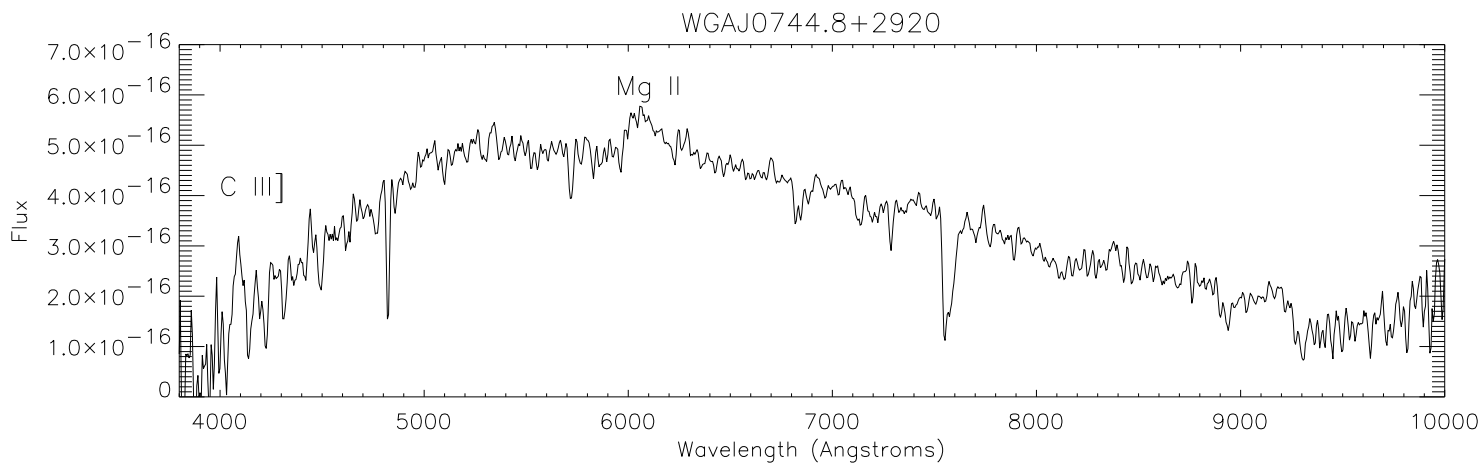


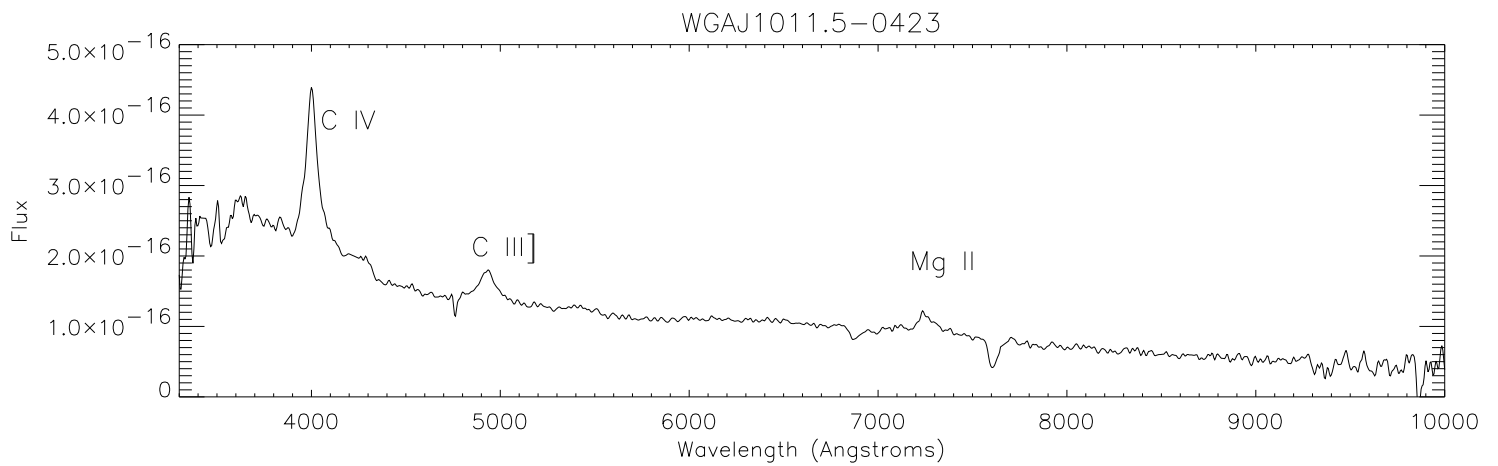
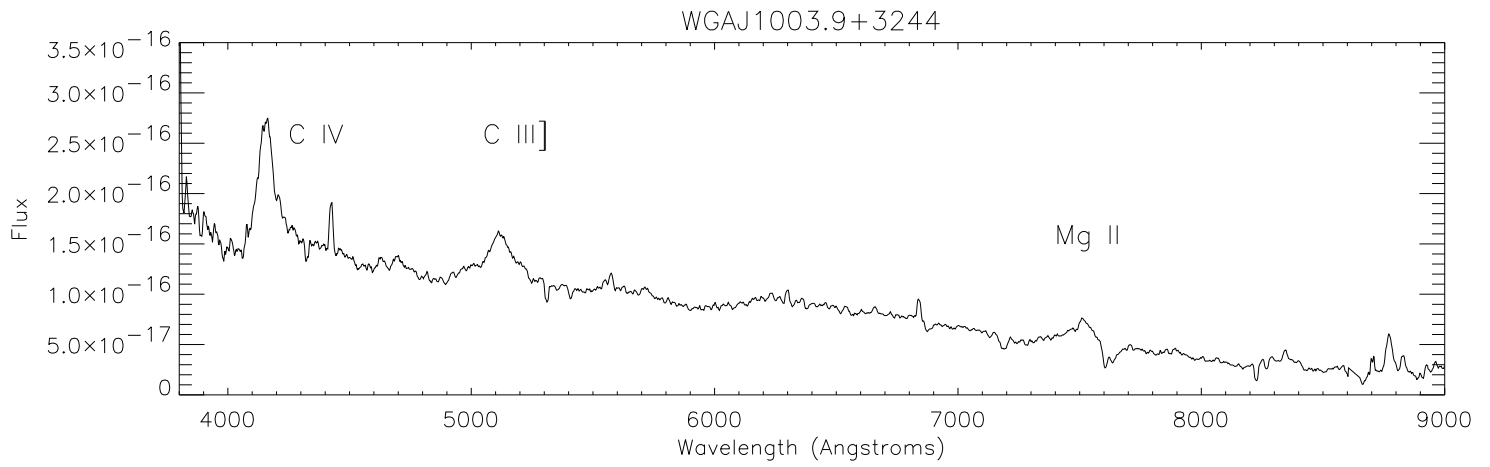
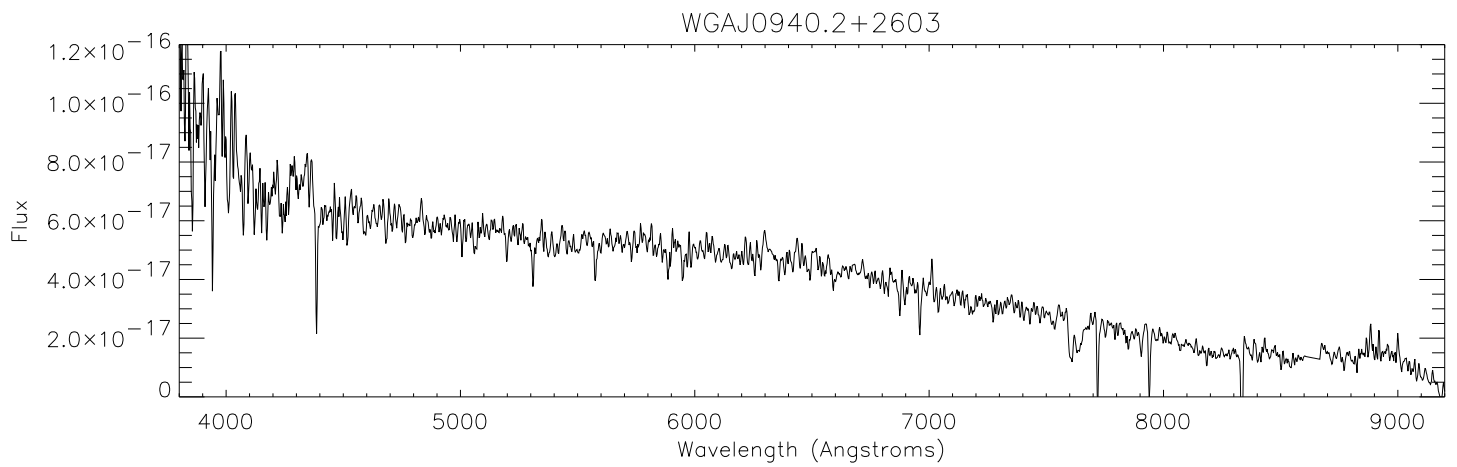
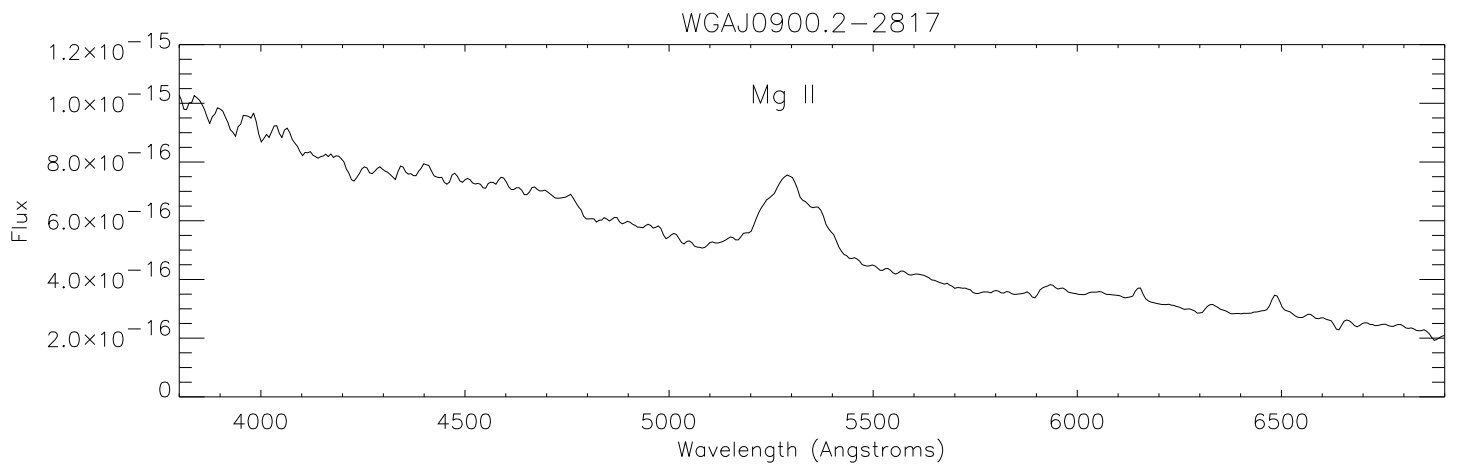


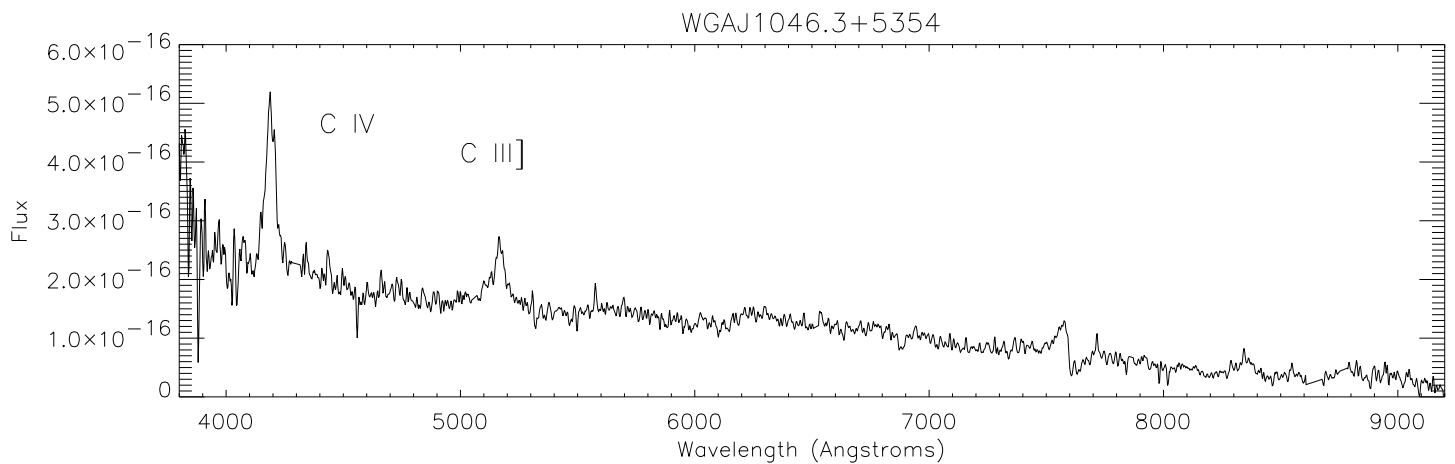
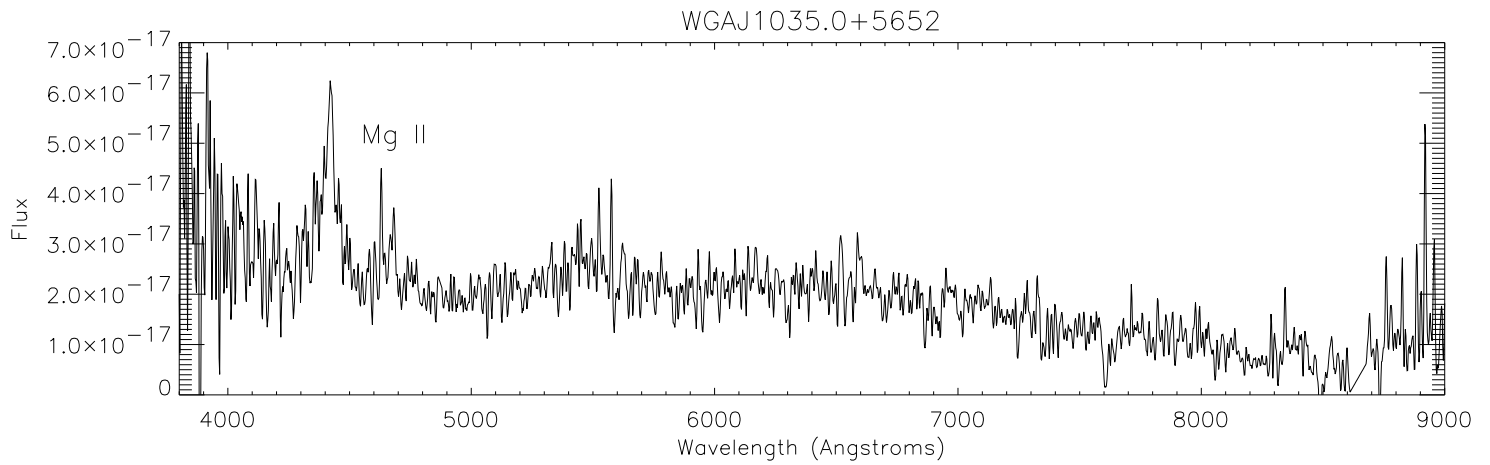
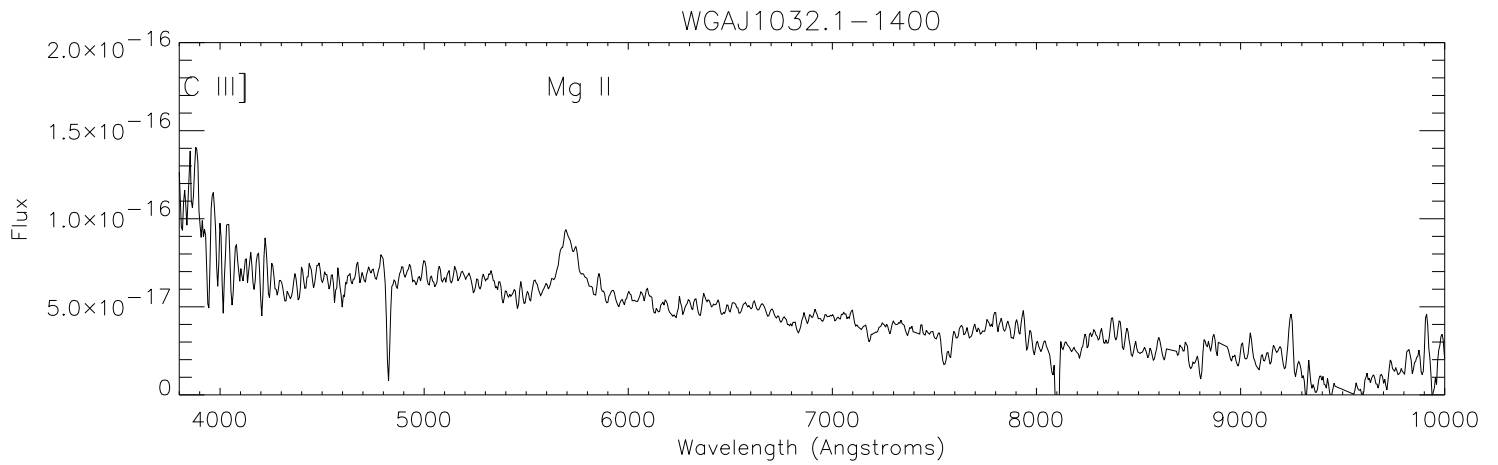
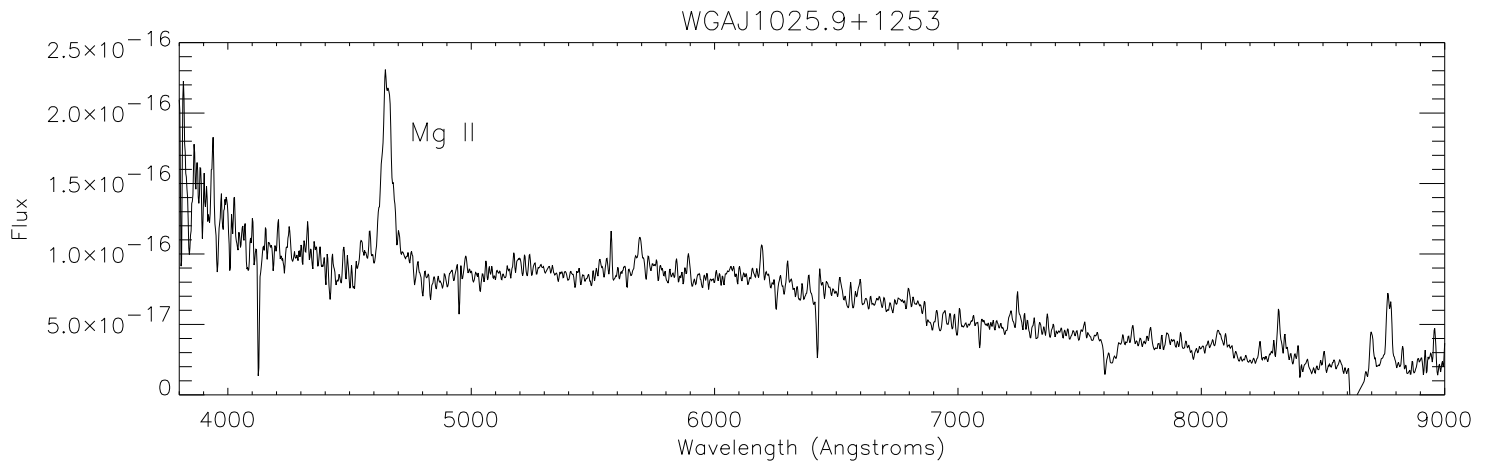




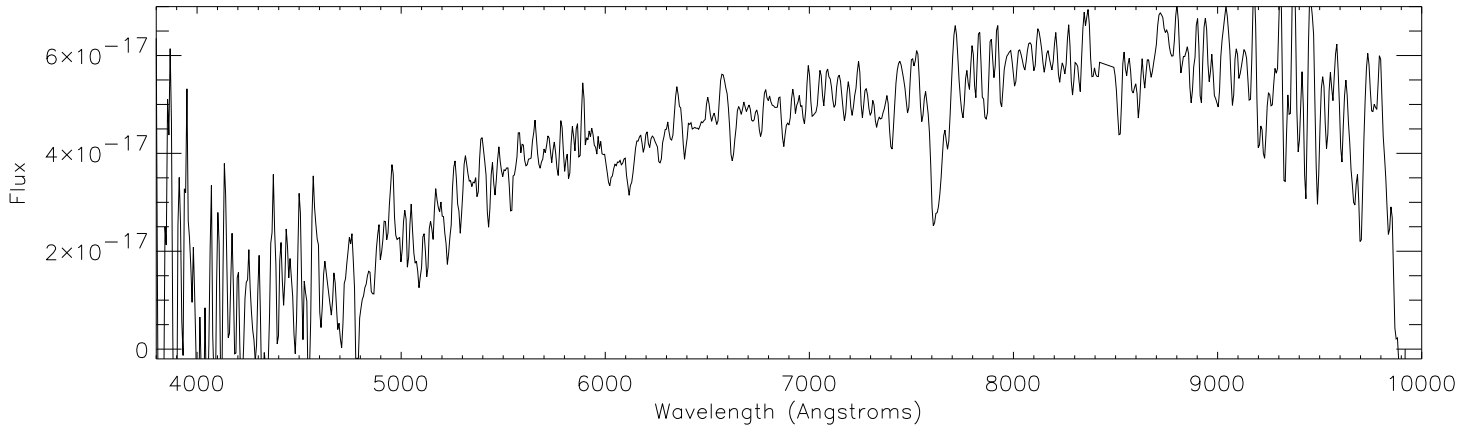




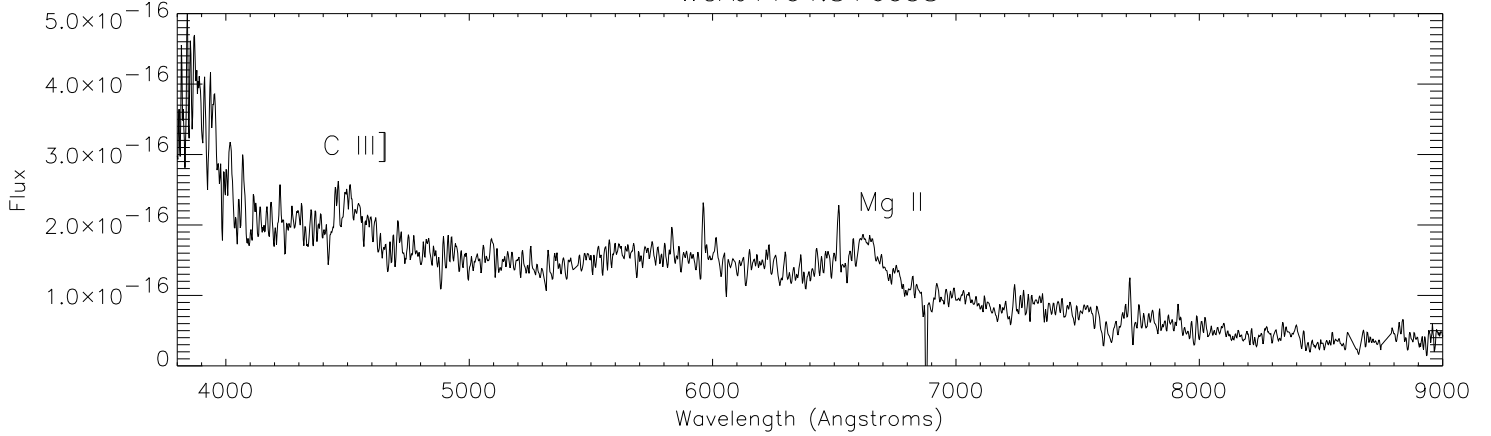




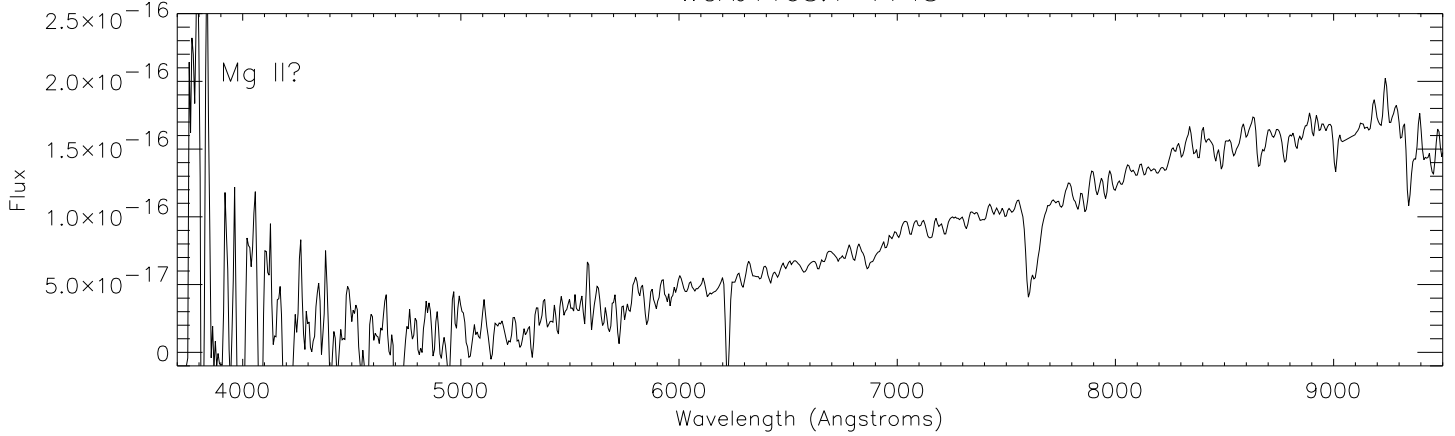
WGAJ1057.7-7724



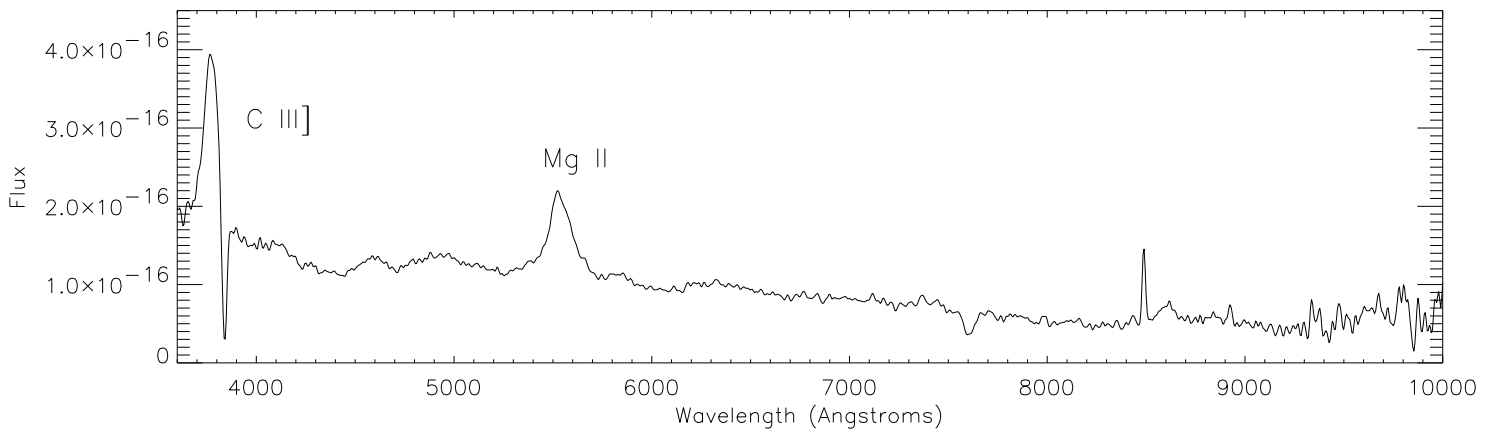
WGAJ1104.8+6038

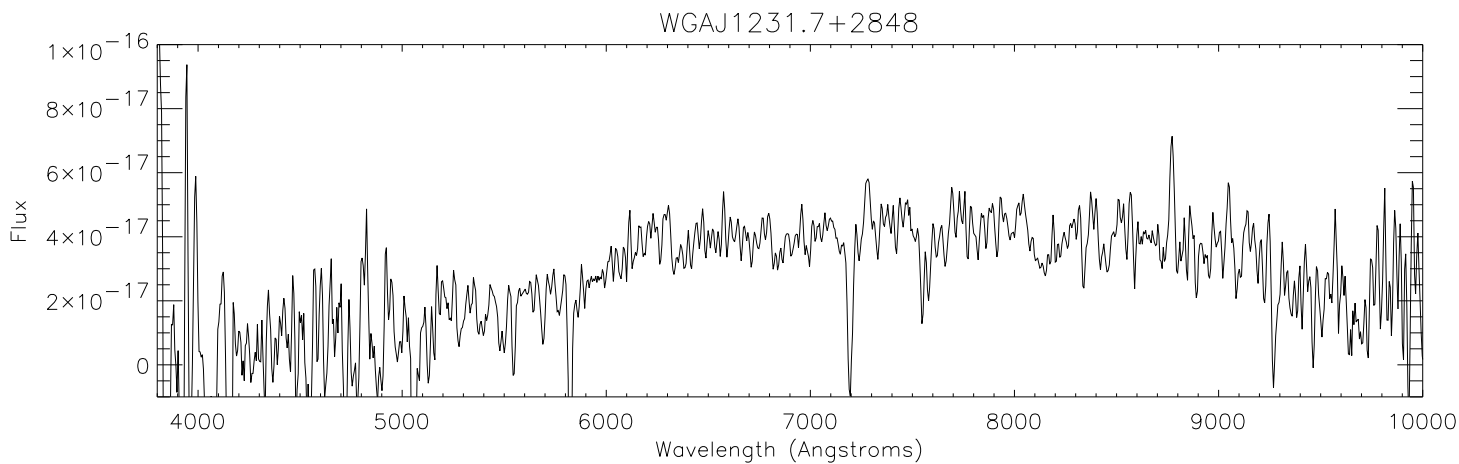
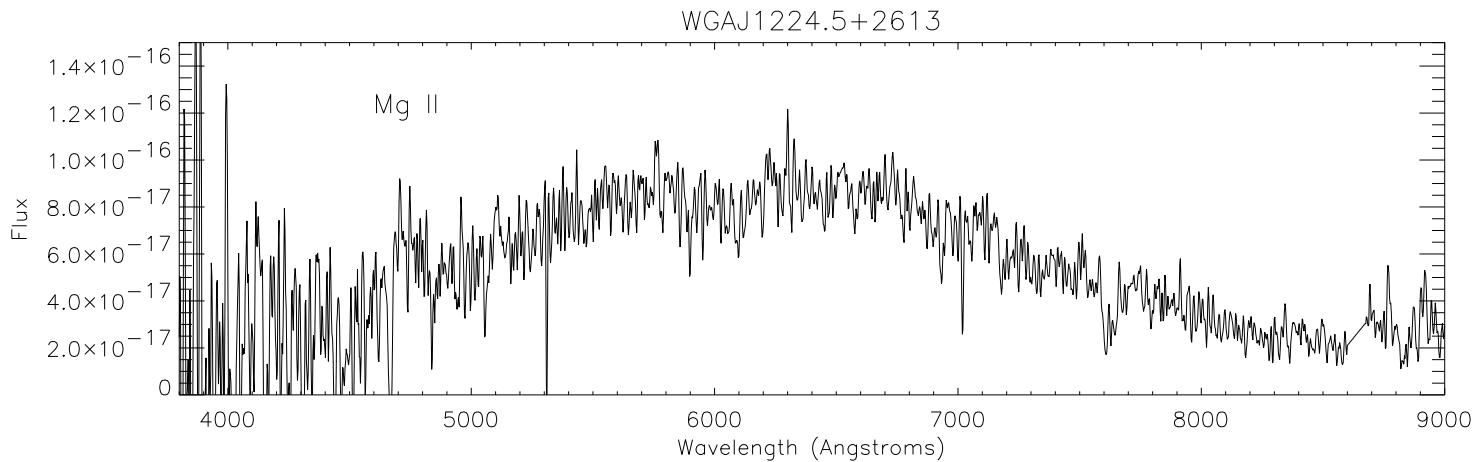
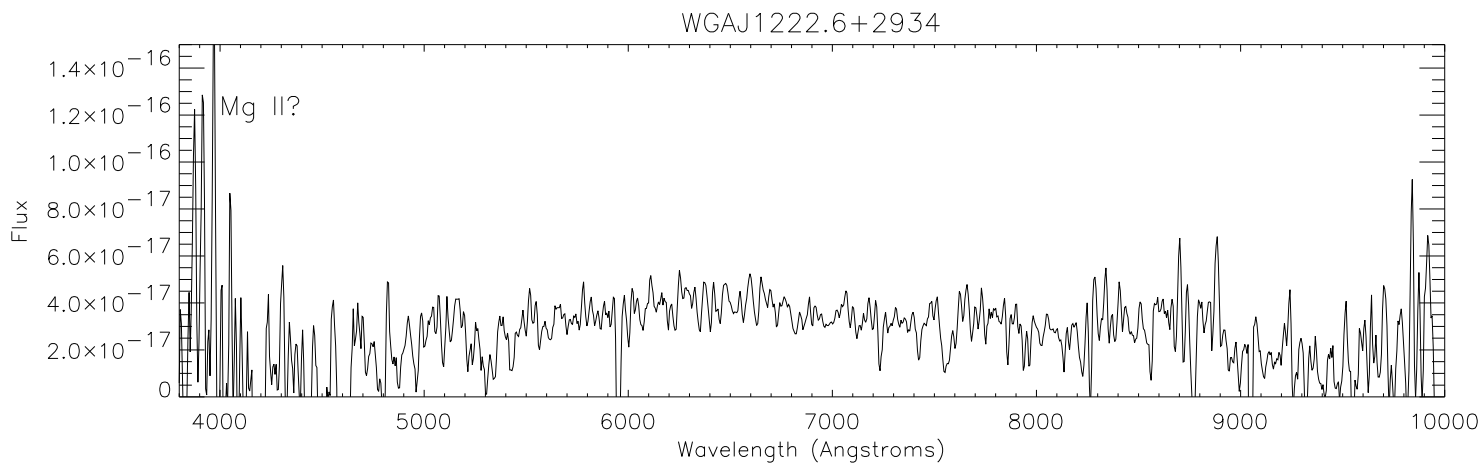
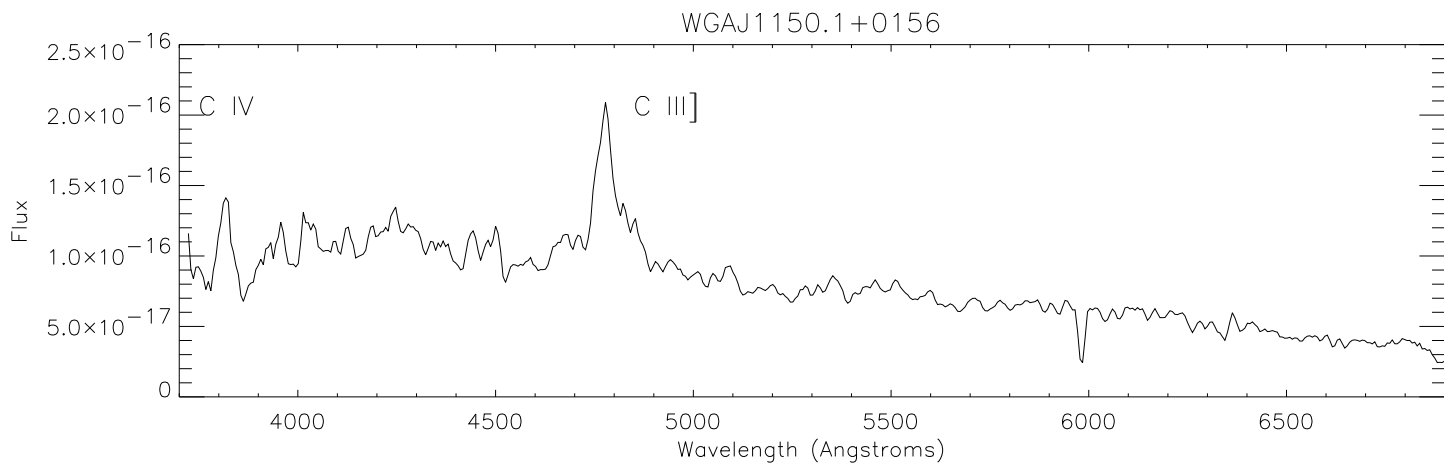


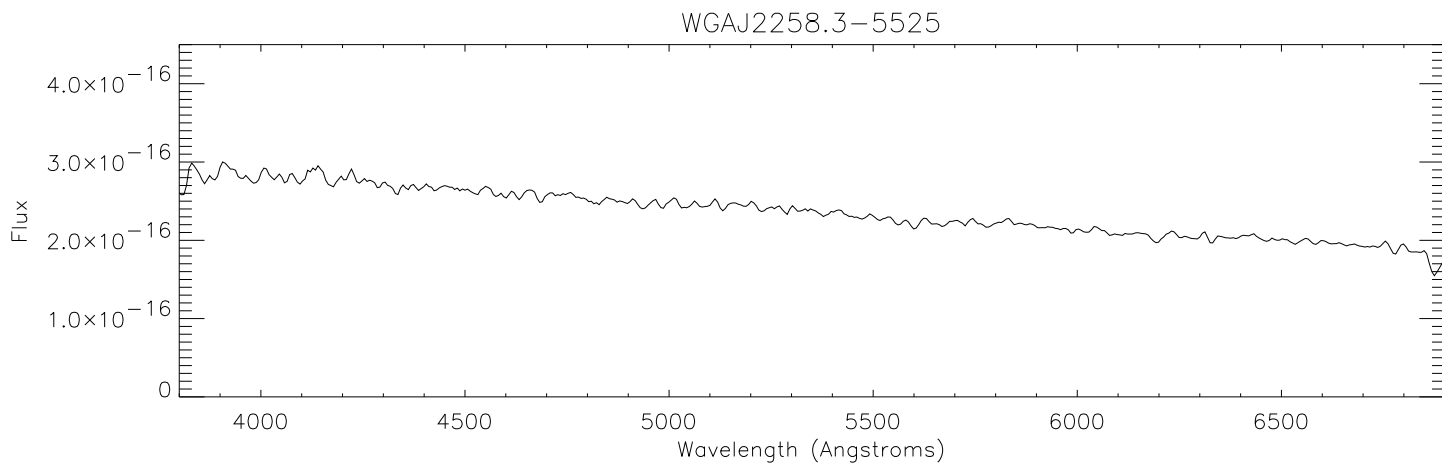
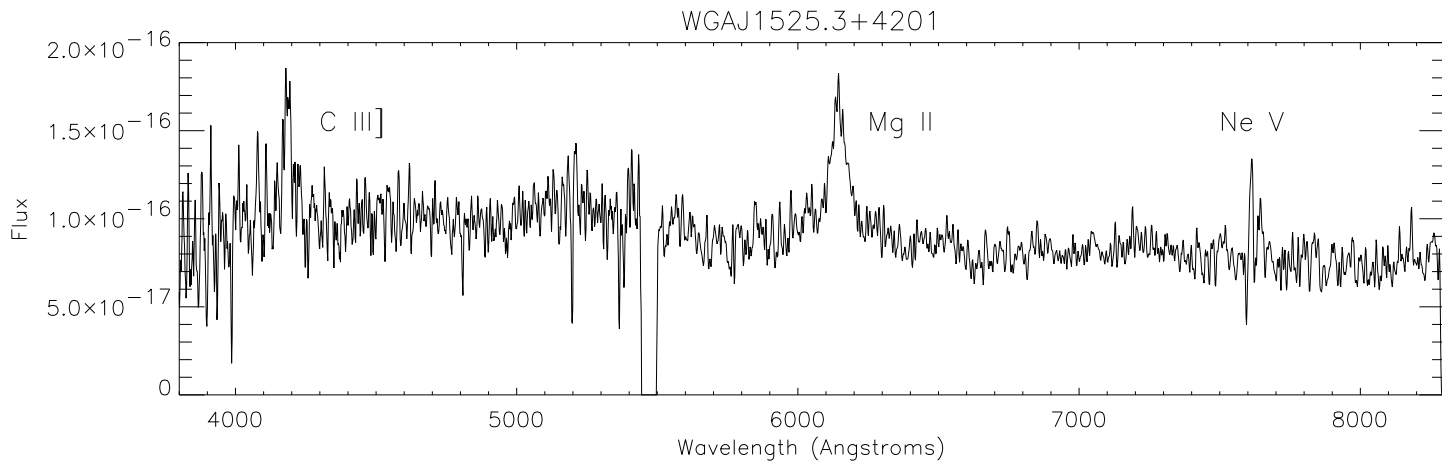
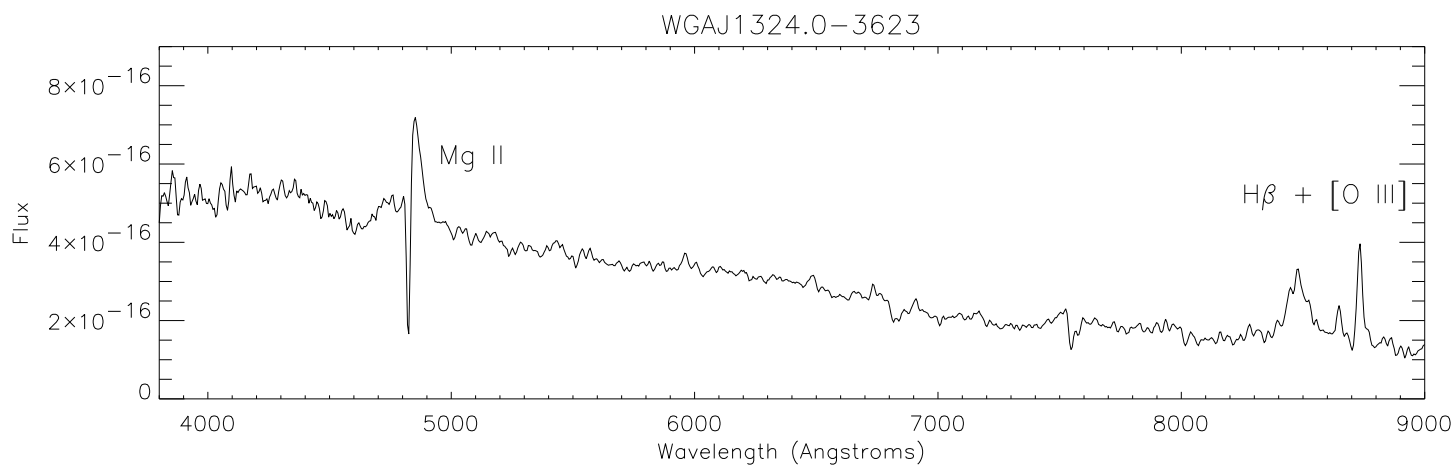
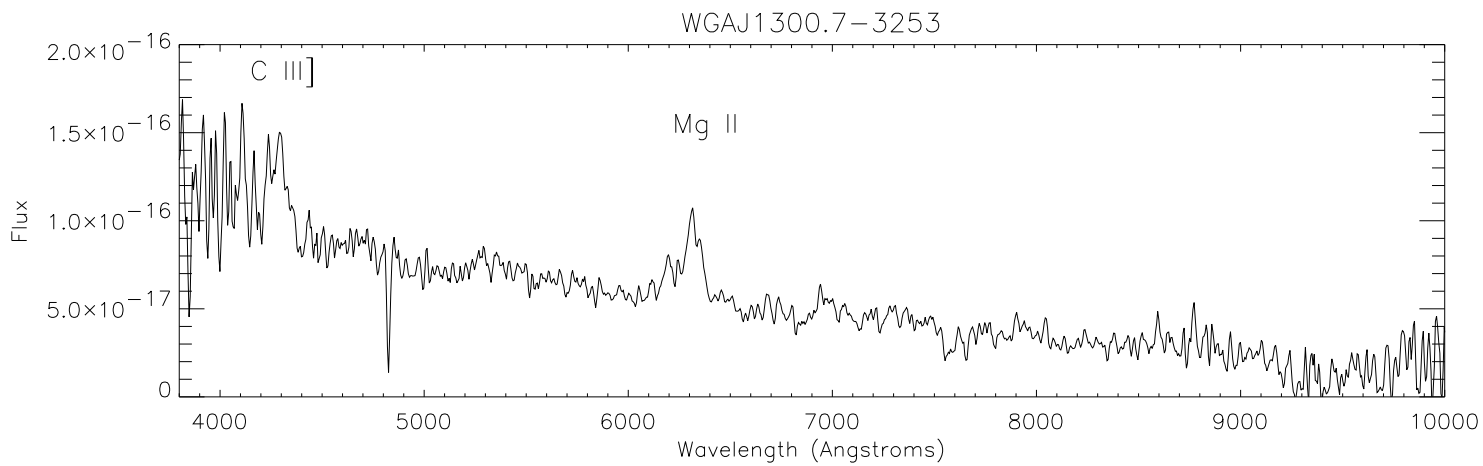
WGAJ1108.1-7748

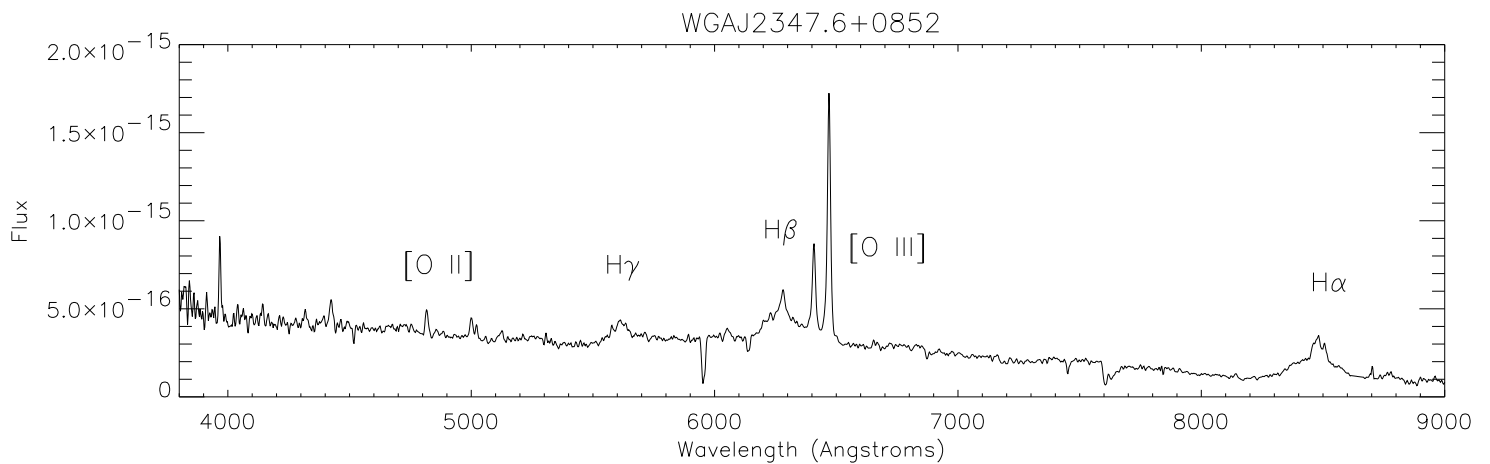
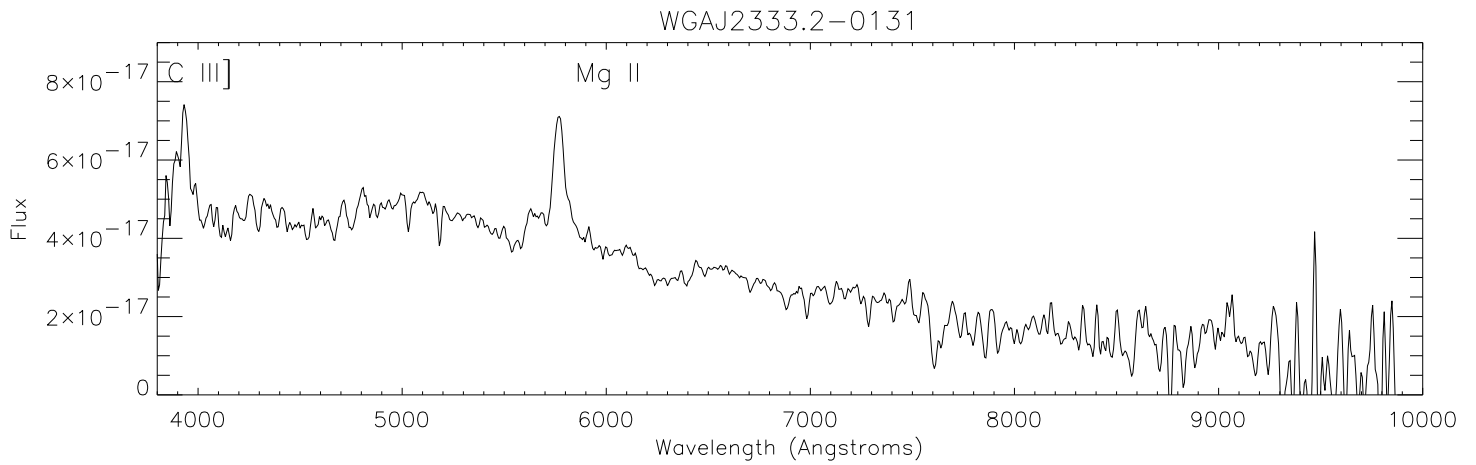
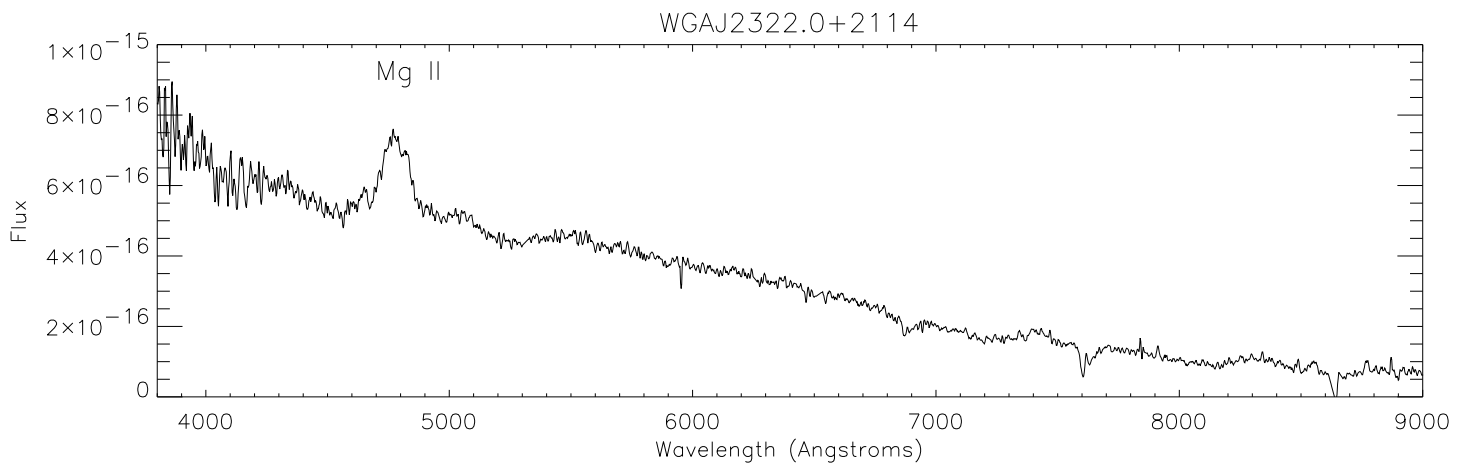
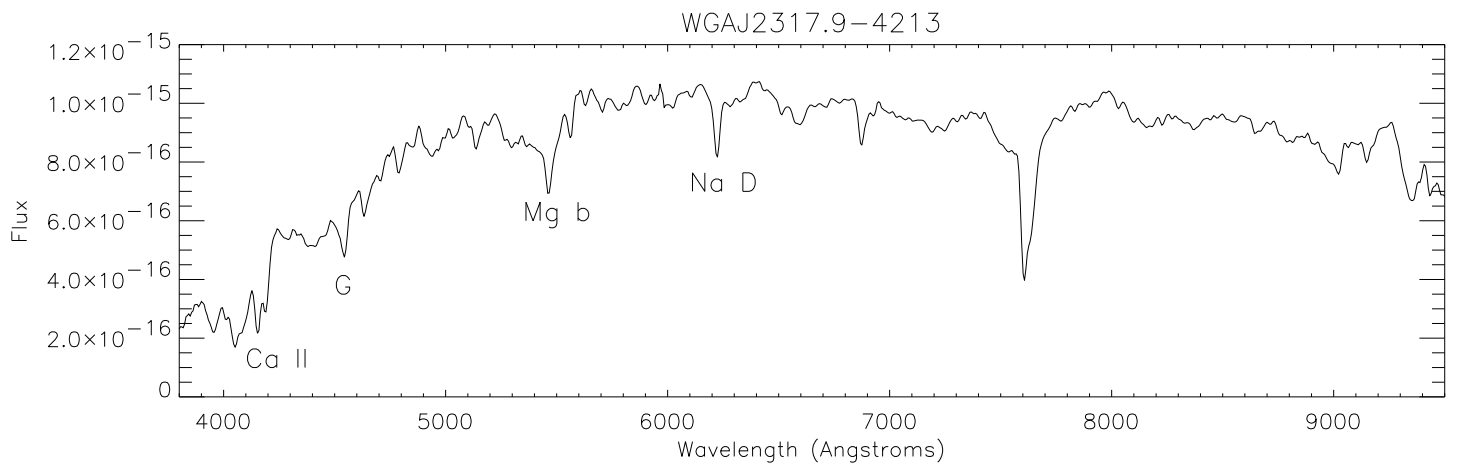


WGAJ1112.1-3745









WGAJ2350.6+3622

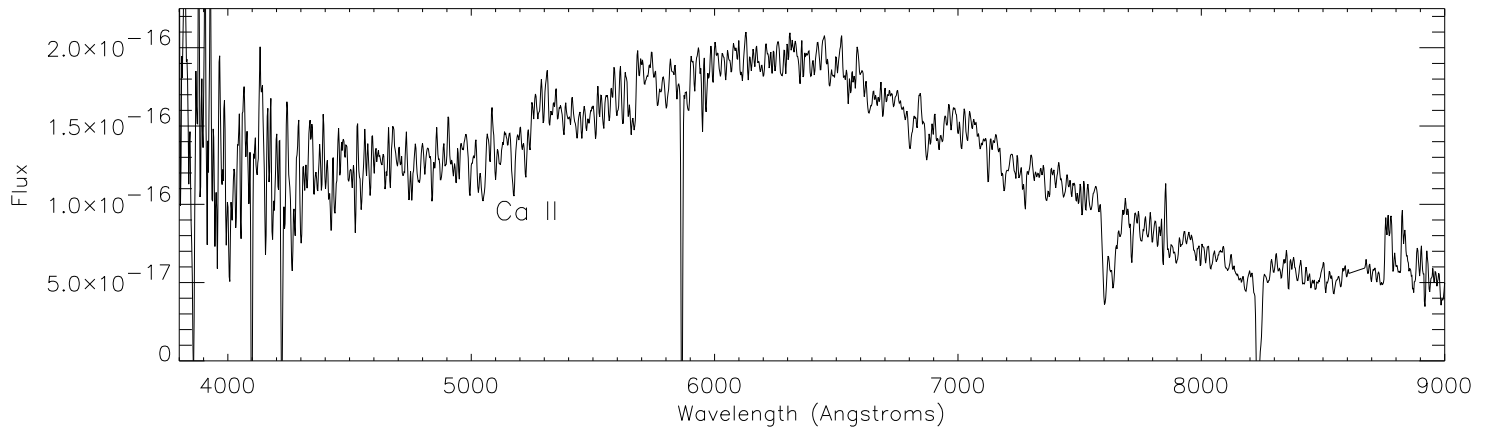


TABLE 2
LOG OF OBSERVATIONS

Name	Where Observed	Date (MM/YY)	Observers
WGAJ0011.2-3620	ES 3.6m	12/96	Giommi, Padovani
WGAJ0012.5-1629	KP 2.1m	12/96	Perlman, Sambruna
WGAJ0015.5+3052	MMT	12/96	Perlman
WGAJ0029.0+0509	KP 2.1m	12/96	Perlman, Sambruna
WGAJ0032.5-2849	ES 3.6m	12/96	Giommi, Padovani
WGAJ0032.5-2648	KP 2.1m	12/96	Perlman, Sambruna
WGAJ0043.3-2638	CT 1.5m	01/97	Perlman
WGAJ0049.5-2509	ES 3.6m	12/96	Giommi, Padovani
WGAJ0057.3-2212	ES 3.6m	12/96	Giommi, Padovani
WGAJ0100.1-3337	ES 3.6m	12/96	Giommi, Padovani
WGAJ0110.5-1647	KP 2.1m	12/96	Perlman, Sambruna
WGAJ0125.0+0146	KP 2.1m	12/96	Perlman, Sambruna
WGAJ0136.0-4044	ES 3.6m	12/96	Giommi, Padovani
WGAJ0143.2-6813	ES 3.6m	12/96	Giommi, Padovani
WGAJ0204.8+1514	ES 3.6m	12/96	Giommi, Padovani
WGAJ0210.0-1004	ES 2.2m	12/96	Giommi, Padovani
WGAJ0216.6-7331	ES 3.6m	12/96	Giommi, Padovani
WGAJ0217.7-7347	ES 3.6m	12/96	Giommi, Padovani
WGAJ0245.2+1047	MMT	12/96	Perlman
WGAJ0304.9+0002	MMT	12/96	Perlman
WGAJ0313.9+4115	KP 2.1m	12/96	Perlman, Sambruna
WGAJ0314.4-6548	CT 1.5m	01/97	Perlman
WGAJ0322.2-5042	ES 2.2m	12/96	Giommi, Padovani
WGAJ0324.9-2140	ES 2.2m	12/96	Giommi, Padovani
WGAJ0325.0-4926	ES 2.2m	12/96	Giommi, Padovani
WGAJ0340.8-1814	ES 3.6m	12/96	Giommi, Padovani
WGAJ0357.6-4158	ES 3.6m	12/96	Giommi, Padovani
WGAJ0411.0-1637	KP 2.1m	12/96	Perlman, Sambruna
WGAJ0414.0-1307	ES 3.6m	12/96	Giommi, Padovani
WGAJ0414.0-1224	ES 2.2m	12/96	Giommi, Padovani
WGAJ0421.5+1433	ES 2.2m	12/96	Giommi, Padovani
	CT 1.5m	01/97	Perlman
WGAJ0428.8-3805	ES 2.2m	12/96	Giommi, Padovani
WGAJ0434.3-1443	ES 3.6m	12/96	Giommi, Padovani
WGAJ0435.1-0811	KP 2.1m	12/96	Perlman, Sambruna
WGAJ0447.9-0322	KP 2.1m	12/96	Perlman, Sambruna
WGAJ0448.2-2110	KP 2.1m	12/96	Perlman, Sambruna
WGAJ0449.4-4349	CT 4m	01/96	Ruiz(1)
WGAJ0500.0-3040	ES 2.2m	12/96	Giommi, Padovani
WGAJ0502.5+1338	ES 3.6m	12/96	Giommi, Padovani
WGAJ0510.0+1800	ES 3.6m	12/96	Giommi, Padovani
WGAJ0513.8+0156	ES 2.2m	12/96	Giommi, Padovani
WGAJ0518.2+0624	ES 3.6m	12/96	Giommi, Padovani
WGAJ0528.5-5820	CT 1.5m	01/97	Perlman
WGAJ0535.1-0239	ES 2.2m	12/96	Giommi, Padovani
WGAJ0539.0-3427	ES 2.2m	12/96	Giommi, Padovani
WGAJ0544.1-2241	KP 2.1m	12/96	Perlman, Sambruna
	ES 2.2m	12/96	Giommi, Padovani

TABLE 2—*Continued*

Name	Where Observed	Date (MM/YY)	Observers
WGAJ0546.6–6415	CT 1.5m	01/97	Perlman
WGAJ0558.1+5328	KP 2.1m	12/96	Perlman, Sambruna
WGAJ0600.5–3937	ES 2.2m	12/96	Giommi, Padovani
WGAJ0624.7–3230	CT 1.5m	01/97	Perlman
WGAJ0628.4–3208	ES 3.6m	12/96	Giommi, Padovani
WGAJ0631.9–5404	CT 1.5m	01/97	Perlman
WGAJ0633.1–2333	ES 3.6m	12/96	Giommi, Padovani
WGAJ0648.2–4347	ES 2.2m	12/96	Giommi, Padovani
WGAJ0656.3–2403	CT 1.5m	01/97	Perlman
WGAJ0724.3–0715	CT 1.5m	01/97	Perlman
WGAJ0744.8+2920	CT 1.5m	01/97	Perlman
WGAJ0748.2–5257	ES 2.2m	12/96	Giommi, Padovani
WGAJ0750.9–6726	ES 2.2m	12/96	Giommi, Padovani
WGAJ0816.0–0736	ES 2.2m	12/96	Giommi, Padovani
	CT 1.5m	01/97	Perlman
WGAJ0900.2–2817	ES 3.6m	12/96	Giommi, Padovani
WGAJ0940.2+2603	KP 2.1m	12/96	Perlman, Sambruna
WGAJ1003.9+3244	KP 2.1m	12/96	Perlman, Sambruna
WGAJ1011.5–0423	ES 2.2m	12/96	Giommi, Padovani
WGAJ1025.9+1253	KP 2.1m	12/96	Perlman, Sambruna
WGAJ1032.1–1400	CT 1.5m	01/97	Perlman
WGAJ1035.0+5652	KP 2.1m	12/96	Perlman, Sambruna
WGAJ1046.3+5354	KP 2.1m	12/96	Perlman, Sambruna
WGAJ1057.6–7724	ES 3.6m	12/96	Giommi, Padovani
WGAJ1104.8+6038	KP 2.1m	12/96	Perlman, Sambruna
WGAJ1108.1–7748	ES 3.6m	12/96	Giommi, Padovani
WGAJ1112.5–3745	ES 2.2m	12/96	Giommi, Padovani
WGAJ1150.4+0156	ES 3.6m	12/96	Giommi, Padovani
WGAJ1222.6+2934	CT 1.5m	01/97	Perlman
WGAJ1224.5+2613	KP 2.1m	12/96	Perlman, Sambruna
WGAJ1231.7+2848	CT 1.5m	01/97	Perlman
WGAJ1300.7–3253	CT 1.5m	01/97	Perlman
WGAJ1324.0–3623	CT 1.5m	01/97	Perlman
WGAJ1525.3+4201	Lick 3m	06/95	Jones
WGAJ2258.3–5525	ES 3.6m	12/96	Giommi, Padovani
WGAJ2317.4–4213	ES 3.6m	12/96	Giommi, Padovani
WGAJ2322.0+2114	KP 2.1m	12/96	Perlman, Sambruna
WGAJ2333.2–0131	ES 3.6m	12/96	Giommi, Padovani
WGAJ2347.6+0852	KP 2.1m	12/96	Perlman, Sambruna
WGAJ2350.6+3622	KP 2.1m	12/96	Perlman, Sambruna

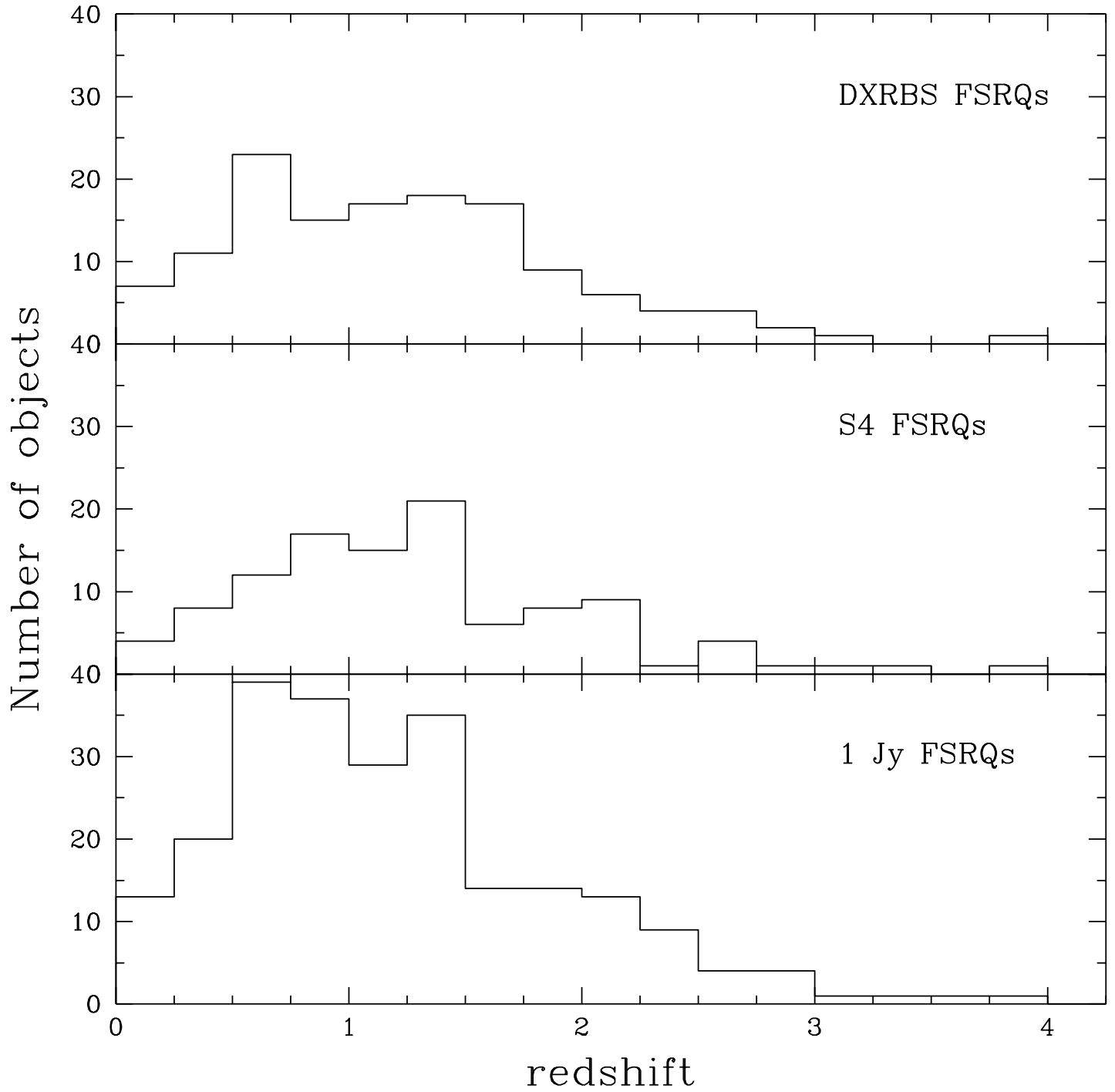


TABLE 3
POSITIONAL INFORMATION

Name	WGACAT Position		Center Offset	WGA error	PMN or GB6 Position		Counterpart Position		Source	Offset (X-O)	Ctrpart Error	Cum. Error	Offset/ Error
	RA	DEC			RA	DEC	RA	DEC					
WGAJ0011.2 – 3620	00 11 14.0	– 36 20 35	3.2	13	00 11 15.5	– 36 20 33	00 11 14.6	– 36 20 39	ATCA	8.34	5	13.93	0.60
WGAJ0012.5 – 1629	00 12 33.7	– 16 29 01	45.9	42	00 12 33.2	– 16 28 06	00 12 33.9	– 16 28 07	ATCA	54.08	5	42.30	1.28
WGAJ0015.5 + 3052	00 15 35.2	+ 30 52 19	34.7	36	00 15 36.1	+ 30 52 21	00 15 36.0	+ 30 52 30	APM+NVS	15.07	3	36.22	0.42
WGAJ0015.6 + 3052	00 15 39.7	+ 30 52 43	33.3	36	00 15 36.1	+ 30 52 21	00 15 36.0	+ 30 52 30	APM+NVS	49.38	3	36.22	1.36
WGAJ0029.0 + 0509	00 29 04.6	+ 05 09 42	22.9	29	00 29 03.8	+ 05 09 31	00 29 03.5	+ 05 09 34	NVSS	18.28	3	28.76	0.64
WGAJ0032.5 – 2849	00 32 31.8	– 28 49 48	34.8	36	00 32 31.2	– 28 49 20	00 32 33.1	– 28 49 19	ATCA	33.79	5	36.44	0.93
WGAJ0032.5 – 2648	00 32 33.0	– 26 48 54	24.3	29	00 32 37.7	– 26 49 29	00 32 33.0	– 26 49 17	NVSS	23.00	3	28.76	0.80
WGAJ0043.3 – 2638	00 43 22.5	– 26 38 57	32.4	36	00 43 24.0	– 26 39 06	00 43 22.7	– 26 39 07	ATCA	10.35	5	36.44	0.28
WGAJ0049.5 – 2509	00 49 33.5	– 25 09 44	28.7	29	00 49 34.2	– 25 09 34	00 49 33.7	– 25 09 34	ATCA	10.36	5	29.03	0.36
WGAJ0057.3 – 2212	00 57 18.6	– 22 12 30	8.9	13	00 57 21.8	– 22 12 33	00 57 18.8	– 22 12 34	NVSS	4.87	5	13.93	0.35
WGAJ0057.3 – 2212	00 57 18.8	– 22 12 17	9.1	13	00 57 21.8	– 22 12 33	00 57 18.8	– 22 12 34	NVSS	17.00	5	13.93	1.22
WGAJ0057.3 – 2212	00 57 19.5	– 22 12 32	8.9	13	00 57 21.8	– 22 12 33	00 57 18.8	– 22 12 34	NVSS	9.95	5	13.93	0.71
WGAJ0100.1 – 3337	01 00 08.9	– 33 37 21	6.0	42	01 00 07.6	– 33 37 20	01 00 09.4	– 33 37 32	ATCA	12.69	5	42.30	0.91
WGAJ0110.5 – 1647	01 10 35.4	– 16 47 56	28.3	29	01 10 36.3	– 16 48 42	01 10 35.5	– 16 48 23	ATCA	27.04	5	29.03	0.93
WGAJ0125.0 + 0146	01 25 05.4	+ 01 46 33	5.0	13	01 25 04.1	+ 01 46 14	01 25 05.4	+ 01 46 26	NVSS	7.00	3	13.34	0.52
WGAJ0136.0 – 4044	01 36 02.0	– 40 44 46	17.0	18	01 36 06.3	– 40 44 29	01 36 02.9	– 40 44 50	ATCA	11.19	5	18.78	0.60
WGAJ0143.2 – 6813	01 43 16.2	– 68 13 06	25.5	29	01 43 22.9	– 68 13 18	01 43 19.2	– 68 13 27	ATCA	27.03	5	29.03	0.93
WGAJ0204.8 + 1514	02 04 49.7	+ 15 14 20	28.7	29	02 04 50.8	+ 15 14 10	02 04 50.3	+ 15 14 11	NVSS	12.51	3	28.76	0.44
WGAJ0210.0 – 1004	02 10 00.6	– 10 04 07	9.1	13	02 09 59.4	– 10 03 31	02 10 00.1	– 10 03 54	NVSS	14.95	5	13.93	1.07
WGAJ0216.6 – 7331	02 16 37.7	– 73 31 35	32.9	18	02 16 47.3	– 73 31 42	02 16 44.6	– 73 31 40	ATCA	31.57	5	18.78	0.87
WGAJ0217.7 – 7347	02 17 44.8	– 73 47 31	17.4	18	02 17 48.2	– 73 47 18	02 17 45.1	– 73 47 23	ATCA	8.12	5	18.78	0.43
WGAJ0217.7 – 7346	02 17 46.4	– 73 46 21	18.6	29	02 17 48.2	– 73 47 18	02 17 45.1	– 73 47 23	ATCA	62.29	5	29.03	3.32
WGAJ0245.2 + 1047	02 45 13.5	+ 10 47 20	34.9	36	02 45 14.7	+ 10 47 12	02 45 13.7	+ 10 47 23	APM+NVS	4.21	3	36.22	0.12
WGAJ0304.9 + 0002	03 04 57.9	+ 00 02 28	30.6	36	03 04 58.8	+ 00 02 07	03 04 59.2	+ 00 02 33	NVSS	20.13	5	36.44	0.55
WGAJ0313.9 + 4115	03 13 56.9	+ 41 15 37	16.9	18	03 13 58.0	+ 41 15 21	03 13 57.8	+ 41 15 23	NVSS	17.31	3	18.35	0.94
WGAJ0314.4 – 6548	03 14 24.4	– 65 48 20	45.7	42	03 14 19.3	– 65 48 39	03 14 22.4	– 65 48 25	ATCA	13.98	5	42.30	0.33
WGAJ0314.4 – 6548	03 14 27.6	– 65 48 21	45.5	42	03 14 19.3	– 65 48 39	03 14 22.4	– 65 48 25	ATCA	34.19	5	42.30	0.81
WGAJ0322.2 – 5042	03 22 12.3	– 50 42 26	22.9	29	03 22 10.3	– 50 42 21	03 22 12.4	– 50 42 33	ATCA	7.07	5	29.03	0.24
WGAJ0324.9 – 2140	03 24 59.6	– 21 40 41	32.6	36	03 25 01.3	– 21 40 19	03 25 00.8	– 21 40 41	NVSS	16.88	5	36.44	0.46
WGAJ0325.0 – 4926	03 25 00.1	– 49 26 44	18.9	18	03 25 03.5	– 49 27 24	03 25 02.6	– 49 27 05	ATCA	32.51	5	18.78	1.73
WGAJ0325.0 – 4927	03 25 00.2	– 49 27 05	18.9	18	03 25 03.5	– 49 27 24	03 25 02.6	– 49 27 05	ATCA	23.83	5	18.78	1.27
WGAJ0325.0 – 4926	03 25 03.2	– 49 26 44	19.4	18	03 25 03.5	– 49 27 24	03 25 02.6	– 49 27 05	ATCA	21.83	5	18.78	1.16
WGAJ0340.8 – 1814	03 40 49.1	– 18 14 00	21.9	29	03 40 45.5	– 18 13 39	03 40 47.8	– 18 14 00	NVSS	18.57	5	29.03	0.64
WGAJ0357.6 – 4158	03 57 39.5	– 41 58 57	31.4	36	03 57 36.8	– 41 58 59	03 57 36.8	– 41 59 01	ATCA	31.27	5	36.44	0.86
WGAJ0411.0 – 1637	04 11 00.0	– 16 37 00	51.0	53	04 10 59.4	– 16 36 08	04 10 59.5	– 16 36 11	ATCA	49.53	5	53.63	0.92

TABLE 3—*Continued*

Name	WGACAT Position RA DEC	Center Offset	WGA error	PMN or GB6 Position RA DEC	Counterpart Position RA DEC	Source	Offset (X-O)	Ctrpart Error	Cum. Error	Offset/ Error
WGAJ0414.0 – 1307	04 14 02.9 – 13 07 13	24.4	29	04 14 02.3 – 13 06 44	04 14 03.1 – 13 06 38	NVSS	35.12	5	29.03	1.21
WGAJ0414.0 – 1224	04 14 05.7 – 12 24 30	18.4	18	04 14 03.1 – 12 23 38	04 14 05.9 – 12 24 17	NVSS	13.33	3	41.18	0.30
WGAJ0421.5 + 1433	04 21 33.4 + 14 33 44	11.8	18	04 21 33.1 + 14 33 43	04 21 33.1 + 14 33 54	OPT+NVS	10.91	3	18.35	0.59
WGAJ0428.8 – 3805	04 28 50.5 – 38 05 44	11.4	18	04 28 52.6 – 38 05 23	04 28 50.9 – 38 05 52	NVSS	9.30	5	18.78	0.50
WGAJ0434.3 – 1443	04 34 18.7 – 14 43 01	5.9	13	04 34 19.0 – 14 43 09	04 34 19.0 – 14 42 55	NVSS	7.43	5	13.93	0.53
WGAJ0435.1 – 0811	04 35 06.6 – 08 11 05	28.6	29	04 35 05.9 – 08 11 15	04 35 07.8 – 08 11 22	OPT+NVS	24.64	5	29.03	0.85
WGAJ0447.9 – 0322	04 47 54.6 – 03 22 28	38.4	36	04 47 57.5 – 03 22 40	04 47 54.7 – 03 22 43	NVSS	15.07	5	36.44	0.41
WGAJ0448.2 – 2110	04 48 14.9 – 21 10 18	30.4	36	04 48 18.0 – 21 09 47	04 48 17.4 – 21 09 45	NVSS	48.14	5	36.44	1.32
WGAJ0449.4 – 4349	04 49 24.6 – 43 49 39	2.0	13	04 49 24.3 – 43 50 04	04 49 24.7 – 43 50 09	ATCA	30.02	3	13.34	2.25
WGAJ0500.0 – 3040	05 00 04.6 – 30 40 49	26.4	29	05 00 07.5 – 30 41 14	05 00 05.0 – 30 41 09	ATCA	20.67	5	29.03	0.71
WGAJ0502.5 + 1338	05 02 33.0 + 13 38 17	18.6	18	05 02 33.4 + 13 38 14	05 02 33.2 + 13 38 11	NVSS	6.67	3	18.35	0.36
WGAJ0502.5 + 1338	05 02 33.1 + 13 38 33	18.4	18	05 02 33.4 + 13 38 14	05 02 33.2 + 13 38 11	NVSS	22.05	3	18.35	1.20
WGAJ0510.0 + 1800	05 10 02.6 + 18 00 48	9.6	13	05 10 02.4 + 18 00 41	05 10 02.3 + 18 00 41	NVSS	8.20	3	13.34	0.61
WGAJ0513.8 + 0156	05 13 52.3 + 01 56 59	14.9	18	05 13 52.7 + 01 56 50	05 13 51.9 + 01 56 55	NVSS	8.50	3	18.35	0.46
WGAJ0513.8 + 0156	05 13 53.4 + 01 56 21	14.3	18	05 13 52.7 + 01 56 50	05 13 51.8 + 01 56 55	NVSS	41.61	3	18.35	2.27
WGAJ0518.2 + 0624	05 18 14.7 + 06 24 17	26.3	29	05 18 15.8 + 06 24 00	05 18 15.9 + 06 24 22	NVSS	18.57	3	28.76	0.65
WGAJ0528.5 – 5820	05 28 34.7 – 58 20 12	33.4	36	05 28 33.2 – 58 20 25	05 28 34.7 – 58 20 18	ATCA	6.00	5	36.44	0.16
WGAJ0535.1 – 0239	05 35 11.9 – 02 39 05	11.5	18	05 35 10.8 – 02 39 11	05 35 12.2 – 02 39 06	NVSS	4.61	5	18.78	0.25
WGAJ0539.0 – 3427	05 39 03.4 – 34 27 12	25.2	29	05 39 06.2 – 34 27 35	05 39 05.4 – 34 27 13	ATCA	25.02	5	29.03	0.86
WGAJ0544.1 – 2241	05 44 07.0 – 22 41 16	17.2	18	05 44 05.7 – 22 41 23	05 44 07.5 – 22 41 10	ATCA	9.21	5	18.78	0.49
WGAJ0546.6 – 6415	05 46 36.1 – 64 15 06	52.8	53	05 46 42.9 – 64 15 22	05 46 41.8 – 64 15 22	ATCA	41.06	5	53.63	0.77
WGAJ0546.6 – 6415	05 46 40.5 – 64 15 27	42.2	42	05 46 42.9 – 64 15 22	05 46 41.8 – 64 15 22	ATCA	9.97	5	42.30	0.24
WGAJ0558.1 + 5328	05 58 09.6 + 53 28 37	27.0	29	05 58 12.0 + 53 28 32	05 58 11.6 + 53 28 19	NVSS	25.35	3	28.76	0.88
WGAJ0600.5 – 3937	06 00 31.0 – 39 37 11	23.6	29	06 00 32.5 – 39 36 60	06 00 31.4 – 39 37 02	ATCA	10.15	5	29.03	0.35
WGAJ0624.7 – 3230	06 24 47.3 – 32 30 38	41.2	42	06 24 46.1 – 32 31 07	06 24 44.9 – 32 30 53	ATCA	34.17	5	42.30	0.81
WGAJ0628.4–3208	06 28 27.9 – 32 08 11	25.7	28	06 28 32.6 – 32 07 35	06 28 30.7 – 32 08 14	NVSS	35.74	3	28.76	1.24
WGAJ0628.4–3208	06 28 28.4 – 32 08 06	25.8	28	06 28 32.6 – 32 07 35	06 28 30.7 – 32 08 14	NVSS	30.33	3	28.76	1.05
WGAJ0631.9 – 5404	06 31 59.6 – 54 04 31	45.2	42	06 31 57.8 – 54 05 02	06 32 01.7 – 54 04 57	ATCA	31.94	5	42.30	0.76
WGAJ0633.1 – 2333	06 33 11.8 – 23 33 18	22.3	29	06 33 12.7 – 23 33 05	06 33 12.8 – 23 33 09	ATCA	16.53	5	29.03	0.57
WGAJ0648.2 – 4347	06 48 16.7 – 43 47 01	30.9	36	06 48 12.4 – 43 46 39	06 48 13.4 – 43 47 15	ATCA	39.24	5	36.44	1.08
WGAJ0656.3 – 2403	06 56 21.5 – 24 03 30	32.4	29	06 56 22.0 – 24 03 48	06 56 22.7 – 24 03 18	ATCA	20.35	5	29.03	0.56
WGAJ0724.3 – 0715	07 24 19.0 – 07 15 56	34.3	36	07 24 16.3 – 07 15 23	07 24 17.3 – 07 15 19	NVSS	38.44	3	36.22	1.06
WGAJ0744.8 + 2920	07 44 51.6 + 29 20 05	33.7	36	07 44 51.5 + 29 20 27	07 44 51.2 + 29 20 11	FIRST	7.96	1	36.11	0.22
WGAJ0744.8 + 2920	07 44 51.8 + 29 20 11	33.8	36	07 44 51.5 + 29 20 27	07 44 51.2 + 29 20 11	FIRST	7.84	1	36.11	0.22
WGAJ0748.2 – 5257	07 48 13.2 – 52 57 45	31.1	29	07 48 10.8 – 52 58 29	07 48 12.7 – 52 58 32	ATCA	47.24	5	29.03	1.30

TABLE 3—*Continued*

Name	WGACAT Position		Center Offset	WGA error	PMN or GB6 Position		Counterpart Position		Source	Offset (X-O)	Ctrpart Error	Cum. Error	Offset/ Error
	RA	DEC			RA	DEC	RA	DEC					
WGAJ0750.9 – 6726	07 50 55.1	– 67 26 16	22.8	29	07 50 56.8	– 67 26 36	07 50 59.5	– 67 26 23	ATCA	27.17	5	29.03	0.94
WGAJ0751.0 – 6726	07 51 02.4	– 67 26 22	23.2	29	07 50 56.8	– 67 26 36	07 50 59.5	– 67 26 23	ATCA	17.33	5	29.03	0.60
WGAJ0751.0 – 6725	07 51 04.2	– 67 25 54	23.7	29	07 50 56.8	– 67 26 36	07 50 59.5	– 67 26 23	ATCA	40.34	5	29.03	1.39
WGAJ0816.0 – 0736	08 16 01.7	– 07 36 16	20.2	29	08 16 04.1	– 07 36 42	08 16 04.3	– 07 35 57	NVSS	43.16	5	29.03	1.49
WGAJ0900.2 – 2817	09 00 14.0	– 28 17 49	31.2	29	09 00 15.8	– 28 17 60	09 00 15.4	– 28 17 58	NVSS	20.66	5	29.03	0.57
WGAJ0940.2 + 2603	09 40 14.0	+ 26 03 39	35.2	36	09 40 14.6	+ 26 03 38	09 40 13.6	+ 26 03 26	NVSS	14.07	3	36.22	0.39
WGAJ1003.9 + 3244	10 03 58.1	+ 32 44 02	18.3	18	10 03 58.4	+ 32 44 03	10 03 57.5	+ 32 44 03	NVSS	7.64	3	18.35	0.42
WGAJ1011.5 – 0423	10 11 30.1	– 04 23 13	18.7	18	10 11 30.7	– 04 23 33	10 11 30.2	– 04 23 28	PMN+APM	21.92	12	21.47	1.02
WGAJ1025.9 + 1253	10 25 56.0	+ 12 53 36	9.7	13	10 25 56.4	+ 12 53 48	10 25 56.4	+ 12 53 49	TEXS	14.26	3	14.45	1.07
WGAJ1032.1 – 1400	10 32 06.6	– 14 00 13	15.7	18	10 32 07.4	– 14 00 19	10 32 06.3	– 14 00 20	NVSS	8.25	5	18.78	0.44
WGAJ1035.0 + 5652	10 35 04.8	+ 56 52 57	13.4	18	10 35 06.0	+ 56 52 57	10 35 05.9	+ 56 52 57	NVSS	9.01	3	18.35	0.49
WGAJ1046.3 + 5354	10 46 23.7	+ 53 54 19	26.4	29	10 46 23.8	+ 53 54 38	10 46 24.0	+ 53 54 26	NVSS	7.49	3	28.76	0.26
WGAJ1057.6 – 7724	10 57 41.0	– 77 24 13	26.7	29	10 57 31.1	– 77 24 24	10 57 32.7	– 77 24 29	ATCA	33.00	5	29.03	1.14
WGAJ1104.8 + 6038	11 04 53.0	+ 60 38 54	22.8	29	11 04 54.5	+ 60 38 57	11 04 53.6	+ 60 38 55	NVSS	4.52	3	28.76	0.16
WGAJ1108.1 – 7748	11 08 07.7	– 77 48 11	18.6	18	11 08 11.3	– 77 48 25	11 08 11.3	– 77 48 17	ATCA	14.21	5	18.78	0.76
WGAJ1112.5 – 3745	11 12 34.7	– 37 45 24	30.2	36	11 12 38.6	– 37 45 49	11 12 36.8	– 37 45 45	ATCA	32.96	5	36.44	0.90
WGAJ1150.4 + 0156	11 50 24.5	+ 01 56 11	8.7	13	11 50 23.9	+ 01 56 02	11 50 24.8	+ 01 56 16	TEXS	7.50	3	13.34	0.56
WGAJ1222.6 + 2934	12 22 39.5	+ 29 34 40	41.9	42	12 22 42.4	+ 29 34 39	12 22 43.1	+ 29 34 40	NVSS	46.83	3	42.11	1.11
WGAJ1222.7 + 2934	12 22 42.5	+ 29 34 54	20.1	29	12 22 42.4	+ 29 34 39	12 22 43.1	+ 29 34 40	NVSS	16.59	3	28.76	0.58
WGAJ1224.5 + 2613	12 24 32.2	+ 26 13 34	26.8	29	12 24 33.0	+ 26 13 00	12 24 32.1	+ 26 13 14	OPT+NVS	20.05	3	28.76	0.70
WGAJ1231.7 + 2848	12 31 46.8	+ 28 48 03	46.6	42	12 31 44.0	+ 28 48 03	12 31 43.7	+ 28 47 50	NVSS	42.77	3	42.11	1.02
WGAJ1300.7 – 3253	13 00 42.3	– 32 53 01	28.2	29	13 00 41.9	– 32 53 02	13 00 42.4	– 32 53 12	ATCA	11.07	5	29.03	0.38
WGAJ1324.0 – 3623	13 24 02.6	– 36 23 16	29.6	29	13 24 04.1	– 36 23 51	13 24 03.5	– 36 23 35	ATCA	21.94	5	29.03	0.76
WGAJ1525.3 + 4201	15 25 22.5	+ 42 01 02	20.5	29	15 25 25.2	+ 42 01 15	15 25 23.6	+ 42 01 17	NVSS	12.61	3	28.76	0.44
WGAJ1525.3 + 4201	15 25 23.9	+ 42 01 15	17.4	18	15 25 25.2	+ 42 01 15	15 25 23.6	+ 42 01 17	NVSS	3.90	3	18.35	0.21
WGAJ2258.3 – 5525	22 58 18.1	– 55 25 31	34.5	36	22 58 16.5	– 55 26 14	22 58 19.0	– 55 25 37	ATCA	9.86	5	36.44	0.27
WGAJ2317.4 – 4213	23 17 55.7	– 42 13 29	7.9	13	23 17 52.3	– 42 13 52	23 17 56.4	– 42 13 33	ATCA	8.79	5	13.93	0.63
WGAJ2322.0 + 2114	23 22 02.1	+ 21 14 02	15.8	18	23 22 03.3	+ 21 14 09	23 22 01.8	+ 21 13 48	NVSS	14.61	3	18.35	0.80
WGAJ2322.0 + 2113	23 22 02.7	+ 21 13 36	15.4	18	23 22 03.3	+ 21 14 09	23 22 01.8	+ 21 13 48	NVSS	17.39	3	18.35	0.95
WGAJ2333.2 – 0131	23 33 14.0	– 01 31 29	30.0	36	23 33 16.3	– 01 31 07	23 33 16.7	– 01 31 07	GB6+APM	39.54	9	37.21	1.06
WGAJ2347.6 + 0852	23 47 36.3	+ 08 52 10	45.9	42	23 47 38.1	+ 08 52 52	23 47 38.1	+ 08 52 46	OPT+NVS	44.81	3	42.11	1.06
WGAJ2350.6 + 3622	23 50 37.0	+ 36 22 04	13.8	18	23 50 37.4	+ 36 21 54	23 50 36.7	+ 36 22 11	TEXS	7.87	3	18.34	0.43

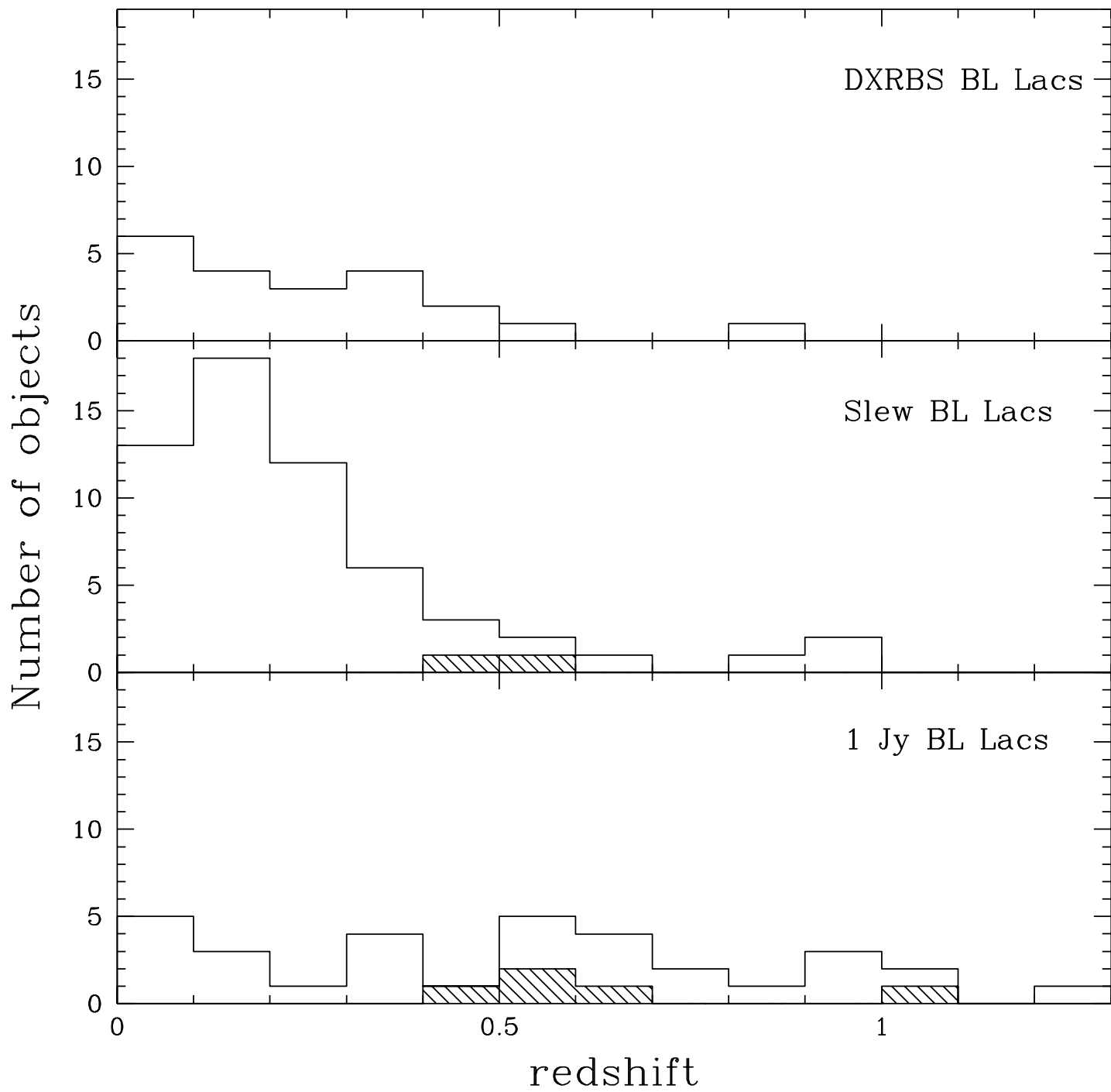


TABLE 4
NEWLY IDENTIFIED OBJECTS

Name	ROSAT ct/s	F(0.1-2.0 keV) erg cm ⁻² s ⁻¹	F(1 keV) μJy	log F _X /F _R	F(6 cm) mJy	α _r	B	R	Class	z	Other Catalogs
WGAJ0011.2 – 3620	0.002	1.73E – 14	0.003	–12.73	96	0.12		21.3	FSRQ	2.324	
WGAJ0012.5 – 1629	0.097	1.28E – 12	0.29	–10.53	50	0.62	17.7		FSRQ	0.151	1
WGAJ0015.5 + 3052	0.019	2.82E – 13	0.083	–11.37	89	0.62	16.3	17.2	FSRQ	1.619	
	0.023	3.16E – 13	0.095								
WGAJ0029.0 + 0509	0.006	6.33E – 14	0.014	–12.71	377	0.00	19.3	18.1	FSRQ	1.633	
WGAJ0032.5 – 2849	0.016	1.82E – 13	0.047	–11.74	146	0.42	18.8		BL Lac	0.324	
WGAJ0032.5 – 2648	0.015	1.15E – 13	0.028	–11.67	71	0.55	18.3		FSRQ	1.470	
WGAJ0043.3 – 2638	0.054	8.16E – 13	0.062	–11.13	81	–0.03	17.3		BL Lac	0.451	2
WGAJ0049.5 – 2509	0.007	5.81E – 14	0.013	–11.98	68	0.58		21.5	FSRQ	1.472	
WGAJ0057.3 – 2212	0.007	4.94E – 14	0.004	–12.10	70	0.31	> 23.0	20.6	BL Lac	?	
	0.007	6.56E – 14	0.013								
	0.007	5.83E – 14	0.016								
WGAJ0100.1 – 3337	0.008	6.18E – 14	0.010	–12.39	127	0.16	20.2		BL Lac	0.875	
WGAJ0110.5 – 1647	0.161	1.17E – 12	0.18	–10.87	72	0.28	15.6		FSRQ	0.780	1
WGAJ0125.0 + 0146	0.016	1.89E – 13	0.046	–11.65	95	0.59	19.6	19.0	FSRQ	1.559	
WGAJ0136.0 – 4044	0.017	1.62E – 13	0.039	–11.84	137	–0.25	20.7		FSRQ	0.649	
WGAJ0143.2 – 6813	0.006	5.42E – 14	0.002	–12.37	51	0.39	21.2		FSRQ	1.223	
WGAJ0204.8 + 1514	0.020	2.60E – 13	0.077	–12.94	3073	0.32	21.0	> 20.0	FSRQ	0.405	3
WGAJ0210.0 – 1004	0.006	6.84E – 14	0.015	–12.50	244	0.09	19.7	19.5	FSRQ	1.976	
WGAJ0216.6 – 7331	0.006	5.89E – 14	0.013	–11.98	62	0.60	19.5		FSRQ	2.679	
WGAJ0217.7 – 7347	0.013	1.50E – 13	0.039	–12.36	143	0.57	19.0		FSRQ	1.234	
	0.002	1.75E – 14	0.005								
WGAJ0245.2 + 1047	0.053	7.80E – 13	0.26	–11.24	217	0.55		15.7	BL Lac	0.070	3
WGAJ0304.9 + 0002	0.026	4.02E – 13	0.12	–11.14	75	0.42	17.8	18.4	FSRQ	0.563	
WGAJ0313.9 + 4115	0.024	3.66E – 13	0.11	–11.12	48	0.00		17.0	BL Lac?	0.029	4
WGAJ0314.4 – 6548	0.023	2.36E – 13	0.021	–11.67	179	0.42	19.0		FSRQ	0.636	
	0.083	9.58E – 13	0.21								
WGAJ0322.2 – 5042	0.025	2.59E – 13	0.057	–11.45	78	–0.12	18.2		FSRQ	0.651	
WGAJ0324.9 – 2140	0.014	1.08E – 13	0.007	–12.03	59	0.46	17.8		FSRQ	2.828	
WGAJ0325.0 – 4926	0.023	1.87E – 13	0.027	–11.40	67	0.36	19.2		FSRQ	0.259	1
	0.018	1.60E – 13	0.039								
	0.089	7.21E – 13	0.11								
WGAJ0340.8 – 1814	0.002	3.01E – 14	0.005	–12.75	148	0.60	19.6		RG?	0.195	
WGAJ0357.6 – 4158	0.012	1.08E – 13	0.024	–11.99	118	0.40	20.9		FSRQ	1.271	
WGAJ0411.0 – 1637	0.034	3.92E – 13	0.087	–11.45	124	–0.18	16.7		FSRQ	0.622	

TABLE 4—*Continued*

Name	ROSAT ct/s	F(0.1-2.0 keV) erg cm ⁻² s ⁻¹	F(1 keV) μJy	log F _X /F _R	F(6 cm) mJy	α _r	B	R	Class	z	Other Catalogs
WGAJ0414.0 – 1307	0.007	7.95E – 14	0.026	–12.01	152	0.62	22.0		FSRQ	0.463	
WGAJ0414.0 – 1224	0.021	2.47E – 13	0.060	–11.17	42		18.3		FSRQ	0.569	
WGAJ0421.5 + 1433	0.003	3.51E – 14	0.017	–12.42	114	0.63	18.8	15.2	BL Lac	?	
WGAJ0428.8 – 3805	0.010	7.59E – 14	0.004	–12.22	51	–0.03	18.9		BL Lac	0.150	
WGAJ0434.3 – 1443	0.004	6.04E – 14	0.009	–12.85	281	0.16	21.2	19.8	FSRQ	1.899	
WGAJ0435.1 – 0811	0.011	1.26E – 13	0.028	–11.75	73	–0.27	21.1	19.5	FSRQ	0.791	
WGAJ0447.9 – 0322	0.103	1.38E – 12	0.35	–10.54	56	0.38	16.3	16.0	FSRQ	0.774	1
WGAJ0448.2 – 2110	0.008	1.10E – 13	0.028	–12.25	227	0.06	19.0		FSRQ	1.971	
WGAJ0449.4 – 4349	0.497	7.46E – 12	0.48	–10.51	242	0.32	15.9		BL Lac	0.205	
WGAJ0500.0 – 3040	0.010	6.57E – 14	0.017	–12.07	108	0.56	19.4		RG	0.417	
WGAJ0502.5 + 1338	0.015	1.97E – 13	0.084	–12.33	459	0.20		18.3	BL Lac	?	
	0.011	1.34E – 13	0.064								
WGAJ0510.0 + 1800	0.027	3.39E – 13	0.21	–12.23	796	0.10		20.0	FSRQ	0.416	
WGAJ0513.8 + 0156	0.031	4.24E – 13	0.12	–11.38	131	0.45		14.8	BL Lac?	0.084	3
	0.023	3.02E – 13	0.095								
WGAJ0518.2 + 0624	0.007	9.69E – 14	0.037	–12.30	230	0.62		19.0	FSRQ	0.891	
WGAJ0528.5 – 5820	0.014	1.37E – 13	0.031	–11.80	99	0.46	19.2		BL Lac	0.302	
WGAJ0535.1 – 0239	0.009	1.05E – 13	0.051	–11.48	42	0.05	18.7		FSRQ	1.033	
WGAJ0539.0 – 3427	0.014	1.76E – 13	0.042	–11.95	195	0.47	19.9		FSRQ	0.263	
WGAJ0544.1 – 2241	0.043	4.56E – 13	0.085	–11.74	234	–0.45	17.0		FSRQ	1.537	
WGAJ0546.6 – 6415	0.221	4.24E – 12	1.2	–10.66	287	–0.18	18.0		FSRQ	0.323	1,5
	0.341	5.83E – 12	1.7								
WGAJ0558.1 + 5328	0.006	8.42E – 14	0.040	–12.31	234	0.59		14.0	BL Lac?	0.036	
WGAJ0600.5 – 3937	0.029	4.08E – 13	0.12	–12.08	623	0.13	18.6		FSRQ	1.661	
WGAJ0624.7 – 3230	0.062	8.16E – 13	0.21	–10.95	86	–0.56	19.7		BL Lac	0.252	
WGAJ0628.4 – 3208	0.019	2.56E – 13	0.075	–11.60	86	0.78	18.5		SSRQ	2.077	
	0.008	9.95E – 14	0.032								
WGAJ0631.9 – 5404	0.141	2.26E – 12	0.71	–10.76	155	0.45	18.7		FSRQ	0.193	1,5
WGAJ0633.1 – 2333	0.003	4.52E – 14	0.017	–12.16	99	0.57	21.5		FSRQ	2.928	
WGAJ0648.2 – 4347	0.026	3.67E – 13	0.11	–11.44	126	0.43	18.3		FSRQ	1.029	
WGAJ0656.3 – 2403	0.011	1.61E – 13	0.10	–11.81	104	0.43	19.5		BL Lac	0.371	
WGAJ0724.3 – 0715	0.017	2.49E – 13	0.23	–12.29	482	–0.28	18.0		FSRQ	0.270	
WGAJ0744.8 + 2920	0.035	5.25E – 13	0.12	–11.50	179	0.40	16.4	15.9	FSRQ	1.168	6
	0.041	6.15E – 13	0.078								
WGAJ0748.2 – 5257	0.006	9.29E – 14	0.035	–12.28	230	–0.10	18.4		FSRQ	1.802	

Other Catalogs

1. RASS Bright Source Catalog
2. HPQS
3. V Zwicky Catalog of Galaxies
4. 4C
5. *Einstein* Slew Survey
6. FIRST Bright Quasar Survey
7. B3
8. Las Campanas Redshift Survey

TABLE 4—*Continued*

Name	ROSAT ct/s	F(0.1-2.0 keV) erg cm ⁻² s ⁻¹	F(1 keV) μJy	log F _X /F _R	F(6 cm) mJy	α _r	B	R	Class	z	Other Catalogs
WGAJ0750.9 – 6726	0.011	1.61E – 13	0.059	–11.45	52	0.46	17.7		FSRQ	1.237	
	0.018	2.68E – 13	0.10								
	0.008	1.18E – 13	0.039								
WGAJ0816.0 – 0736	0.008	1.22E – 13	0.040	–11.55	61	–0.29	16.1		BL Lac?	0.040	
WGAJ0900.2 – 2817	0.022	3.74E – 13	0.14	–11.74	234	0.66	21.0		FSRQ	0.894	
WGAJ0940.2 + 2603	0.037	3.51E – 13	0.082	–11.83	292	0.05	20.9	19.2	BL Lac	0.498?	
WGAJ1003.9 + 3244	0.006	4.57E – 14	0.006	–13.01	371	0.20	18.8	18.2	FSRQ	1.682	
WGAJ1011.5 – 0423	0.006	6.41E – 14	0.019	–12.22	189	–0.07	20.0		FSRQ	1.588	
WGAJ1025.9 + 1253	0.028	3.27E – 13	0.076	–12.25	631	0.34	18.2		FSRQ	0.663	
WGAJ1032.1 – 1400	0.012	1.41E – 13	0.040	–12.12	223	–0.11	18.8	18.4	FSRQ	1.039	
WGAJ1035.0 + 5652	0.005	2.81E – 14	0.001	–13.38	205	0.24	19.8	19.1	FSRQ	0.577	
WGAJ1046.3 + 5354	0.016	1.46E – 13	0.023	–12.34	271	0.38	19.2	18.4	FSRQ	1.704	
WGAJ1057.6 – 7724	0.005	7.12E – 14	0.020	–12.76	431	0.70	21.0		BL Lac	0.541?	
WGAJ1104.8 + 6038	0.018	1.35E – 13	0.015	–12.32	187	0.18	19.0	18.1	FSRQ	1.373	
WGAJ1108.1 – 7748	0.003	4.21E – 14	0.011	–11.79	73	0.68		21.0	BL Lac	0.351?	
WGAJ1112.5 – 3745	0.023	3.62E – 13	0.12	–11.47	132	0.36	18.3		FSRQ	0.979	
WGAJ1150.4 + 0156	0.018	1.57E – 13	0.019	–11.93	95	0.35		19.5	FSRQ	1.502	
WGAJ1222.6 + 2934	0.016	1.53E – 13	0.029	–11.57	60	0.55		18.7	FSRQ	0.401	
	0.016	1.45E – 13	0.033								
WGAJ1224.5 + 2613	0.015	1.04E – 13	0.011	–12.59	272	0.67	21.3	17.9	FSRQ	0.687	4
WGAJ1231.7 + 2848	0.117	1.08E – 12	0.15	–11.14	114	0.52	16.4	15.6	BL Lac	?	
WGAJ1300.7 – 3253	0.017	2.17E – 13	0.059	–11.98	238	–0.10	18.7		FSRQ	1.256	
WGAJ1324.0 – 3623	0.022	2.78E – 13	0.074	–11.82	202	0.17	16.6		FSRQ	0.739	
WGAJ1525.3 + 4201	0.015	1.52E – 13	0.031	–11.74	103	0.24	18.0	17.2	FSRQ	1.189	4,7
	0.019	1.81E – 13	0.042								
WGAJ2258.3 – 5525	0.167	1.43E – 12	0.20	–10.66	51	0.61	17.9		BL Lac	?	1
WGAJ2317.4 – 4213	0.003	2.42E – 14	0.006	–12.58	133	0.34	15.4		RG	0.056	8
WGAJ2322.0 + 2114	0.011	1.49E – 13	0.041	–11.63	100	0.31	17.1	16.9	FSRQ	0.707	
	0.019	2.42E – 13	0.064								
WGAJ2333.2 – 0131	0.013	1.61E – 13	0.043	–12.21	314	0.16	19.6	17.3	FSRQ	1.062	
WGAJ2347.6 + 0852	0.043	6.40E – 13	0.18	–10.91	60	0.58	17.1	16.2	FSRQ	0.292	
WGAJ2350.6 + 3622	0.009	1.17E – 13	0.038	–11.99	154	0.42	19.6	17.3	BL Lac	0.317	

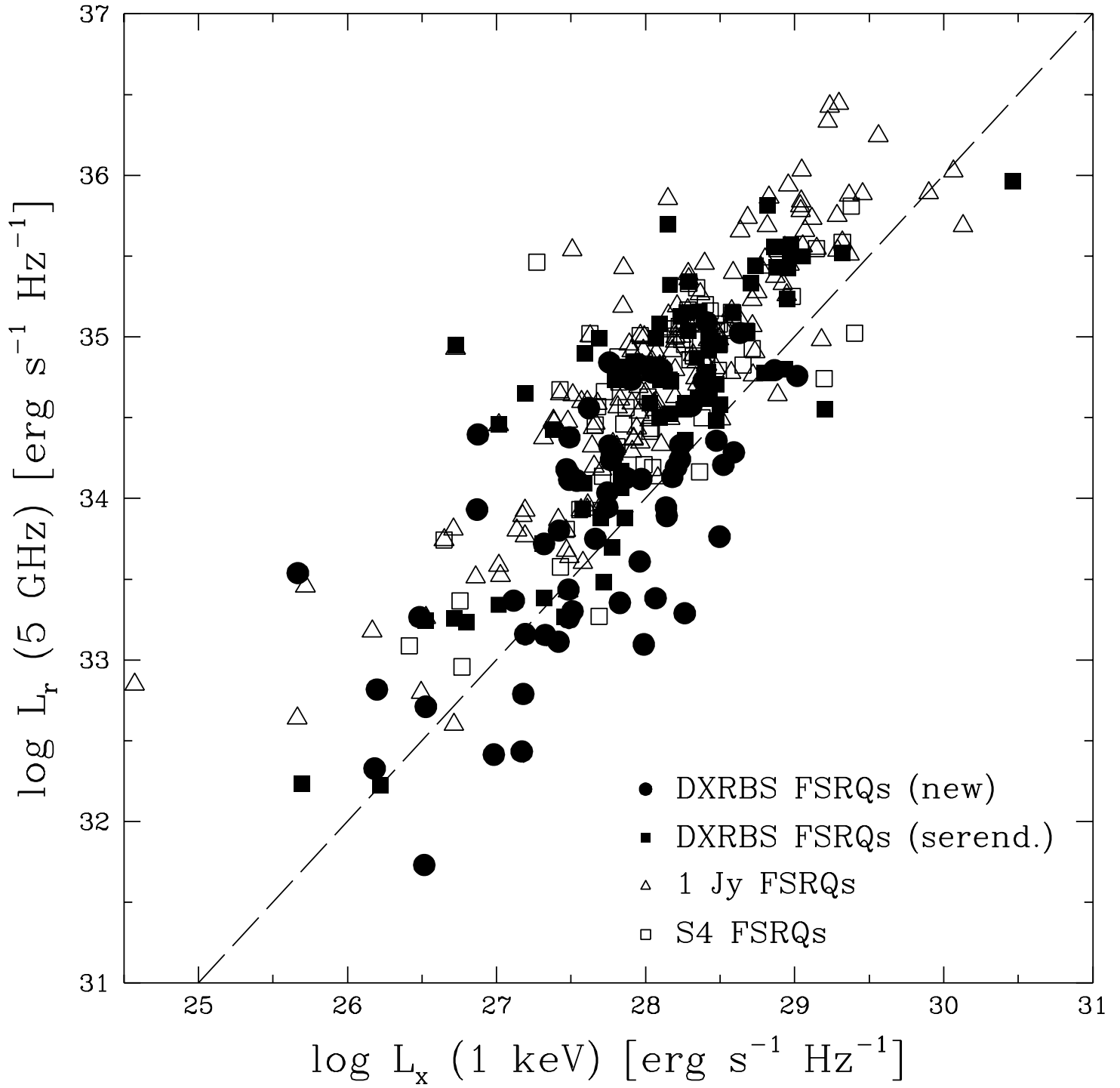


TABLE 5
SPECTRAL CHARACTERISTICS OF BL LACS AND RADIO GALAXIES

Object	C	W_λ (Å)
WGAJ0032.5–2849	0.22 ± 0.08	< 1.1
WGAJ0043.3–2638	< 0.06	9.6 ± 5.3
WGAJ0057.3–2212	< 0.30	< 5.0
WGAJ0100.1–3337	< 0.13	9.8 ± 1.4
WGAJ0245.2+1047	0.26 ± 0.08	19.1 ± 3.9
WGAJ0313.9+4115	0.38 ± 0.12	13.0 ± 1.7
WGAJ0340.8–1814	0.40 ± 0.08	16.0 ± 3.0
WGAJ0421.5+1433	0.30	< 8.2
WGAJ0428.8–3805	0.32 ± 0.05	< 0.7
WGAJ0449.4–4349	< 0.01	< 0.1
WGAJ0500.1–3040	< 0.17	52.6 ± 8.9
WGAJ0502.5+1338	< 0.21	< 3.0
WGAJ0513.8+0156	0.34 ± 0.12	< 1.3
WGAJ0528.5–5820	0.23 ± 0.06	< 0.8
WGAJ0558.1+5328	0.29 ± 0.16	9.8 ± 0.4
WGAJ0624.7–3230	0.22 ± 0.05	8.5 ± 1.6
WGAJ0656.3–2403	< 0.15	24.5 ± 9.3
WGAJ0816.0–0736	0.37 ± 0.18	< 1.8
WGAJ0940.2+2603	< 0.14	13.7 ± 5.3
WGAJ1057.7–7724	< 0.29	< 3.2
WGAJ1108.1–7748	< 0.15	< 2.6
WGAJ1222.6+2934	< 0.33	< 4.5
WGAJ1231.7+2848	< 0.28	< 4.0
WGAJ2258.3–5525	< 0.07	< 1.0
WGAJ2317.9–4213	0.52 ± 0.08	< 0.5
WGAJ2350.6+3622	0.22 ± 0.10	< 0.5

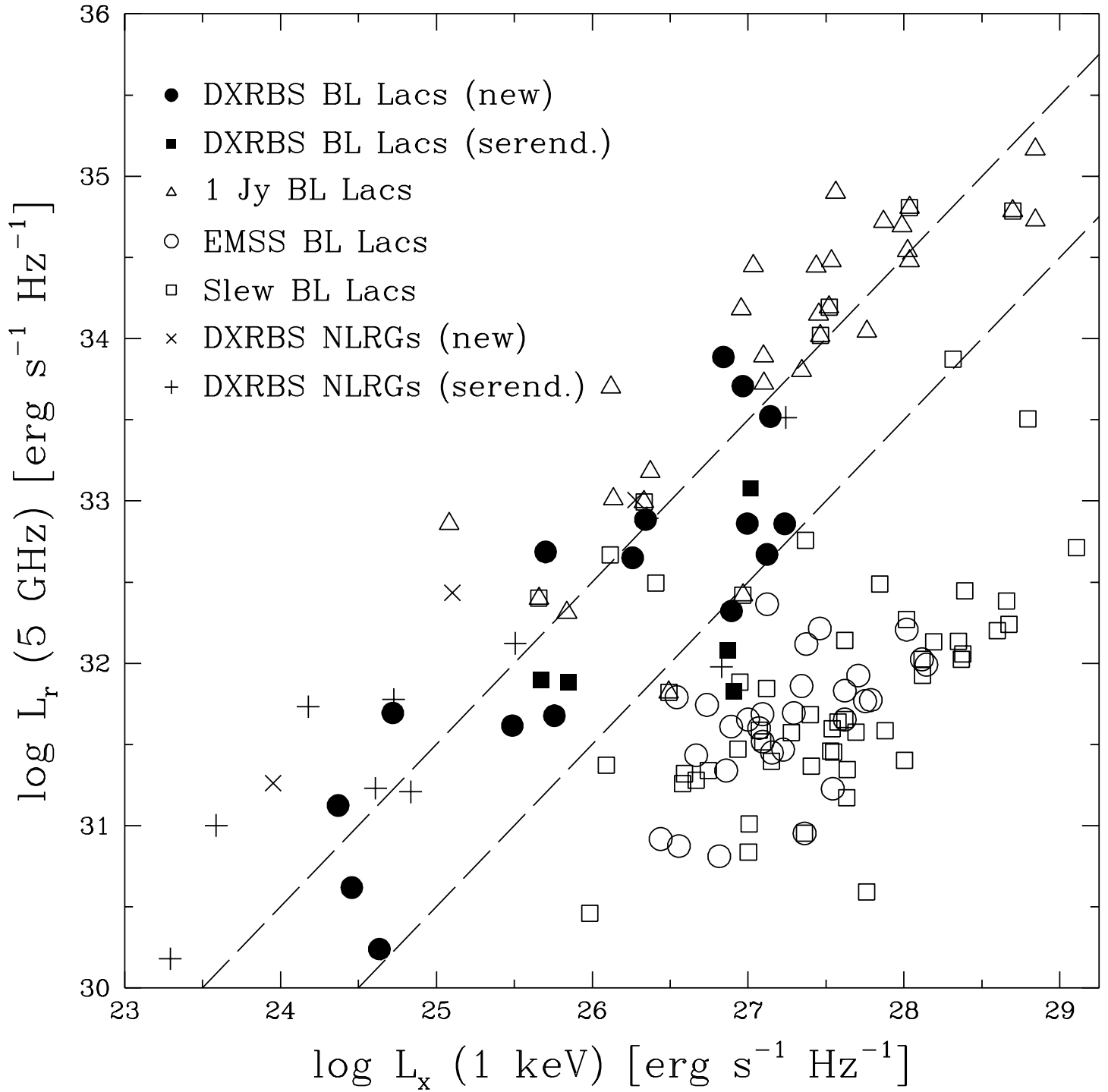


TABLE 6
PREVIOUSLY IDENTIFIED BLAZARS

Name	ROSAT ct/s	F(0.1–2.0 keV) erg cm ⁻² s ⁻¹	F(1 keV) μJy	log F _X /F _R	F(6 cm) mJy	α _r	V	Class	z
PKS 0027–426	0.046	0.55E–12	0.14	–11.80	419	0.00	19.0	FSRQ	1.660
PKS 0035+23	0.012	0.16E–12	0.032	–12.49	463	0.54	19.0	FSRQ	2.270
PKS 0100–270	0.030	0.27E–12	0.045	–11.92	201	0.42	18.1	FSRQ	1.597
TEX 0109+200	0.017	0.24E–12	0.058	–12.01	281	0.31	17.0	FSRQ	0.746
PKS 0112–017	0.026	0.36E–12	0.092	–12.56	1540	–0.48	17.4	FSRQ	1.381
PKS 0119+041	0.024	0.26E–12	0.050	–12.70	1235	–0.24	19.5	FSRQ	0.637
UM 320	0.010	0.12E–12	0.031	–12.22	259	0.13	18.6	FSRQ	2.280
PKS 0122–003	0.066	0.76E–12	0.20	–12.11	1234	0.09	16.7	FSRQ	1.070
I 0115	0.005	0.65E–13	0.019	–12.82	671	0.64	14.0	RG	0.043
PKS 0142–278	0.050	0.56E–12	0.14	–12.01	833	–0.03	19.0	FSRQ	1.157
S4 0206+355	0.022	0.31E–12	0.086	–12.39	976	0.68	13.0	RG	0.037
PKS 0247–207	0.029	0.33E–12	0.092	–11.90	389	0.54	15.5	RG	0.087
PKS 0256–005	0.023	0.34E–12	0.10	–12.04	500	–0.59	17.2	FSRQ	1.995
PKS 0335–364	0.048	0.49E–12	0.070	–12.19	583	–0.39	18.0	FSRQ	1.537
PKS 0406–127	0.013	0.13E–12	0.021	–12.63	517	0.22	19.0	FSRQ	1.563
PKS 0422–380	0.064	0.67E–12	0.011	–12.49	1706	–2.06	18.1	FSRQ	0.782
PKS 0439–433	0.100	0.10E–11	0.16	–11.53	285	0.19	16.4	FSRQ	0.593
PKS 0514–459	0.067	0.84E–12	0.16	–12.10	990	0.44	17.5	FSRQ	0.194
S4 0537+531	0.007	0.83E–13	0.040	–12.82	668	–0.02	18.0	FSRQ	1.275
EXO0556.4–3838	0.956	0.11E–10	3.01	–9.73	68	0.00	17.1	BL Lac	?
S5 0743+74	0.009	0.12E–12	0.034	–12.45	445	–0.19	19.3	FSRQ	1.629
0822+27W01	0.054	0.64E–12	0.16	–11.31	150	–0.03	17.7	FSRQ	2.060
B2 0834+25	0.035	0.41E–12	0.11	–11.94	458	0.14	18.0	FSRQ	1.122
TEX 0836+182	0.014	0.11E–12	0.016	–12.52	310	0.17	17.0	BL Lac	?
PKS 0839+187	0.051	0.54E–12	0.104	–12.23	898	0.24	16.4	FSRQ	1.272
S4 0847+37	0.043	0.64E–12	0.15	–11.75	391	0.37	19.5	RG	0.407
4C 58.17	0.023	0.28E–12	0.071	–12.51	1184	0.15	18.0	FSRQ	1.322
OJ–297	0.004	0.58E–13	0.022	–13.40	2216	–0.17	16.6	FSRQ	2.160
4C 47.29	0.032	0.27E–12	0.044	–12.73	1264	0.48	18.7	FSRQ	1.462
RXJ09168+5238	0.252	0.22E–11	0.36	–10.55	69	0.58	18.9	BL Lac	0.190
S5 0916+718	0.026	0.36E–12	0.094	–11.78	295	0.22	19.5	FSRQ	0.594
4C 55.17	0.076	0.46E–12	0.034	–12.94	2015	0.33	16.5	FSRQ	0.909
S4 0955+476	0.036	0.34E–12	0.028	–12.77	1005	–0.32	18.0	FSRQ	1.873
0959+68W01	0.029	0.42E–12	0.11	–11.18	86	0.41	15.9	FSRQ	0.773
WGAJ1012.2+063	0.021	0.21E–12	0.055	–12.03	300	0.45	16.8	BL Lac	?
4C 19.34	0.103	0.12E–11	0.28	–11.75	765	–0.11	17.5	FSRQ	0.828
S5 1027+74	0.066	0.84E–12	0.22	–11.38	250	0.19	17.2	FSRQ	0.123
B2 1048+34	0.011	0.86E–13	0.015	–12.56	312	0.44	19.0	FSRQ	2.520
5C 02.56	0.004	0.32E–13	0.006	–12.52	100	0.50	20.0	FSRQ	2.396
4C 72.16	0.034	0.49E–12	0.13	–12.03	858	0.44	17.9	FSRQ	1.460
1104+72W01	0.008	0.99E–13	0.026	–12.26	271	0.30	18.9	FSRQ	2.100
PKS 1145–071	0.031	0.37E–12	0.093	–12.27	791	0.00	18.0	FSRQ	1.342
B2 1147+245	0.017	0.15E–12	0.022	–12.72	645	–0.02	16.2	BL Lac	> 0.2
WGAJ1202.1+444	0.210	0.13E–11	0.11	–10.98	69	1.43	18.1	BL Lac	?
7C 1159+2813	0.043	0.34E–12	0.036	–11.70	107	0.16	...	FSRQ	0.672
DW 1211+13	0.011	0.98E–13	0.023	–12.89	894	0.42	18.1	FSRQ	1.137
B2 1211+33	0.039	0.25E–12	0.041	–12.44	627	0.54	17.9	FSRQ	1.598
1ES1212+078	0.506	0.54E–11	0.95	–10.37	117	–0.04	16.0	BL Lac	0.136

TABLE 6—*Continued*

Name	ROSAT ct/s	F(0.1–2.0 keV) erg cm ⁻² s ⁻¹	F(1 keV) μJy	log F _X /F _R	F(6 cm) mJy	α _r	V	Class	z
B2 1215+33	0.007	0.49E-13	0.004	-12.67	117	0.46	18.1	FSRQ	2.605
ON 325	0.382	0.27E-11	0.27	-11.44	478	0.09	15.6	BL Lac	0.130
3C 273	9.060	0.91E-10	17.2	-11.68	43572	0.12	12.8	FSRQ	0.158
GB 1231+482	0.140	0.86E-12	0.036	-11.93	268	0.27	17.4	FSRQ	0.375
RX J12368+2507	0.083	0.81E-12	0.10	-11.26	109	0.54	17.6	FSRQ	0.546
PKS 1240-294	0.042	0.59E-12	0.17	-11.83	472	0.31	17.7	FSRQ	1.133
PKS 1255-316	0.019	0.23E-12	0.061	-12.74	1410	0.09	18.7	FSRQ	1.924
1308+328	0.014	0.12E-12	0.027	-12.76	870	-0.62	19.5	FSRQ	1.650
PKS 1324-300	0.031	0.40E-12	0.097	-11.96	406	0.59	18.0	RG	0.200
NGC 5232	0.010	0.11E-12	0.020	-12.72	529	-0.09	13.0	RG	0.021
1339+274	0.027	0.19E-12	0.021	-12.44	347	-0.29	19.0	FSRQ	1.185
PKS 1402+044	0.012	0.13E-12	0.031	-12.80	1008	-0.49	19.0	FSRQ	3.202
S4 1435+638	0.078	0.89E-12	0.13	-12.02	757	0.51	16.1	FSRQ	2.068
MS 14428+6344	0.022	0.17E-12	0.030	-12.43	442	0.36	17.2	FSRQ	1.380
3C 309.1	0.077	0.78E-12	0.17	-12.63	3567	0.64	16.8	FSRQ	0.904
PKS 1502+106	0.023	0.22E-12	0.032	-13.14	2325	-0.33	18.6	FSRQ	0.563
B2 1506+33A	0.007	0.55E-13	0.005	-12.57	115	0.14	18.5	FSRQ	2.200
MC 1524+101	0.024	0.24E-12	0.043	-12.15	316	0.26	19.0	FSRQ	1.358
1555+3538	0.226	0.28E-11	0.55	-10.44	80	0.68	14.7	RG	0.158
NGC6034	0.032	0.38E-12	0.077	-11.99	343	0.58	13.5	RG	0.034
NGC6061	0.048	0.52E-12	0.10	-11.71	258	0.61	13.6	RG	0.038
OS319	0.103	0.12E-11	0.22	-12.31	2324	0.18	17.5	FSRQ	1.401
4C 38.41	0.100	0.10E-11	0.15	-12.61	3221	-0.44	18.0	FSRQ	1.814
S4 1637+574	0.105	0.10E-11	0.19	-12.24	1750	-0.29	17.0	FSRQ	0.750
S4 1638+398	0.028	0.26E-12	0.050	-12.61	1117	-0.44	16.5	FSRQ	1.666
3C 345	0.317	0.35E-11	0.75	-12.31	8719	-0.08	16.0	FSRQ	0.594
B2 1656+34	0.030	0.26E-12	0.046	-12.28	474	0.02	18.5	FSRQ	1.936
S4 1656+571	0.021	0.20E-12	0.037	-12.61	764	0.04	17.6	FSRQ	1.293
4C 45.34	0.042	0.55E-12	0.17	-11.65	461	0.70	17.4	FSRQ	0.646
PKS 1725+044	0.049	0.70E-12	0.18	-12.07	885	-0.44	17.0	FSRQ	0.293
7C 1753+6543	0.020	0.23E-12	0.046	-11.92	186	0.61	17.4	FSRQ	0.140
S4 1806+456	0.027	0.30E-12	0.077	-11.99	351	-0.68	19.0	FSRQ	0.830
EXO1811.7+3143	0.036	0.48E-12	0.090	-11.45	127	0.17	17.4	BL Lac	0.117
4C 50.47	0.023	0.38E-12	0.11	-11.93	345	0.53	17.9	FSRQ	1.098
PKS 1937-101	0.029	0.46E-12	0.18	-12.15	750	0.09	17.0	FSRQ	3.787
PKS 2058-425	0.097	0.10E-11	0.20	-11.86	721	0.56	17.2	FSRQ	0.221
MH 2136-428	0.120	0.97E-12	0.11	-11.17	108	0.00	16.2	BL Lac	?
4C 06.69	0.186	0.33E-11	0.91	-12.02	4135	-0.30	16.5	FSRQ	0.990
OY-106	0.008	0.72E-13	0.016	-13.73	4271	0.36	19.5	FSRQ	0.618
PKS 2212-299	0.032	0.21E-12	0.022	-12.54	450	0.30	17.4	FSRQ	2.706
3C 446	0.088	0.12E-11	0.32	-12.62	6382	0.00	18.0	FSRQ	1.404
I 1459	0.084	0.88E-12	0.15	-12.16	1151	-0.14	11.8	RG	0.006
PKS 2316-423	0.207	0.17E-11	0.34	-11.52	595	0.43	14.5	BL Lac	0.055
PKS 2319+07	0.013	0.19E-12	0.047	-12.63	857	0.18	18.5	FSRQ	2.090
PKS 2329-384	0.019	0.19E-12	0.048	-12.47	784	-0.05	17.0	FSRQ	1.195
PG 2344+092	0.085	0.13E-11	0.36	-11.97	1392	0.32	16.0	FSRQ	0.673
PKS 2352-342	0.182	0.12E-11	0.11	-11.53	241	0.62	16.4	FSRQ	0.702
PKS 2357-318	0.037	0.32E-12	0.085	-12.19	747	-1.62	17.6	FSRQ	0.991

TABLE 6—*Continued*

Name	ROSAT ct/s	F(0.1–2.0 keV) erg cm ⁻² s ⁻¹	F(1 keV) μJy	log F_X/F_R	F(6 cm) mJy	α_r	V	Class	z
PKS 2357–326	0.007	0.41E–13	0.003	–13.37	535	0.02	18.7	FSRQ	1.275

